



**This document was prepared by the Nondestructive Testing Information Analysis Center (NTIAC), Southwest Research Institute, 6220 Culebra Road, San Antonio, Texas 78284. NTIAC is a full service information analysis center sponsored by the U.S. Department of Defense, serving the information needs of the Department of Defense, other U.S. Government agencies, and the private sector, in the field of nondestructive testing.**

**NTIAC is operated under Contract DLA900-79-C-1266 with the Defense Logistics Agency. Technical aspects of NTIAC operations are monitored by the U.S. Army Materials and Mechanics Research Center.**

**This document was prepared under the sponsorship of the U.S. Department of Defense. Neither the United States Government nor any person acting on behalf of the United States Government assumes any liability resulting from the use or publication of the information contained in this document or warrants that such use or publication of the information contained in this document will be free from privately owned rights.**

**All rights reserved. This document, or parts thereof, may not be reproduced in any form without written permission of the Nondestructive Testing Information Analysis Center.**

# SOUTHWEST RESEARCH INSTITUTE

POST OFFICE BOX 21700 • 5420 CULBERTSON ROAD • SAN ANTONIO, TEXAS 78284 • 512-684-5111

Nondestructive Testing Information Analysis Center

22 March 1982

Defense Technical Information Center  
Attn: DDA2  
Cameron Station  
Alexandria, VA 22314

Gentlemen:

In accordance with our contract requirements, we are enclosing two (2) copies of "Nondestructive Evaluation of Fiber Reinforced Composites, Part I", by G. A. Matzkanin.

This publication is an IAC-originated document and should be considered an "exception-priced" document. NTIAC will sell this publication for \$40.00 domestic, and \$45.00 foreign.

Very truly yours,

*Richard T. Smith, by mfa*

Richard T. Smith, Director  
Nondestructive Testing  
Information Analysis Center

RTS:mfa

Enclosures



NTIAC is operated for the U.S. Department of Defense by Southwest Research Institute under Contract No. DLA 900 79 C 1265  
SAN ANTONIO HOUSTON TEXAS AND WASHINGTON D.C.

2

NTIAC-82-1

# **NONDESTRUCTIVE EVALUATION OF FIBER REINFORCED COMPOSITES**

A State-of-the-Art Survey

Volume I

**NDE OF GRAPHITE FIBER-REINFORCED PLASTIC COMPOSITES**

(Part I. Radiography and Ultrasonics)

by

**George A. Matzkanin  
Senior Research Scientist**

**SOUTHWEST RESEARCH INSTITUTE  
San Antonio, Texas**

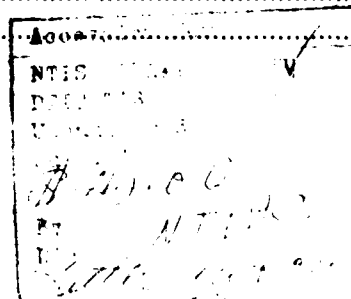
March 1982

**NONDESTRUCTIVE TESTING INFORMATION ANALYSIS CENTER**

**Approved for public release; distribution unlimited**

## TABLE OF CONTENTS

	Page
LIST OF ILLUSTRATIONS .....	iii
LIST OF TABLES .....	iv
I. INTRODUCTION .....	1
II. MATERIAL DESCRIPTION .....	3
A. Constituent Materials .....	3
1. Matrix .....	3
2. Reinforcement .....	4
B. Fabrication .....	4
1. Primary Fabrication .....	5
2. Secondary Fabrication .....	6
C. Properties .....	6
III. SURVEY OF NDE RESULTS .....	9
A. Radiography .....	9
1. Methodology .....	9
2. General Application to Fiber Reinforced Composites .....	11
3. Use of Opaque Additives .....	14
4. Computer Assisted Radiography .....	16
5. Commercial Aircraft Inspection .....	21
B. Ultrasonics .....	21
1. Methodology .....	21
2. General Application to Composites .....	26
3. Fatigue Damage .....	34
4. Measurement of Strength .....	40
5. Measurement of Void Content .....	43
6. Detection of Moisture Degradation .....	46
7. Commercial Aircraft Inspection .....	48
IV. DISCUSSION .....	51
V. REFERENCES .....	54
APPENDIX A—LITERATURE SEARCH STRATEGY .....	57
APPENDIX B—BIBLIOGRAPHY .....	60



A. B. C.

## LIST OF ILLUSTRATIONS

Figure	Page
1. Specific Strength of Selected Composites .....	8
2. Specific Stiffness of Selected Composites .....	8
3. Strength Loss of Carbon-Reinforced Plastics Due to Environmental Aging .....	8
4. Diagram of Radiographic Process .....	9
5. The Two Principal Types of Damage in Fibrous Composites .....	12
6. Cracking in the Plies of a $0^\circ$ - $45^\circ$ Laminate with Load Applied in the $0^\circ$ Direction .....	12
7. Damage Line Growth for a $[\pm 45]_3$ Specimen Under Ramp Loading .....	14
8. Summation of $\pm 45^\circ$ Crack Lengths from Notch vs Load Squared for $[\pm 45]_3$ Under Ramp Loading .....	15
9. Schematic Representation of the Addition of Boron Fiber to the Edges of Composite Tape by an Automatic Tape-Laying Machine .....	16
10. Schematic of Radiographic Inspection Facility .....	17
11. Images of Damaged Zone in Composite Fan Frame Ring .....	18
12. Electronically Processed Radiographic Images .....	19
13. Electronic Images of Section of Damaged Area .....	20
14. Particle Displacements in Elastic Waves .....	22
15. Refraction and Mode Conversion at an Interface .....	22
16. Block Diagram of Ultrasonic Velocity Measuring Apparatus .....	23
17. Ultrasonic Transmission Setup Using the Pulsed Through-Transmission Technique .....	24
18. Main Features of a Basic General-Purpose Ultrasonic Test Unit in the A-Scan Mode .....	24
19. Basic Features of B-Scan System with a Persistent-Phosphor Cathode-Ray Oscilloscope Display .....	25
20. A Pulse-Echo C-Scan Presentation System .....	26
21. Alternative Ultrasonic Inspection Procedures .....	27
22. Block Diagram for Spectral Analysis of Ultrasound for NDT .....	29
23. Ultrasonic Spectra From Flat-Bottom Holes (b, c, d) and a Good Area (a) .....	29
24. Ultrasonic Spectra For Crack-Like Defects .....	30
25. Ultrasonic Spectrum for a Void Defect .....	30
26. Examples of Discriminator Level Settings in Ultrasonic C-Scan .....	31
27. Ultrasonic C-Scan Showing Poor Fiber Alignment .....	32
28. Ultrasonic C-Scan of Impact Damage .....	32
29. Schematic Diagram of a Double-Focused Imaging System .....	33
30. Block Diagram of Lockheed Acoustic Imaging System .....	33
31. Ultrasonic C-Scan and Acoustic Image of a Flat, 14-Ply Graphite/Epoxy Laminate .....	33
32. Ultrasonic C-Scans of $90 \pm 45^\circ$ Carbon Fiber Composite Made Before and After Fatiguing .....	35
33. Flaw Growth Under Spectrum Fatigue Loading in Graphite/Epoxy Specimens with 6.4 mm (0.25 in.) Diameter Hole .....	36
34. Flaw Growth Under Spectrum Fatigue Loading in Graphite/Epoxy Specimens with 9.4 mm (0.37 in.) Square Embedded Kapton Patch .....	37

## LIST OF ILLUSTRATIONS (cont'd)

Figure	Page
35. Flaw Growth Under Spectrum Fatigue Loading in Graphite/Epoxy Specimens with 3.2 mm (0.125 in.) Gap in Outermost 45-Deg. Ply .....	38
36. Flaw Growth Under Spectrum Fatigue Loading in Graphite/Epoxy Specimens with 0.25 mm (0.01 in.) Deep Surface Scratches .....	39
37. Attenuation Change Versus Number of Load Cycles for a Type I Specimen (2309 #7) .....	39
38. Attenuation Change Versus Number of Load Cycles for a Type II Specimen (2649 #6) .....	39
39. Initial Attenuation at 2.0 MHz Versus Cycles to Failure for Transfiber Compression-Compression Fatigue of Laminate No. 1 Specimen at $\sigma_{max}=0.8\sigma_f$ .....	40
40. Attenuation at 2.0 MHz Versus Cycles to Failure for Transfiber Compression-Compression Fatigue of Laminates No. 1 and 2 Specimens at $\sigma_{max}=0.8\sigma_f$ .....	41
41. Apparatus and Signal Treatment Used for Measuring the Stress Wave Propagation Factor .....	42
42. Correlation of Interlaminar Shear Strength with Stress Wave Factor for Graphite-Polyimide Composite ..	42
43. Variation of Stress Wave Factor Along Tensile Specimen for Three Typical Cases .....	43
44. Use of Ultrasonic Pulse-Echo Technique for Delaminated Detection .....	44
45. Relationship Between the Coefficient of Attenuation of Ultrasound by CFRP and the Void Content .....	45
46. Use of Bilinear Function to Describe the Relationship Between Void Content and Attenuation Coefficient .....	45
47. Effects of Varied Moisture Exposure and Subsequent Thermal Cycles on the Acoustic Attenuation $\alpha_1$ of Composite SC4 .....	46
48. Effects of Varied Moisture Exposure and Subsequent Thermal Cycles on the Ultrasonic Velocity $C_1$ of Composite SC4 .....	47
49. Moisture Effect on Acoustic Velocity .....	47
50. Moisture Effect on Acoustic Attenuation .....	47
51. Hygrothermal Cycling History of FRP Specimens .....	48
52. Normalized Flexural and Tensile Strengths Versus Ultrasonic Attenuation for Different Fiber Reinforced Plastic Systems .....	49

## LIST OF TABLES

Table	Page
I. Properties of the More Common Fibers Used in Reinforced Plastics .....	4
II. Typical Properties of Carbon Fibers .....	5
III. Typical Longitudinal Properties of Unidirectional Reinforced-Plastic Composites .....	7
IV. Typical Tensile Properties of Carbon-Fiber Composites at Room Temperatures .....	7
V. Thermal Neutron and X-Ray Elemental Mass Absorption Coefficients .....	13
VI. Calculated X-Ray and Thermal Neutron Mass Absorption Coefficients versus Composite Resin Content ...	13
VII. Results of Ultrasonic Spectral Analysis Technique on Graphite-Epoxy Composite Specimen with Flat-Bottom Holes .....	30
VIII. Application of Radiography and Ultrasonics to Nondestructive Evaluation of Graphite Fiber Reinforced Plastic Composites .....	53

## I. INTRODUCTION

Composite materials are being increasingly used as structural components because of their high strength-to-weight ratio. In fact, advanced structural composites are rapidly finding their way from aerospace applications into automotive, industrial, and consumer products. From a technical standpoint, advanced plastic matrix composites could easily replace metal or load-bearing components in structures in many consumer and industrial products. Composites offer some of the standard advantages of plastics processing. A number of parts can be grouped into one structure; the structure can be large, and secondary operations can be minimized. Composites can supply characteristics other than strength or rigidity; for instance, exceptional thermal oxidative stability, good bearing or wear characteristics, or electrical conductivity. However, current primary use is associated with the structural characteristics of composites.

While glass fiber reinforced plastic composites were the first composite materials to be used for structural applications, advanced composites containing graphite, aramid or boron fibers in a plastic matrix have been used increasingly in recent years. Even more exotic composites such as carbon/carbon composites and metal-matrix composites are finding expanded application, especially in harsh environments. Because of their primary utilization in structural applications, the non-destructive evaluation of composites has become increasingly important. In addition, the trend towards damage tolerant design philosophy in aerospace applications places emphasis on accurate NDE. Given defects must be found with specified probability and degree of confidence, and once found, they must be characterized in such a way that their effects on structural performance can be determined. Because of the heterogeneous nature of composites, the form of defects is often very different from a metal and fracture mechanisms are more complex. One result is that the effects of various defects on performance of composites are at present not well understood. The extent to which any combination of defects will prove detrimental is governed by the geometry (including layup order) of the structure, the exact location and orientation of the defects, the nature of the applied stress field, and the environment in which a given component is required to operate. On such factors there is a lack of information. From the standpoint of the user of NDE, there is a need to be able to differentiate between defects potentially detrimental to the performance of the structure and those which are not. To achieve this differentiation, it is necessary to ensure

good collaboration among design, fabrication, NDE, and mechanical or structural testing groups.

The purpose of this state-of-the-art survey is to provide a review of, and a ready reference to, the technical literature available and applicable to the nondestructive evaluation of graphite fiber reinforced epoxy composite materials. Previous state-of-the-art surveys on NDE of composites have been documented by the Air Force on carbon/carbon composites (Ref. 1) and by the Army on glass fiber reinforced composites (Ref. 2). This survey, published under the auspices of NTIAC, is intended to be the first volume in a series of surveys on NDE of composite materials. Future volumes will be directed toward NDE of metal-matrix composites, ceramic materials, and updates of carbon/carbon composites and glass fiber reinforced composites. Because of the large amount of literature available on graphite fiber reinforced composites, this particular volume has been divided into two parts. Part I will cover the two principal NDE methods in use for composites, namely ultrasonics and radiography, while Part II will cover all other NDE techniques.

In order to orient the reader, a brief description of composite materials is presented in Chapter II. The constituent matrix and reinforcement materials are discussed, as well as the more common fabrication techniques, and relevant physical properties. References are provided to more extensive descriptions of composite materials. The primary results of the literature survey are presented in Chapter III, which is subdivided into sections on radiography and ultrasonics. A brief description of the methodology is provided, and then a summary of illustrative NDE literature is presented.

Chapter IV contains a discussion of the overall survey results and includes an application table which provides the reader with a ready reference to the literature. This table lists documents indicating which NDE techniques have been reported for specific defect and property determinations in graphite fiber composites. Two appendices are included to provide additional information to the reader. Appendix A contains a description of the information retrieval procedures. Appendix B is a Bibliography containing a comprehensive listing of pertinent articles retrieved through the Defense Technical Information Center, NTIAC, and open literature sources.

Throughout the text the International System (SI) of units is used in accordance with the American National Standard ANSI Z210.1-1976. In some cases, approximate English or customary unit equivalents are included in parentheses following SI units. In the illustrations which are extracted from referenced papers, measurement units by the authors are retained and no conversions to either SI or English units, as the case may

be, are provided.

Hopefully, the information provided in this survey will serve as an introduction to the important area of *NDE of graphite fiber reinforced composite materials* for the casual reader, and also as a guide to further in-depth reading for those interested themselves in advancing the state-of-the-art.

## II. MATERIAL DESCRIPTION

Presented in this section is a general review of the characteristics and physical properties of the composite materials which are the subject of this survey. An excellent source for further details is Reference 3 from which much of the following information has been extracted.

### A. Constituent Materials

#### 1. Matrix

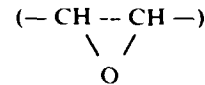
The matrix performs several important functions: (1) it acts as a bridge to hold the fibers in place, (2) it protects the filaments from damage by abrasion and chemical attack, and (3) it transmits stresses. Several polymer matrices are used in composites, but they may be divided into two categories: (1) the thermosets (comprising epoxy, polyester, phenolic, polyimide resins), and (2) the thermoplastics (polyethylene, polystyrene, nylon, and others). These two groups of matrices demand different methods of processing. The shear, chemical, and electrical properties of the composite depend primarily on the resin. Also, the usefulness of the laminate in the presence of a corroding environment is primarily determined by the nature of the resin.

The thermoplastics are largely one- or two-dimensional in molecular structure. At high temperatures, they soften, and indeed in the case of crystalline materials, show a discreet melting point. The process of softening at elevated temperatures and regaining rigidity upon cooling is a reversible one. Generally, the thermoplastics are used in chopped fiber composites in which the starting material is a premix or molding compound containing fibers in the desired quantity and of desired aspect ratio. These molding compounds are processed using conventional techniques of compression, transfer, or injection molding or extrusion.

Thermosets, on the other hand, develop a well-bonded, three-dimensional molecular structure upon curing. Once cross-linked or hardened these polymers will decompose rather than melt. The conditions necessary to effect cure and the characteristics of the uncured resin can be varied by changing the basic formulation. Moreover, some thermosets can be held in a partially cured condition for prolonged periods of time. This inherent flexibility makes the thermosets ideally suited to use as matrix materials for advanced continuous fiber composites.

Of the thermosets, polyesters and epoxies are perhaps the most widely used in fiber reinforced

composites. The epoxies have generally been preferred for use in advanced composites because of their higher strength, greater temperature resistance, excellent adhesion, and low shrinkage on curing. Epoxies, by definition, are polymers containing one or more epoxide groups,



In the usual case, epoxies consist of a resin system containing the base resin, a curing agent, and in certain cases, a filler or thixotropic addition.

Uncured epoxy can be advanced to the cured stage by catalyzed self polymerization, or by use of hardeners which are reactive cross-linking agents. In the resin systems used for composites, catalysts such as the tertiary amines are used almost exclusively as accelerators in conjunction with a reactive curing agent. Processability and properties of cured epoxy material are highly dependent on the type of hardener used to cure it. Aliphatic amines provide optimum handling characteristics; aromatic amines provide good short time heat resistance; anhydrides yield the best thermal stability; polyamides are used where increased resin flexibility is required.

In the curing reaction the resin passes from the uncured stage through a partially cured state in which the epoxy exists as a thermoplastic. Although the curing reaction to final cure is irreversible, by controlling the temperature one may maintain the resin in the thermoplastic stage for prolonged periods of time. This flexibility makes possible the use of prepregs, i.e., pre-impregnated fibers or fabrics, in composite fabrication. Depending upon the particular system, subzero storage may be needed to prevent the thermoplastic resin from completely curing.

Epoxies have superior chemical resistance, good adhesion to most substrates, very low water absorption and cure shrinkage, good electrical properties, and high strength. The standard epoxy resin systems, after curing, are generally limited to a use temperature of approximately 149°C. Epoxy-novolac systems with an anhydride cure have been the basis for most of the high temperature resistant epoxy formulations. Such systems have retained fair strength to 260°C, and have been tested at temperatures up to 399°C for short exposures.

Epoxy resins are among the most important of the matrix materials used in structural composites. It is estimated that over 90% of all high-performance composites presently used have an epoxy resin matrix (Ref. 3).

## 2. Reinforcement

By carrying the load and imparting stiffness to the structure, the fiber phase is literally the backbone of advanced fiber reinforced composites and determines the mechanical properties. Fibers are used in composites in three different forms:

- (1) in long filaments to provide the utmost in strength from filament winding,
- (2) in the form of cloths where a simpler fabrication technique is possible and the orthogonal properties of the layup are predictable,
- (3) by using chopped fibers sprayed with resin directly on a form.

The third form is by far the cheapest method of fabrication, but the strength is less than the other two.

Glass is the most widely used reinforcing fiber material for composites. It offers excellent strength at a low cost; unfortunately, it also has a low modulus and is not suited for stiffness-limited applications. The new high-strength, high modulus fibers have opened new doors for application of reinforced composites. Properties of the more important fibrous materials used in advanced composites are compared in Table I.

Although glass fiber reinforced composites have been used extensively in recent years, graphite fiber reinforcement is fast becoming the number one fiber re-

inforcement of the future. Recent expansions of existing production facilities as well as new planned construction are anticipated to meet the near term increased demand. The total U.S. market for graphite fibers, which in 1978 was about 159,000 kg, is expected to grow 30% to 40% annually, and along with the multimillion pound production, prices of less than \$22/kg are projected (Ref. 4).

Most carbon fibers are produced by the thermal decomposition of an inorganic precursor, usually rayon or polyacrylonitrile (PAN), although some are made from extruded pitch. PAN-based carbon fibers have been the standard in many applications, such as aircraft, for years, but pitch-based fibers offer better processability and a potential cost break as well. Currently, pitch-based fibers have a modulus equivalent to PAN-based, but they are not yet up to the same strength levels (Ref. 4).

Although the terms "carbon" and "graphite" are used interchangeably when describing fibers, there is a difference. Typically, PAN-based carbon fibers are 93% to 95% carbon by elemental analysis, whereas graphite fibers are usually 99 + % carbon. The basic difference is the temperature at which the fibers are made or heat treated. PAN-based carbon is produced at about 1590°C, while higher modulus graphite fibers are graphitized at 2283° to 3283°C.

The final mechanical properties of carbon fibers are controlled by the processing parameters. Generally, as modulus increases, ultimate strength and elongation decrease. Thus, it is impossible to obtain ultra high strength and modulus in the same fiber. A high modulus graphite fiber, for example, exhibits a lower strain-to-failure than a high strength carbon fiber. In some aircraft applications, where composite parts are continually stressed and flexed, the fiber with a higher strain-to-failure (higher elongation) may be the one of choice. Most suppliers of carbon fibers market several types, as shown in Table II.

TABLE I  
PROPERTIES OF THE MORE COMMON FIBERS USED  
IN REINFORCED PLASTICS (Ref. 3)

Material	Tensile Strength, ksi (N/cm <sup>2</sup> × 10 <sup>3</sup> )	Modulus, psi × 10 <sup>6</sup> (N/cm <sup>2</sup> × 10 <sup>6</sup> )	Density (g/cm <sup>3</sup> )
E Glass	500 (345)	10.5 (7.2)	2.55
S Glass	650 (450)	12.5 (8.6)	2.50
PRD-49-III	400 (275)	19 (13)	1.45
Boron	400-450 (275-310)	55-60 (38-41)	2.4
Carbon	150-450 (103-310)	10-90 (69-62)	1.4-1.9
Steel Wire	300-600 (206-512)	30 (20)	7.7-7.8

## B. Fabrication

In fabrication of polymeric composites, there are two aspects which must be considered. The first, termed primary fabrication, is the actual combination of fiber and matrix into a dense well-bonded body. The composite structures produced by primary fabrication must then be machined and attached to some other structure to be of use. The necessary machining and joining operations comprise secondary fabrication.

TABLE II  
TYPICAL PROPERTIES OF CARBON FIBERS (Ref. 3)

Vendor (Trade Name)	Grade	Precursor <sup>(a)</sup>	Tensile Strength, ksi/N/cm <sup>2</sup> × 10 <sup>3</sup>	Tensile Modulus, psi × 10 <sup>6</sup> / N/cm <sup>2</sup> × 10 <sup>6</sup>	Density, lb./in. <sup>3</sup> (g/cm <sup>3</sup> )	Form
Union Carbide (Thornel)	T-25	R	180/125	25/17	0.052 (1.43)	2 ply yarn
	T-40	R	250/172	40/28	0.056 (1.56)	2 ply yarn
	T-50	R	300/207	50/35	0.059 (1.65)	2 ply yarn
	T-75	R	365/252	75/52	0.066 (1.82)	2 ply yarn
	T-400	P	450/310	30/21	0.064 (1.78)	1 ply yarn
Hitco	HMG-25	R	150/103	25/17	0.054 (1.5)	yarn
	HMG-40	R	250/172	40/28	0.061 (1.7)	yarn
	HMG-50	R	300/207	50/35	0.065 (1.8)	yarn
Celanese (Celion)	GY-70	P	300/207	75/52	0.069 (1.9)	--
Hercules/Courtaulds (Grafil) (Magnamite)	A	P	390/269	31/21	0.065 (1.8)	10,000 tow
	HM <sup>(b)</sup>	P	300/207	55/38	0.068 (1.88)	10,000 tow
	HT <sup>(b)</sup>	P	350/241	40/28	0.062 (1.72)	10,000 tow
Great Lakes (Fortafil)	3-T	P	250/172	28/19	0.064 (1.76)	150,000 tow
	4-T	P	350/241	37/25	0.064 (1.78)	50,000 tow
	5-T	P	400/276	48/33	0.065 (1.79)	--
	6-T	P	420/290	59/41	0.069 (1.9)	50,000 tow
Whittaker Morganite (Modmor)	I	P	250/172	60/41	0.072 (2.0)	10,000 tow
	II	P	400/276	40/28	0.064 (1.76)	10,000 tow
Polycarbon	A	P	300/207	35/24	0.063 (1.75)	tow
	T	P	350/241	40/28	0.063 (1.75)	tow
	M	P	300/307	60/41	0.069 (1.90)	tow
Kureha	Corbis	T	75-250/51-172	4-38/2.7-2.6	0.058-0.061 (1.6-1.7)	--
Tokai (Thermalon)	T-S	P	230/159	70/48	0.072 (2.0)	--
Stackpole (Panex)	30	P	400-470/275-324	30/21	--	160,000 tow
Nippon	G.L.	L	85/58	--	0.065 (1.8)	--
Sigr (Sigrafil)		P	215-355/148-245	28-70/19-48	0.065-0.072 (1.8-2.0)	--

(a) R = Rayon P = Polyacrylonitrile L = Lignin

Source: Manufacturers' Literature

(b) Surface-treated versions also available under designations HM-S and HT-S

### 1. Primary Fabrication

Fabrication of continuous fiber reinforced composite involves three basic operations: (1) positioning of the fibers (layup), (2) introduction of the polymeric matrix, and (3) compaction and curing of the composite. In some processing schemes, dry fiber and catalyzed resin are combined during the fabrication se-

quence. For these wet layups, as they are called, resin viscosity and gel time must be controlled to assure wetting of the fiber and to achieve a uniform distribution of the matrix. Many glass fabric reinforced composites are made by the wet layup method. An alternative approach, which is the dominant method in the area of high performance composites, such as graphite fiber reinforced composites, is the prepreg or dry layup

method. Here the fiber and matrix are combined prior to layup. These pre-impregnated fibrous materials are available in the form of yarn or roving as well as narrow tape and broadgoods. As mentioned earlier, prepregs are generally advanced to the thermoplastic stage and held under refrigeration until needed. The prepregs offer the user controlled resin content, fiber distribution, flow, volatile content, gel time, and tack. As a result, producibility often is better for prepreg than for wet layups.

A variety of approaches are utilized for actual layup. Many users make their own prepreg by drum winding over prepregged film or drum winding and then resin coating. For single parts, hand layup, i.e., the manual positioning of each ply of prepreg is not uncommon. Templates are usually used as patterns for cutting the prepreg and to guide the layup for various plies. As a result of a need for automation to cut costs, highly versatile and complex tape laying machines have been developed.

Filament or tape winding is a machine controlled process for wrapping a mandrel with continuous reinforcement. Basically, the process involves the wrapping of successive layers of resin-impregnated fibers over the part in a prescribed pattern. In wet winding the impregnation is effected just prior to application onto the mandrel, whereas prepregged tape or roving is used in dry winding. The tack inherent in prepreg systems often is an asset, in that fiber slippage is greatly reduced. The principal winding patterns are hoop or circumferential winding at approximately 90° to the mandrel axis, helical winding at some angle to the axis, and polar or longo winding (essentially a very low helix angle) nearly parallel to the axis. Usually the mandrel used in filament winding must be removed after the matrix is cured. However, in some cases, the mandrel may be an integral part of the final assembly as in a fiber overwrapped pressure vessel.

Prior to, or in conjunction with, the curing of the composite, entrapped air must be removed and the layup debulked or consolidated. Almost all high performance continuous fiber composites are produced by some variation of the open molding or bag molding process. The layup is positioned over a tool or mold and covered with a porous non-adherent material. A porous bleeder material such as glass fabric is then added to absorb excess resin. Finally, the layup is covered with a flexible membrane or bag which is sealed to the mold. In vacuum-bag molding the air inside the bag is evacuated, allowing ambient air pressure to effect the compaction of the laminate. Usually the vacuum is maintained

throughout the cure cycle to eliminate the accumulation of evolved volatile matter. Vacuum-bag molding is relatively uncomplicated, but the maximum pressure which can be achieved is less than one atmosphere. For some systems the vacuum does not provide sufficient pressure differential and an external pressure must be applied. Thus, the term pressure-bag molding. Usually the pressure is applied in a gas or steam autoclave. The bagging operation is essentially the same as for vacuum-bag molding, and in fact, most autoclave cure cycles employ a vacuum assist. Pressure-bag molding usually produces a lower void content and dimensional control is better than with vacuum-bag molding. Some composites, especially those requiring very high curing pressures, are molded in presses using closed dies. Very close dimensional tolerances and high production rates are possible, but tooling costs and press capacity are often limiting factors. One problem area in the fabrication of composite structures is residual stresses due to thermal expansion mismatch between the composite and the tooling.

## 2. Secondary Fabrication

Secondary fabrication of composites, that is, the joining and machining of cured panels poses some unique problems. Most composites, with the exception of those having rather complex ply orientations, have relatively low shear strengths. Thus, mechanical fasteners are not satisfactory unless some provision is made for increasing the shear strength in the joint area. One common technique involves the addition of metal shims into the layup at strategic locations. Stress concentration at holes and cutouts is also of concern. One effective way to reduce the stress concentration is to reduce the modulus stepwise in the vicinity of the cutout. This is readily accomplished by inserting softening strips or individual plies of low modulus carbon or glass prepreg into the layup in the areas where cuts are to be made.

## C. Properties

In a composite, the shear properties and high temperature resistant properties are most directly related to the matrix while the mechanical properties depend primarily on the type of fibers, the quantity of fibers in the laminate, and the direction of the fibers. The characteristics of the fiber, i.e., its tensile strength and its modulus, will determine these properties in the finished laminate, and the tensile strength and modulus of the composite will be directly proportional to the percentage value of the fibers. The direction of the fibers will determine the response of the material to off-axis loads. The properties of the composite depend not only on the identities and relative quantities of the fiber and resin

used, but on the laminate construction as well. For example, a unidirectional composite, one in which all fibers are aligned and parallel, has the highest strength and stiffness in the fiber direction for a given fiber/matrix system. Typical unidirectional properties for several important composite systems are compared in Table III. Such unidirectional composites, however, will have rather poor properties if stressed at some angle oblique to the fiber direction.

Because carbon fibers are available in such wide variety, there is also a broad spectrum of attainable composite properties. Some of these properties are listed for various types of carbon fiber composites in Table IV. Data for two polyimide matrix systems are included for comparison. The carbon/polyimide composites are lower in strength than comparable carbon/epoxies. Stress-strain curves for carbon fiber composite laminates are essentially linear to failure. The strength-

TABLE III  
TYPICAL LONGITUDINAL<sup>(a)</sup> PROPERTIES OF UNIDIRECTIONAL  
REINFORCED-PLASTIC COMPOSITES (Ref. 3)

Fiber	Matrix	Ultimate Tensile Strength ksi/N/cm <sup>2</sup> × 10 <sup>3</sup>	Tensile Modulus psi × 10 <sup>6</sup> / N/cm <sup>2</sup> × 10 <sup>6</sup>	Ultimate Compressive Strength ksi/N/cm <sup>2</sup> × 10 <sup>3</sup>
E glass	Epoxy	150-250/103-172	6.8/4-5.5	87/60
S glass	Epoxy	250-290/172-200	9.6/6.6	200/138
PRD-49	Epoxy	210/144	12.5/8.6	40-60/28-41
Boron	Epoxy	180-210/124-144	30-32/21-22	400-440/275-303
Boron	Polyimide	170-190/117-131	30-31/≈21-21.4	--
Carbon <sup>(b)</sup>	Epoxy	60-200/41-138	18-30/12-21	60-200/41-138
Carbon <sup>(c)</sup>	Polyimide	180-210/124-144	23/16	175/120
Steel	Epoxy	300-425/206-293	15-21/10-15	--

(a) parallel to the fiber direction

(b) various fibers

(c) Modmor II only

TABLE IV  
TYPICAL TENSILE PROPERTIES OF CARBON-FIBER COMPOSITES  
AT ROOM TEMPERATURES (Ref. 3)

Fiber Description	Matrix	Laminate Orientation, degrees	Ultimate Tensile Strength, ksi/N/cm <sup>2</sup> × 10 <sup>3</sup>	Modulus, psi × 10 <sup>6</sup> / N/cm <sup>2</sup> × 10 <sup>6</sup>
HT	Epoxy	0	188/130	20/14
		90	2.4/1.7	1.1/0.80
		0/±45	115/79.0	13.1/9.00
HM	Epoxy	0	104/72.0	24/17
		90	6.8/4.7	1.1/0.80
		±45	21/15	2.5/1.7
		0/90	53/37	14.5/10.0
A	Epoxy	0	168/116	19.7/13.6
GY-70	Epoxy	0	90/62	42/29
		90	3/2	0.86/0.60
Fortafil 5Y	Polyimide	0	91/63	23.6/16.3 <sup>(a)</sup>
		90	2.9/2.0	--
HMG-50	Polyimide	0	69.7/48.0	25.8/17.8
		90	2.6/1.8	--

(a) In flexure.

to-density and modulus-to-density ratios versus temperature behaviors for several important boron and carbon composites are compared in Figures 1 and 2. The width of the range of attainable properties with carbon fiber composites is apparent.

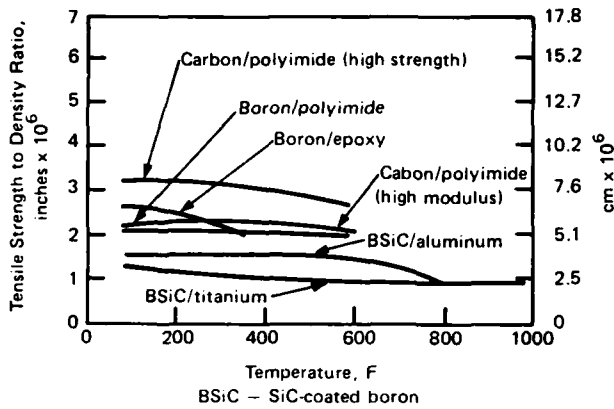


FIGURE 1. SPECIFIC STRENGTH OF SELECTED COMPOSITES (From Ref. 3, Reproduced by permission of The Metallurgical Society of AIME)

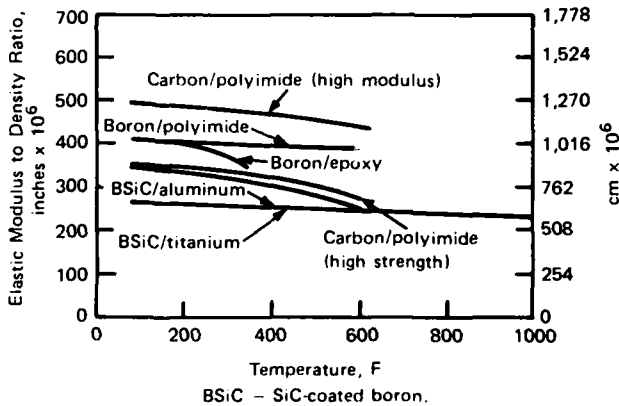


FIGURE 2. SPECIFIC STIFFNESS OF SELECTED COMPOSITES (From Ref. 3, Reproduced by permission of The Metallurgical Society of AIME)

All of the resin matrix composites are subject to degradation as a result of aging. The problem was first encountered in glass fiber reinforced composites in which the fiber surface is subject to a hydrolysis reaction resulting in strength loss. The effect of moisture is accelerated if the fiber is under stress. Many properties,

especially the high temperature properties, of advanced carbon fiber reinforced composites degrade upon aging, even under low humidity, low temperature conditions. The problem is illustrated by data shown in Figure 3. One theory is that water plasticizes the resin, thus lowering its glass transition temperature and heat distortion temperature. However, the fact that aging without the presence of excessive humidity can also result in strength losses, gives rise to speculation that the mechanism may be associated with thermal stress relaxation in the matrix.

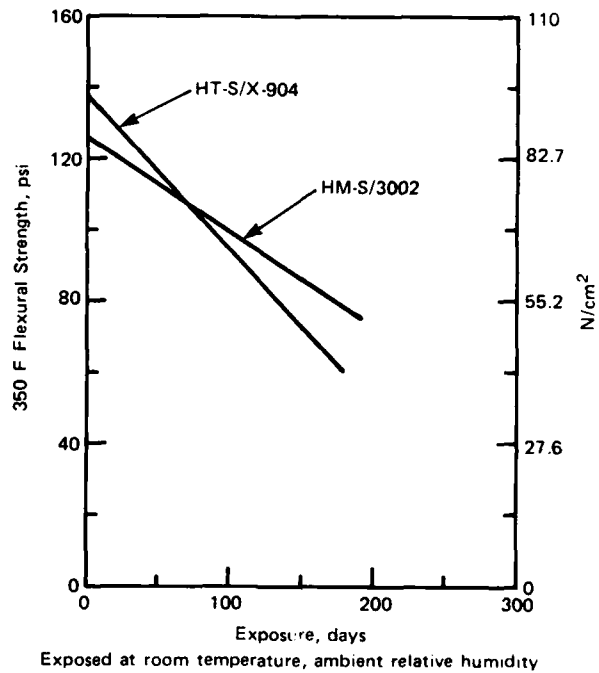


FIGURE 3. STRENGTH LOSS OF CARBON-REINFORCED PLASTICS DUE TO ENVIRONMENTAL AGING (From Ref. 3, Reproduced by permission of The Metallurgical Society of AIME)

### III. SURVEY OF NDE RESULTS

In this chapter a descriptive review is presented of literature relevant to NDE of graphite/epoxy composites. Since it was not possible within the scope of this survey to describe all the literature in this area, documents were selected which illustrate the state-of-the-art in certain broad categories. Preference was given to more recent documents, i.e., those appearing within the last five or six years. Approximately 50 documents are included in the narrative survey presented in this chapter; a more extensive listing of relevant documents resulting from the information retrieval is given in the Bibliography (Appendix B).

As mentioned in the Introduction, the two primary NDE methods used for the inspection of composites are radiography and ultrasonics. In presenting a survey of NDE results for these two methods in this chapter, brief descriptions of the methodologies are provided. While variations of these methods are sometimes used, only the basic principles will be discussed to acquaint the reader with the methodology. This information has been extracted in large measure from References 5 and 6, which provide more complete descriptions of these and other NDE techniques.

With respect to terminology, in the literature survey presented here, the terms "carbon" and "graphite", and "epoxy" and "plastic", are used interchangeably in the context of the particular documents being reviewed. Further specific information regarding materials can be found in the original documents as referenced.

#### A. Radiography

##### 1. Methodology

Radiography basically provides a two-dimensional picture of the intensity distribution of some form of radiation projected from the source, and which has passed through a material object that partially attenuates the intensity of the radiation (Figure 4). Variations in specimen thickness and density, or flaws of a different density affect the intensity of the transmitted radiation, and show up as variations in contrast on developed film. A shadowgraph image of the specimen defects is thus created. Of the three forms of penetrating radiation presently used in radiography, x-rays, gamma rays, and neutrons, x-ray radiography is the most widely used method for NDE of composites.

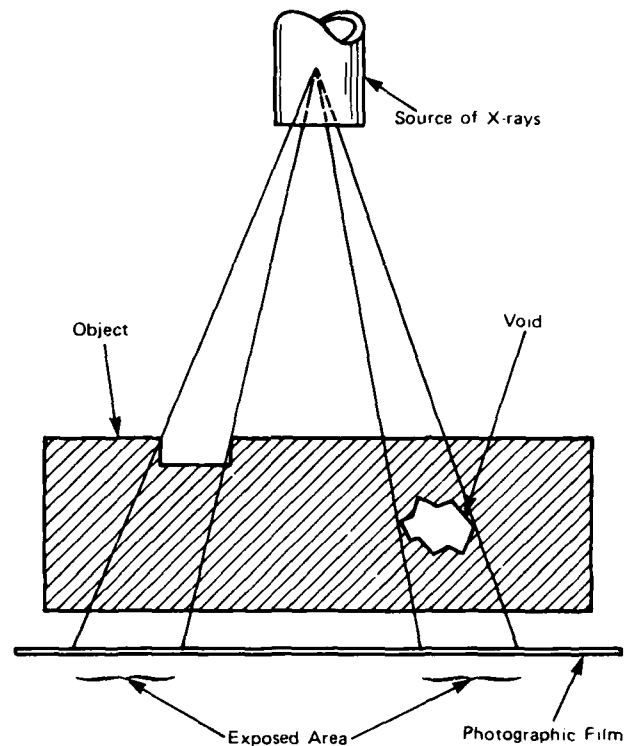


FIGURE 4. DIAGRAM OF RADIOGRAPHIC PROCESS (From Ref. 6)

Radiographic inspection is superior to other NDE methods in a number of applications. For example, it can provide a permanent visual representation of the interior of the test object. Under favorable conditions, radiographic inspection as a quality control procedure can conserve time and materials as given below.

1. It reveals nondestructively the internal nature of a material and can be used to separate acceptable items from unacceptable ones after standards for acceptance have been established.
2. It discloses errors in the manufacturing procedure and process control in sufficient detail to indicate necessary corrective action.
3. It discloses structural unsoundness, assembly errors, and concealed mechani-

cal malfunctions, thereby reducing the unknown or variable factors in a design during the development phase.

4. It is also useful in preventative maintenance in failure analysis.

The cost of industrial x-ray films and their handling and processing are relatively high in comparison to other inspection methods. Radiography of material that is small, easily handled, of simple geometry, and which otherwise lends itself to high rates of inspection, can be accomplished economically. Large items, complex geometries, materials which are difficult to handle, and cases in which the radiographic equipment be brought to the material are all factors that increase costs of inspections substantially.

Radiographic inspection has several inherent limitations. Since radiation traveling in straight lines from a source must intercept a film at nearly right angles, the efficient examination of some items of complex geometries is prevented. These conditions can preclude proper orientation of the film, or subject the film to the adverse effects of scatter radiation or image distortion. It is often desirable to determine the condition of a specific area that is surrounded by component materials or items. In these instances, inspection could be impossible because of the confusion created by superimposed images.

The information recorded on a radiograph is obtained because of density differences brought about by differential absorption of the radiation. These density differences, unless gross in nature, must be oriented almost parallel to the direction in which the radiation is traveling. Discontinuities of small volume such as laminar-type flaws will often be undetected because they do not present a sufficient density differential to the radiation. Fortunately, this limitation is countered to some extent, since the probable orientation of fractures can be approximately predicted and the radiographic setup oriented accordingly. However, the very nature of delaminations precludes their ready detection and radiographic inspection is seldom used to locate this type of flaw (see discussion in Section III.A.3 on the use of radio-opaque enhancement).

Penetrating radiation is attenuated in relation to the thickness of material. As material thickness is increased, the time required to obtain sufficient information on film also increases. For a given radiation energy, a maximum thickness exists beyond which the use of radiography is not economically practical. Radiogra-

phic equipment of higher maximum energy could be obtained, but costs increase markedly because of the barriers required to protect personnel from the harmful effects of the radiation, as well as the greater cost of larger equipment.

X-ray radiography of fiber reinforced composites is performed using state-of-the-art radiography procedures for materials with low absorption. A small x-ray focal spot size (0.35 mm) and a long source-to-film distance give good sensitivity and resolution of small defects. The use of low power and long exposure times enhances sensitivity and contrast. Extra fine grain film also helps provide sharp images and good resolution.

Neutron radiography is performed in a similar manner to x-ray radiography except that a neutron radiation source is used. Neutrons are electrically neutral particles that are constituents of all atomic nuclei except ordinary hydrogen. Neutrons are liberated by various nuclear reactions, including nuclear fission. Unlike x-rays, neutrons do not significantly interact with the electrons in matter. Rather, the neutron interacts directly with the atomic nucleus, either by elastic collision or by being absorbed by the nucleus, where it may subsequently induce a nuclear decay process. Ordinary radiographic film is only weakly sensitive to neutrons. Thus, the neutrons transmitted through the specimen are made to strike a foil such as indium, gadolinium, or lithium which emits secondary radiation to expose the film.

Neutrons for radiographic use are derived from nuclear reactors, nuclear accelerators, and radioactive isotope sources. In reactors, neutrons result from fission of the fuel element nuclei. Accelerators produce neutrons with accelerated charged particles to induce nuclear reactions in which neutrons are emitted. Isotope sources make use of the gamma radiation produced by certain radioactive nuclei to induce neutron-emitting reactions in a secondary element mixed with the radioactive one.

For most radiographic applications, it is necessary to "thermalize" the neutrons, that is, reduce their average energy to that of a gas at a moderate temperature. Since the thermalized neutrons do not radiate from a point source, it is necessary to collimate the neutrons using neutron absorbing materials give a reasonably unidirectional beam. This procedure is very wasteful of neutrons, and the resulting low beam intensity, particularly for non-reactor sources, is a major shortcoming.

## 2. General Application to Fiber Reinforced Composites

A useful review of the literature and state-of-the-art pertaining to radiographic inspection of composites prior to 1973 has been presented by Domanus and Lilholt (Ref. 7). The authors point out that, up to that time, literature on the subject was very scarce and no work had been reported on a systematic investigation of optimum radiographic conditions for the quality control of particular composites. In all of the documents reviewed by Domanus and Lilholt, soft x-ray radiography using beryllium window x-ray tubes was recommended. Many of the papers cited described NDE results for determination of such things as alignment and distribution of the reinforcing phase, fatigue shear cracks, fiber fractures, matrix cracks parallel to fibers, and delaminations between plies. However, little detail is provided regarding the technique itself. To remedy the lack of information on details of the radiographic technique, Domanus and Lilholt performed an investigation to establish the exposure technique for radiographic examination of carbon fiber reinforced composite samples 2 and 3 mm thick. The examination was performed with x-ray film and paper of different brands with different speed and graininess. Two types of samples were used. One was a commercial carbon fiber reinforced epoxy material containing 60 volume percent of continuous fibers, and having cross-sectional dimensions of 2 mm  $\times$  10 mm. A series of laboratory samples were also fabricated from the epoxy LY 554/HY 554 and high modulus carbon fibers of diameter 8 to 9  $\mu$ m. Continuous as well as short (approximately 5 mm) fibers were used in volume fractions of 20 to 30 percent. The samples fabricated in a simple leaky mold had dimensions 15 mm wide by 3 mm thick. The specimens had a somewhat irregular fiber distribution and contained several "natural" defects, mostly voids.

Radiographs were obtained with a constant potential Balteau Baltograph BE 50/20, with a 1 mm beryllium window, 0.5 mm focus, x-ray tube. A film-to-focus distance of 50 cm was used. The authors describe various details of the x-ray radiographic techniques which were investigated such as results obtained on different types of film, the use of different exposure techniques, obtaining dimensional measurements from radiographs, assessment of radiographic quality, and determination of measuring accuracy.

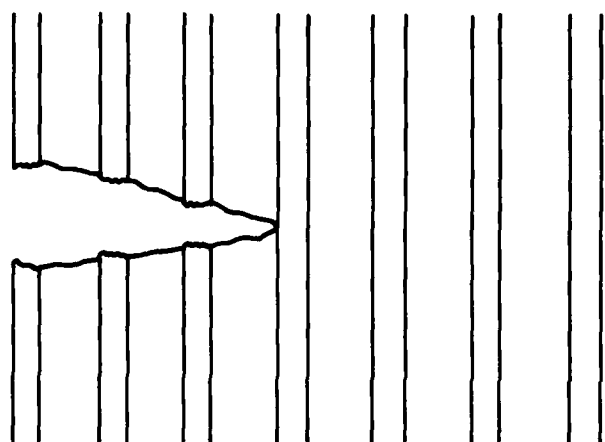
The authors conclude that the best way to determine the detection limit of defects which may occur in the material under examination is to produce artificial defects of known calibrated dimensions. Voids

could be simulated by producing holes of known dimensions which show up on the radiograph as dark spots. Inclusions made of a material with a higher attenuation to radiation will be reproduced as light spots. The smallest defect which could be detected on a projection microscope had a diameter of 100  $\mu$ m and this can be considered as the detection limit for natural defects in the form of voids in a sample 3 mm thick. The detectability of defects in the form of inclusions could be judged by the assessment of radiographs of samples containing tungsten wires. On film radiographs, 5 mm diameter wires could be clearly seen, whereas on paper radiographs the thinnest detectable wire was 20  $\mu$ m diameter.

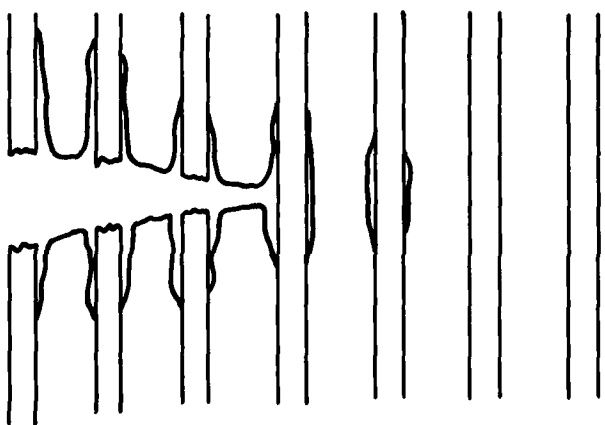
From the investigations performed, Domanus and Lilholt drew the following conclusions.

1. Low voltage radiography with soft x-rays is particularly suitable for the non-destructive examination of carbon fiber reinforced composites.
2. For thin sections of such composites very low voltages are required (10-17 kV) and it is essential to use a beryllium window x-ray tube with a focus as small as possible.
3. Use of fine-grain x-ray films insure good defect detectability. The low speed of these films can be compensated by using relatively high voltages to obtain reasonable exposure times.
4. Use of high speed film, or even radiographic paper with fluorescent intensifying screens, can be recommended only if no high radiographic quality is required.
5. Dimensions can be read from radiographs with a relatively high accuracy if the boundaries are well defined such as at metallic inclusions.
6. It can be expected that natural defects in the form of voids can be detected if they are larger than 0.1 mm.
7. Inclusions in the form of metallic material can be easily detected even if they are so small as a 5-mm tungsten wire.

Fatigue mechanisms and characterization of defects in fiber reinforced composites has recently been treated by Sturgeon (Ref. 8). The author points out that failure types vary quite considerably from one laminate construction to another. There are differences in the fracture process depending on whether the material has a strong or weak fiber/matrix interfacial bond. When the bond is good, cracks can propagate with ease from one fiber to the next, breaking each in turn, and giving a sudden brittle fracture as shown in Figure 5a. When the interface is poor, debonding can occur ahead of a crack so that it may deflect along the fibers instead of continuing to break them, as shown in Figure 5b. Debonding absorbs more energy than simple fracture, thus helping to improve toughness.



(a) Brittle fracture caused by a strong interface



(b) Crack blunting by debonding at a weak interface

**FIGURE 5. THE TWO PRINCIPAL TYPES OF DAMAGE IN FIBROUS COMPOSITES (From Ref. 8, Reproduced by permission of British Crown Copyright)**

In the general case in which load is applied at an arbitrary angle to the fibers the dominant failure modes become shear along the fibers or transverse tension between them. In most cases, failure will be a combination of both these modes, and while they are seldom present in well-designed applications of unidirectional material, they are common in multidirectional composites where fibers are aligned at various angles to resist multidirectional loading and shear stresses.

In describing fatigue damage in a composite, a good example to use is a specimen containing a hole. In isotropic materials, one single or two diametrically opposed cracks grow out from the hole. On the other hand, in composites, cracks usually run from the hole along the fibers in each ply as illustrated in Figure 6. In

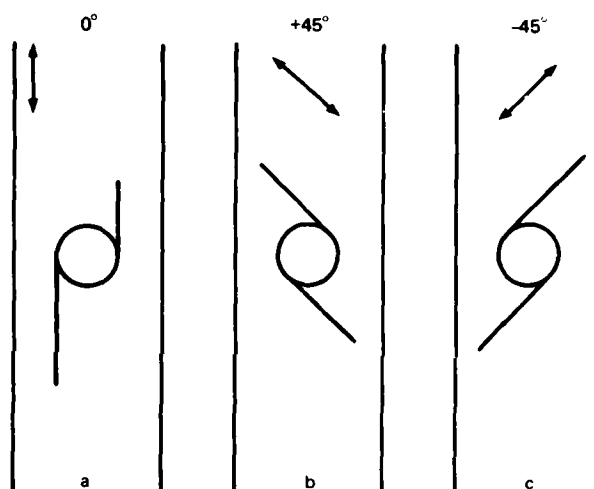


**FIGURE 6. CRACKING IN THE PLYS OF A 0°-45° LAMINATE WITH LOAD APPLIED IN THE 0° DIRECTION (From Ref. 8, Reproduced by permission of British Crown Copyright)**

randomly oriented fibrous composites, the gross damage may resemble cracking of isotropic materials. However, examination on a microscale will show cracks running back along the fibers and an extensive damage zone around the gross crack which has little in common with damage in metals.

This type of fatigue damage is difficult to detect nondestructively using radiography since unenhanced radiographs of many composite materials show only gross differences in the depth of material intercepting the beam, and furthermore, the contrast is often poor. Therefore, they only reveal large splits and give no indication of delamination. However, a radio-

opaque liquid can be used to fill the cracks and delaminations, providing a much clearer picture of fatigue damage. Using this method, it has been shown that matrix crazing and composite cracking occur before delamination around a notch, and the load redistribution resulting from the cracking reduces the stress concentrating effect of a hole in multi-ply material, hence increasing the strength of the material (Ref. 9). This procedure will be discussed in more detail in Section III.A.3.

The feasibility of using radiographic techniques for measuring the resin content in graphite fiber reinforced epoxy composites was investigated by Martin (Ref. 10). The use of both low energy x-rays and thermal neutrons was considered. Specimens were graphite fiber (Thornel 300) reinforced epoxy resin (Narmco 5208) composites fabricated from prepregged tape. Test specimens of different resin contents were fabricated. For purposes of NDE, the basic parameter of interest is the absorption of x-rays and neutrons by the graphite fibers relative to the epoxy resin which is a hydrocarbon.

Computations of mass absorption coefficients for both neutrons and x-rays are shown in Table V. These results show that for thermal neutrons, the mass absorption coefficient for hydrogen is more than two orders of magnitude larger than that for graphite fibers. Consequently, the resin will be much more ab-

sorbing of thermal neutrons than will the graphite fibers, thus providing a basis for considering use of thermal neutrons for measuring the composite resin content. For x-rays, the difference between hydrogen and graphite is not so great. For increasing x-ray energy the differences among the constituent elemental mass absorption coefficients decrease, thus decreasing the ability to distinguish between graphite fibers and resin by means of different radiograph absorption. The mass absorption coefficients were calculated as a function of resin content for low energy x-rays and neutrons, with the results presented in Table VI. These results show that a one percent change in resin content corresponds to a 2.6% change in the neutron mass absorption coefficient, whereas the equivalent change for x-rays is only 0.7%.

Based on his mass absorption coefficient calculations, which were supported by experimental measurements, Martin concluded that the use of x-rays for measuring composite resin content was not feasible. This is because of insufficient sensitivity for detecting small changes in composite density and mass absorption coefficient due to variations in resin content. Changes in the neutron mass absorption coefficient due to changes in the resin content are significantly larger than the corresponding situation for x-rays. However, it was concluded, based upon experimental measurements, that the neutron film technique is not sensitive enough for practical measurement of resin content. It was suggested,

TABLE V  
THERMAL NEUTRON AND X-RAY ELEMENTAL MASS ABSORPTION COEFFICIENTS (Ref. 10)

Element	Thermal Neutron ( $\lambda = 1.08 \text{ \AA}$ )	Mass Absorption Coefficients ( $\text{cm}^2/\text{g}$ )				
		10 keV	15 keV	X Ray 20 keV	50 keV	100 keV
hydrogen	48.5	0.385	0.376	0.369	0.335	0.294
carbon	0.26	2.16	0.721	0.387	0.179	0.149
nitrogen	0.48	3.57	1.09	0.541	0.187	0.150
oxygen	0.15	5.57	1.62	0.754	0.199	0.152
sulfur	0.029	50.3	15.2	6.42	0.527	0.189

TABLE VI  
CALCULATED X-RAY AND THERMAL NEUTRON MASS  
ABSORPTION COEFFICIENTS VERSUS COMPOSITE RESIN CONTENT<sup>(a)</sup> (Ref. 10)

Resin Content (Weight Percent)	Mass Absorption Coefficient ( $\text{cm}^2/\text{g}$ )			
	10 keV	X-ray 15 keV	20 keV	Neutron
25.0	2.72	0.721	0.457	1.07
26.0	2.73	0.714	0.459	1.10
27.0	2.76	0.703	0.462	1.13
28.0	2.78	0.694	0.465	1.16
29.0	2.81	0.687	0.468	1.19
30.0	2.83	0.678	0.471	1.23

(a) Graphite fibers and ERL 0510 epoxy resin (Ciba Epopal hardener)

that since neutron gaging techniques are more accurate than film techniques for hydrocarbons (Ref. 11) it may be possible to detect changes in resin content of  $\pm 1\%$ . However, further experimental work is necessary to determine the practicality of using neutron gaging for measuring composite resin content.

### 3. Use of Opaque Additives

The conventional x-ray technique is not suitable for the detection of delaminations in graphite epoxy composites due to the fact that carbon has a low attenuation coefficient for x-rays. Small differences in attenuation caused by planar delaminations and voids are indistinguishable on x-ray records. The most effective means of detecting damage consisting of cracks and delaminations in graphite epoxy composites is by enhancing the x-ray method with tetrabromoethane (TBE) as described by Chang, et al (Ref. 12). TBE is an x-ray

opaque fluid which penetrates into the delamination and matrix cracks and enhances the radiographic image of the damage. In the investigations reported in Reference 12, center slit specimens were fabricated from Modmor II/Narmco graphite/epoxy laminates with orientations of  $[0/\pm 45]_{2S}$ ,  $[0/\pm 45/90]_{2S}$ , and  $[\pm 45]_{3S}$ . These laminates were chosen to exhibit fiber failure in linear and nonlinear matrix failures.

Using TBE enhanced radiography, the authors were able to monitor the damage zone growth in the composite specimens at increasing load levels in real-time. A common feature found for three laminate configurations was a nonlinear damage growth rate under ramp loading. Typical results are shown in Figure 7. The slow growth rate in the low stress region was separated from the accelerated growth rate in the high stress region by a characteristic stress level. The failure mechanism near this characteristic stress level was found to

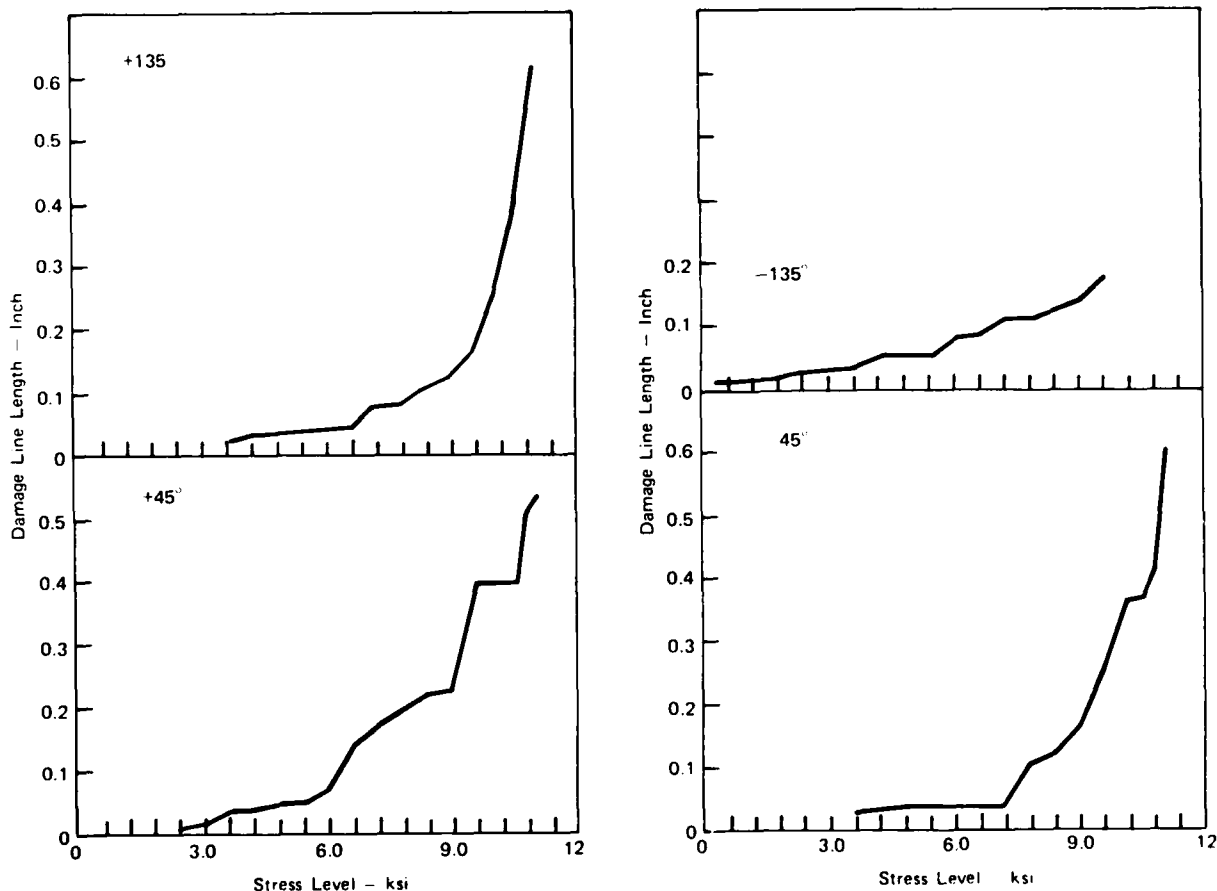


FIGURE 7. DAMAGE LINE GROWTH FOR A  $[\pm 45]_{3S}$  SPECIMEN UNDER RAMP LOADING (From Ref. 12, Reproduced by permission of American Society for Testing & Materials, 1916 Race Street, Philadelphia, PA 19103)

cause small damage growth. The existence of short damage lines prior to load application did not affect the history of damage growth appreciably. At high stress levels in the cyclic tests, the majority of damage growth occurred in the earlier cycles.

In further studies of composite failure mechanisms using TBE enhanced radiography, Chang, et al, investigated the actual stress redistribution in composite laminates and addressed the question of whether matrix failures precede delamination between plies (Ref. 9). For graphite/epoxy specimens it was found that under constant amplitude cyclic loading, specimens failed at a stress level 30 percent higher than the ultimate stress level of similar specimens under tensile ramp loading. By comparing the actual damages observable in the x-ray radiographs at different stress levels, it was found that the main reason the specimen under cyclic loading could withstand higher stress was the fact that it allowed sufficient time for the load to be redistributed as the damage propagated. With respect to whether delaminations or matrix crazing occurs first, it was found from virtually every series of radiographs that delaminations always originated from damage lines caused by matrix crazing. After delamination started, the failure process accelerated until total failure occurred.

Chang, et al (Ref. 9) indicate that TBE enhanced radiographic techniques can provide information on the applicability of linear fracture mechanics to laminate composites. An example of this is shown in Figure 8, which shows a plot of the summation of measured crack lengths of  $\pm 45^\circ$  cracks extending from the notched tips in a ramp-loaded specimen. The linear correlation of crack length with load squared suggests a possible adaptation of a linear fracture mechanics model with total crack length proportional to opening mode stress intensity squared, or strain energy release rate.

In another investigation, Bailey, et al (Ref. 13) report using TBE enhanced radiography to detect and evaluate impact damage in graphite/epoxy composites. Specimens were constructed of 16 plies of pre-impregnated Type HMS 3501-6 amine-cured epoxy resin reinforced with unidirectional graphite fibers. The graphite fibers were the continuous type surface treated to increase the composite shear and transverse tensile strength. The specimens were fabricated in a balanced "cross ply" configuration, i.e., the plies were stacked in a  $+45^\circ$ ,  $-45^\circ$ ,  $0^\circ$ ,  $0^\circ$  . . . orientation with the longitudinal axis of the specimen. Impact damage was imparted to the specimen by dropping a 0.906-kg (2-lb) weight from specified heights to achieve a range of im-

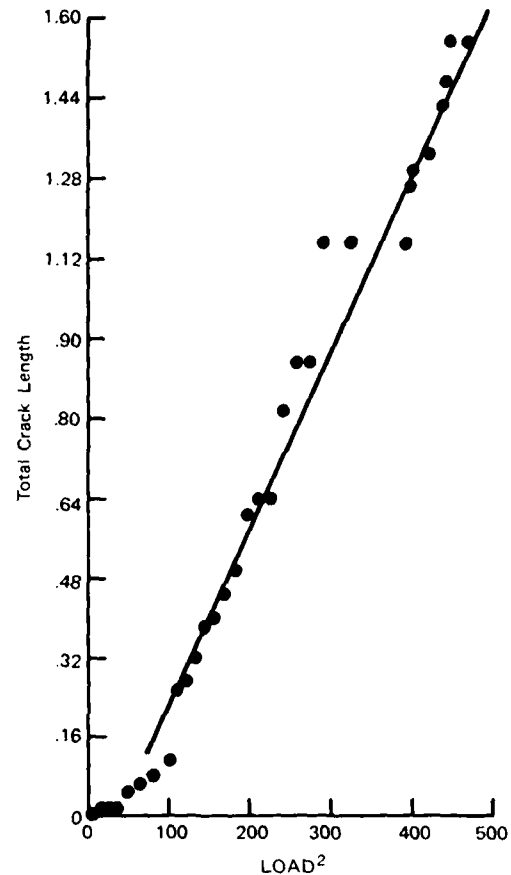


FIGURE 8. SUMMATION OF  $\pm 45^\circ$  CRACK LENGTHS FROM NOTCH VS LOAD SQUARED FOR  $[\pm 45]_s$  UNDER RAMP LOADING (From Ref. 9. Reproduced by permission of Technomic Publishing Co., Inc., Westport, CT 06880)

pact damage levels from 0.0575 kg-m (5 in.-pounds) to 0.575 kg-m (50 in.-pounds). The weight impacted a 16.9-mm (0.625-in.) diameter round-end rod at rest on the surface of the specimen.

TBE was applied to the impact damaged areas on the surfaces of the specimen with a syringe just prior to x-ray exposure. The effectiveness of this method depends upon the ability of the TBE to penetrate the damaged area. The TBE enhanced x-ray radiographs produced images which were indicative of both the size of the damage and the extent of fiber fracture with one restriction, i.e., the flaws had to be connected to the surface. The TBE technique provided no indication of delaminations which were not surface connected.

According to Bailey, et al, it appears that the TBE enhanced technique can be very useful for enhancing the contrast of defects such as voids or cracks associated with fatigue damage or impact damage. But, thus far, the technique remains essentially confined to the laboratory.

Another radiographically opaque technique has recently been described in the literature by R. L. Crane, et al (Ref. 14). The technique described permits the radiographic determination of both the distribution and integrity of fibers on a tape-by-tape level within a component. The technique consists of adding a boron fiber to the edges of each composite tape during the layup process. The boron fiber is first coated with a dilute solution of the epoxy matrix and methylethylketone, and then dusted with a powder fluorescent dye to enhance its visibility. The process is shown schematically in Figure 9. The coated fiber appears as a bright

fiber washing and waviness, and ply overlap or underlap.

One of the major field inspection problems for composite structures is mapping the extent of foreign object damage. While the area of damage may be determined with some difficulty using visual techniques, determining the depth of the damage is almost impossible. Since boron filament is available in a wide variety of strength levels, it may be possible to use fiber with a failure rate approximately equal to that of the composite reinforcing fiber. Thus, an estimate of the depth of internal fiber breakage could be obtained by simply noting the number of boron fibers broken at a specific location. The feasibility of this technique was demonstrated by Crane, et al (Ref. 14).

Three-point bending tests showed that the addition of boron fiber did not affect the mechanical properties of the composite. A limitation, however, in the use of boron marker fibers is in application to areas where the radius of curvature of the part is greater than approximately 0.635 cm (0.25 in.). This value depends on the strength of the boron fiber and the lower limit of curvature and could be calculated with simple beam flexure formulas found in most engineering handbooks.

#### 4. Computer Assisted Radiography

Computer enhanced real-time radiography promises to afford a quick and convenient inspection tool. In a manufacturing situation, there would be little delay between the discovery of anomalies and the opportunity to take corrective action in a part that is still in production. Moreover, with automatic processing of the radiographic image, the operator is relieved of the need to interact with all but the essential details of the image. This is made possible by the fact that image processing routines can extract and emphasize only the essential features and make it easier and less fatiguing for the operator to concentrate on key factors.

An example of a computer based radiography facility for composites is the system developed at NASA Lewis Research Center (Ref. 15). This system uses a computer to provide enhanced images in near real-time. The test facility is composed of discreet modules as shown schematically in Figure 10. The various modules can be grouped into three major components: an image acquisition system, an image conditioning system, and an image processing system. The x-ray signal is sensed by a solid-state electronically excited thin film screen which senses an x-ray field on one face and displays the visual image on the opposite face. The visual

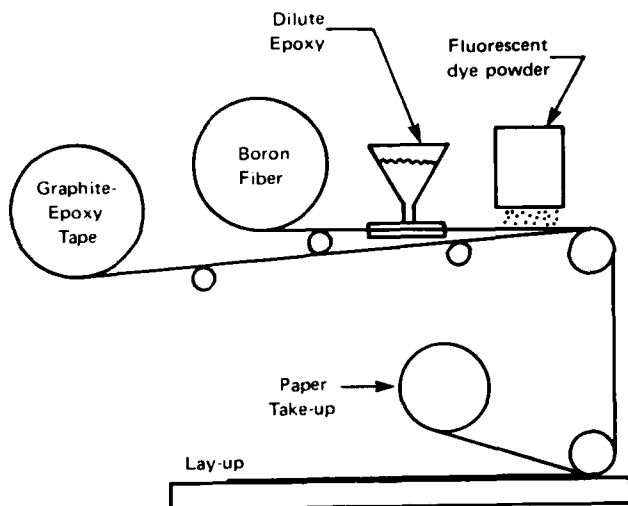


**FIGURE 9. SCHEMATIC REPRESENTATION OF THE ADDITION OF BORON FIBER TO THE EDGES OF COMPOSITE TAPE BY AN AUTOMATIC TAPE-LAYING MACHINE (From Ref. 14, Reproduced by permission of The American Society for Nondestructive Testing)**

yellow line against a black background of the graphite tape. It was suggested by the authors that the distinct color difference could permit automated inspection of the tape position with simple optical readers, thus eliminating a tedious expensive inspection with its possibility of human error. Once the preform is consolidated, the tungsten core of the boron filament permits x-ray radiographic examination for ply orientation and sequencing.

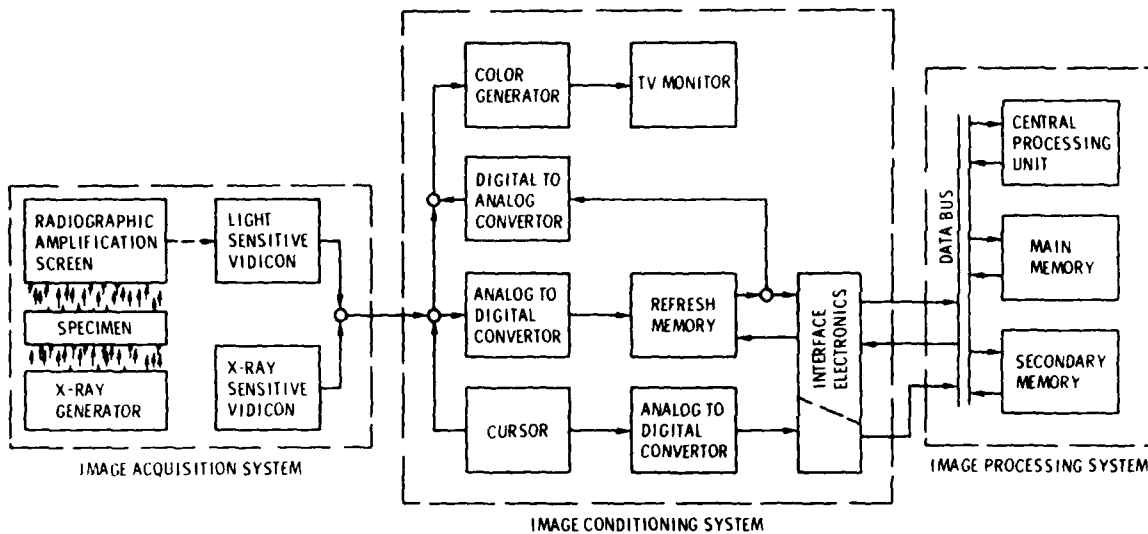


FIGURE 10. SCHEMATIC OF RADIOGRAPHIC INSPECTION FACILITY (From Ref. 15, Reproduced from Proceedings of Second Conf. on Automated Inspection and Product Control)

image is digitized and stored on a high-speed magnetic disc refresh memory. The memory may be modified by the minicomputer contained in the image processing system, and the results displayed on a monitor.

Once digitized, the image appears to the computer as an ordered array of approximately 250,000 numbers, ranging in magnitude from 0 to 255. Any desired mathematical operation may be performed on these numbers. Two types of processing have been found to be most helpful. The first is transforming the numbers representing subject brightness to increase the contrast over a given area of the image. The second is modifying the numbers defining the edges of the object to increase the edge sharpness of a given region of the image.

The computer assisted radiographic technique was applied to the inspection of a fan frame ring for an experimental aircraft gas turbine. The ring was fabricated from 10 plies of carbon fiber reinforced epoxy composite material. Each ply was approximately 2.5 mm thick laid up from pre-impregnated fibers at angles of 0, 45, and 90 degrees. Damage was incurred in the specimen during a previous test.

Results of a standard ultrasonic C-scan and conventional radiography using an opaque photosensitive paper are shown in Figure 11. The ultrasonic C-scan produced little useful information because of extensive delamination in the damaged zone. However, it indi-

cates the existence of damage and shows its location and approximate extent. The radiograph was much more informative. The irregularities known to exist in the test object were evident. Fine details were easily resolved, and there was little extraneous noise in the image. However, these advantages occurred at the cost of an interruption in the continuity of the manufacturing process, that is, a delay for photographic image development was required.

Results of radiographic image processing are shown in Figure 12. The original direct video image, Figure 12a, is very good. In a manufacturing situation, an experienced operator would probably need no further processing to make a judgment on the test piece. A horizontal bright band near the base of the upright indicates that the mechanical damage is extensive. The vertical lines at the lower part of the fillet show the junction or separation of two differently oriented plies. Further processing confirms the nature of the mechanical damage. Figure 12b shows a contrast expansion, and Figure 12c shows a high pass filtered image. The latter shows that the damage is quite extensive, and clearly outlines what appears to be a large through-crack.

Magnifying the fillet region by moving the camera in closer produces the result shown in Figure 13. Although the vertical lines at the root of the fillet are apparent in the unenhanced image, shown in Figure 13a, they are not clear and sharp. A contrast expansion is shown in Figure 13b, and a high pass filtered image in



a. ULTRASOUND SCAN OF DAMAGED AREA



b. CONVENTIONAL RADIOGRAPH OF DAMAGED AREA

*FIGURE 11. IMAGES OF DAMAGED ZONE IN COMPOSITE FAN FRAME RING (From Ref. 15, Reproduced from Proceedings of Second Conference on Automated Inspection and Product Control)*



(a) UNENHANCED IMAGE



(b) BRIGHTNESS EXPANDED IMAGE



(c) HIGH-PASS FILTERED IMAGE

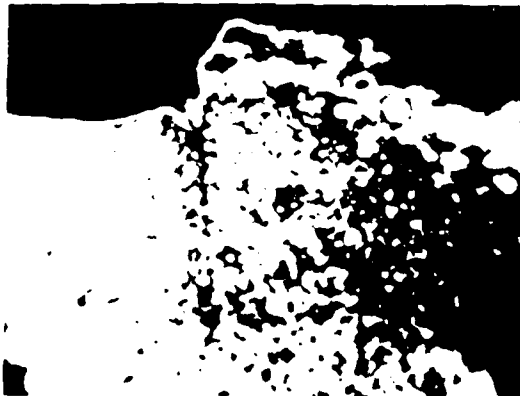
FIGURE 12. ELECTRONICALLY PROCESSED RADIOGRAPHIC IMAGES (From Ref. 15, Reproduced from Proceedings of Second Conf. on Automated Inspection and Product Control)



(a) UNENHANCED IMAGE



(b) BRIGHTNESS EXPANDED IMAGE



(c) HIGH-PASS FILTERED IMAGE

*FIGURE 13. ELECTRONIC IMAGES OF SECTION OF DAMAGED AREA (From Ref. 15, Reproduced from Proceedings of Second Conf. on Automated Inspection and Product Control)*

13c. In the latter image, the lines stand out quite clearly. Furthermore, a subtle gradation in density, not readily apparent in the paper radiograph, becomes prominently revealed.

These results illustrate that computer processing can extract and display key properties of a radiographic image. Two types of irregularities were evident in the multiple-ply carbon fiber reinforced composite structural element examined. One was major mechanical damage producing broken fibers and separated plies. The other was the junction of differently oriented plies. For these types of irregularities in this composite, computer assisted radiographic inspection was clearly superior to either ultrasonic C-scan or film based radiography.

## 5. Commercial Aircraft Inspection

Radiographic inspection of graphite/epoxy composite DC10 structures has recently been discussed by Hagemmaier and Fassbender (Ref. 16). The state-of-the-art for nondestructive evaluation of fabricated composite structures for commercial aircraft, as well as specific results, are discussed in this paper. The authors point out that x-ray radiography is especially useful for detecting porosity, foreign objects, and cracks in laminates. It is also used to inspect composite honeycomb assemblies for core defects, foaming-adhesive voids, and internal structure fit-up. Since graphite/epoxy composite structures are relatively low absorbers of x-ray radiation, low kv machines having beryllium windows are used to make radiographs of these materials.

There are times when edge delaminations are obvious in laminated structures. Radiography may be used to determine the extent of the delamination by brushing an x-ray opaque solution on the edge of the laminate and letting it seep into the defect. The primary penetrant used for this application is 1, 4, Diiodobutane (99%). Although S-Tetrabromoethane (TBE) is more x-ray opaque than Diiodobutane, the authors indicate that TBE is not used since chemical catalogs list it as a severe poison and potent mutagen, whereas Diiodobutane is classified only as an irritant.

DC10 structures examined by NDE include floor beams and struts, vertical stabilizer trailing edge panel, center line gear drag-brace tube, upper aft rudder, aileron access panel, nose landing gear aft door, and fan cowl door.

An extensive assessment of the state-of-the-art of inservice inspection methods for graphite/epoxy

composite structures on commercial transport aircraft has recently been published by Phelps (Ref. 17). In this work, a survey was conducted to determine current inservice inspection practices for all types of aircraft structure, and specifically for advanced composite structures. The survey consisted of written questionnaires to commercial airlines, visits to airlines, aircraft manufacturers, and government agencies, and a literature search. Existing inspection methods and equipment for inservice inspection of aircraft structures are documented in the report. Included as appendices are a reference to inservice inspection baseline and preliminary inservice inspection program for advanced composite structures on commercial transport. Based on the data obtained in the survey, a plan was prepared for development and approval of inservice inspection methods for graphite/epoxy composite aircraft structures. This plan has been presented to NASA-Lewis Research Center for approval.

Results of the survey indicated that none of the airlines had sufficient experience in the use of graphite/epoxy composites to provide comment. Their main concerns included inspection time required, access to structure for inspection purposes, inspections requiring use of nonportable complex inspection instruments, moisture in delamination defects, and lack of appropriate reference standards. Radiography probably defines the limit in inspection cost and time required for current airline inspection practices. Aircraft manufacturers and the military utilize radiography of several components to detect water entrapped in honeycombs and honeycomb core separation from foam adhesive and metal sub-structure.

## B. Ultrasonics

### 1. Methodology

Ultrasonic testing involves the propagation of high frequency sound (between 20 kHz and several MHz) through a material. Characteristics of the transmitted or reflected sound are measured to determine material properties or defects. Some of the advantages of ultrasonics are:

1. Its ability to penetrate to substantial depths in many important materials;
2. Its ability to test from one surface only;
3. Its sensitivity in the detection of minute flaws;

4. Its comparative accuracy to determine flaw size and depth;
5. Its electronic operation which enables rapid and substantially automated inspection.

The chief disadvantages are:

1. Its manual use requires technicians of considerable ability, training, experience, and motivation;
2. It is intrinsically a small area coverage method. Large area coverage requires complex mechanical scanning or the use of numerous transducers in an array;
3. Its use, in general, requires a good essentially direct mechanical coupling to the article to be tested, a requirement which is often difficult to meet in practice.

To provide the basis for better understanding the methodology of ultrasonic NDE, a brief discussion of elementary principles is presented in the following paragraphs.

Sound waves propagate to some extent in any material that is elastic; that is, if a particle of the material is displaced from its equilibrium position by any applied stresses, internal forces tend to restore the system to its original equilibrium. Elastic waves are categorized according to the mode of particle displacement involved. The basic types of waves which propagate in the bulk of a material are longitudinal waves in which the displaced particles vibrate back and forth along a direction parallel to the direction of the wave propagation, as shown in Figure 14a, and transverse waves, in

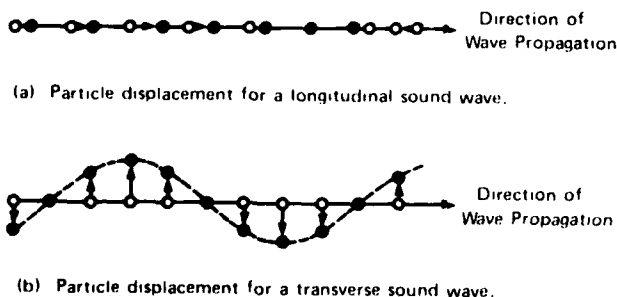
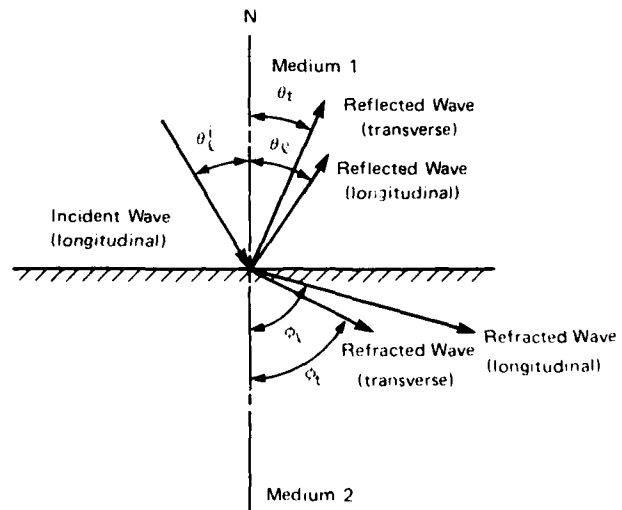


FIGURE 14. PARTICLE DISPLACEMENTS IN ELASTIC WAVES (From Ref. 6)

which the displaced particles vibrate in a direction perpendicular to that of wave propagation, as shown in Figure 14b. Longitudinal waves are also called compression waves; transverse waves are sometimes called shear waves.

When an ultrasonic wave propagating in a medium encounters an interface with another medium, reflection, refraction, and mode conversion may occur. For the case of normal incidence, both reflection and transmission occur, with the amplitudes of the reflected and transmitted waves determined by the ratio of the characteristic acoustic impedances of the two media. For angles of incidence other than zero, refraction also takes place and mode conversion occurs, whether the incident wave is longitudinal or transverse. This is illustrated schematically in Figure 15. The angles of reflec-



Both longitudinal and transverse waves are reflected and refracted (mode conversion).

FIGURE 15. REFRACTION AND MODE CONVERSION AT AN INTERFACE (From Ref. 6)

tion and refraction satisfy a generalized form of Snell's law:

$$\frac{\sin \theta_i}{v_l^1} = \frac{\sin \theta_r}{v_t^1} = \frac{\sin \theta_t}{v_l^2} = \frac{\sin \phi}{v_t^2} = \frac{\sin \phi_t}{v_l^2}$$

An important practical application of mode conversion in ultrasonic NDE is the conversion of longitudinal waves into transverse waves for ultrasonic inspection purposes. This occurs by adjusting the angle of incidence of the longitudinal wave so that the refracted longitudinal wave is effectively eliminated from medium 2, and the angle of refraction of the transmitted shear wave is equal to 90°. In this case, no energy enters the

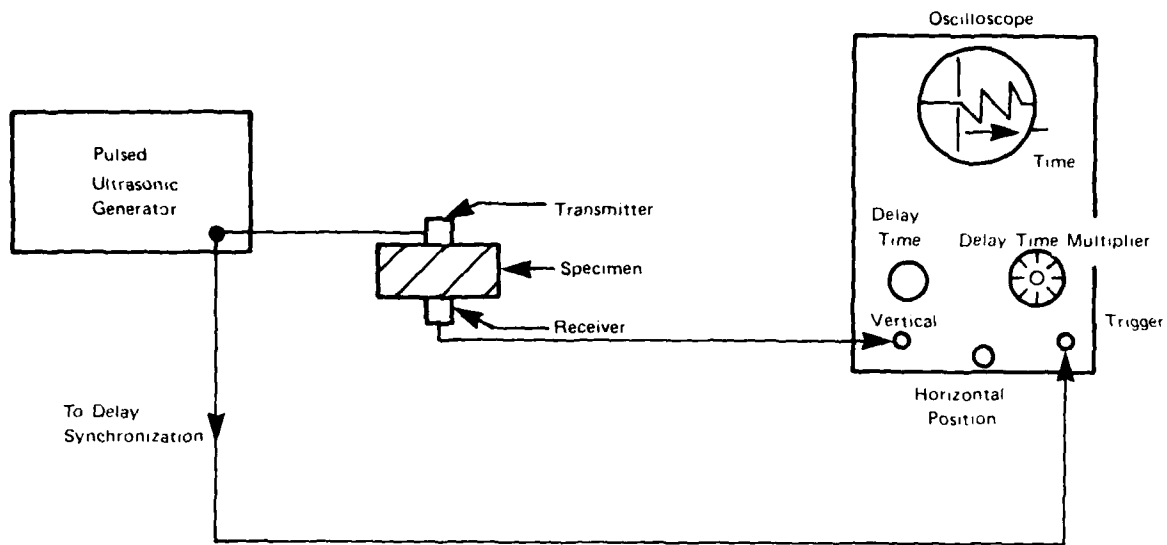


FIGURE 16. BLOCK DIAGRAM OF ULTRASONIC VELOCITY MEASURING APPARATUS (From Ref. 18)

bulk of medium 2. Instead, a complex mode wave (partially longitudinal, partially transverse) propagates along the interface between the two media. This surface wave (called a Rayleigh wave) is very useful for ultrasonic inspection of such surface flaws as cracks.

For the inspection of fiber reinforced composites, the three most common ultrasonic techniques utilized are measurement of ultrasonic velocity, ultrasonic attenuation, and pulse-echo ultrasonics.

Velocity measurements are accomplished by measuring the elapsed time required for an ultrasonic pulse to propagate through the specimen. An ultrasonic transmitting transducer is placed on one side of the specimen and a receiving transducer on the other, with alcohol generally used as a couplant between transducer and specimen. A short pulse of longitudinal mode sound is transmitted through the specimen and its propagation time determined by measuring the elapsed time between transmitted and received pulses on an oscilloscope display. The ultrasonic velocity can be calculated from the elapsed propagation time and the measured specimen length. Figure 16 is a diagram of an ultrasonic velocity measurement arrangement (Ref. 18).

Ultrasonic attenuation measurements are also accomplished by a through-transmission technique, as shown in Figure 17 (Ref. 19). Measurements may be made under immersion conditions to minimize coupling variations which would affect attenuation mea-

surements. An ultrasonic pulse is propagated from the transmitter through the specimen to the receiver. The signal from the receiver is directed through a variable attenuator and displayed on an oscilloscope. The variable attenuator is adjusted to make the signal amplitude from the test specimen the same as that previously obtained from a reference specimen. This value is the relative ultrasonic attenuation of the test specimen compared to a reference specimen.

Ultrasonic pulse-echo measurements are performed with a single transducer which acts alternately as a transmitter and a receiver. Couplant for fiber reinforced composites may be alcohol or an alcohol-water mixture, although for porous surfaces, Teflon tape or other surface sealer such as a strippable vinyl may first be applied to the surface, and couplant then applied to the tape. A short ultrasonic pulse is introduced into the specimen and travels through the material. If a defect with a different ultrasonic impedance, such as a void or a crack is encountered, a portion of the ultrasonic wave is reflected back to the transducer which now acts as a receiver. The reflected pulse is observed on an oscilloscope display, and its amplitude may be used to obtain information regarding the size of the defect. The transducer is usually moved to inspect the entire specimen.

Three types of scan mode presentation are commonly used in ultrasonic NDE. These are the A-scan, the B-scan, and the C-scan.

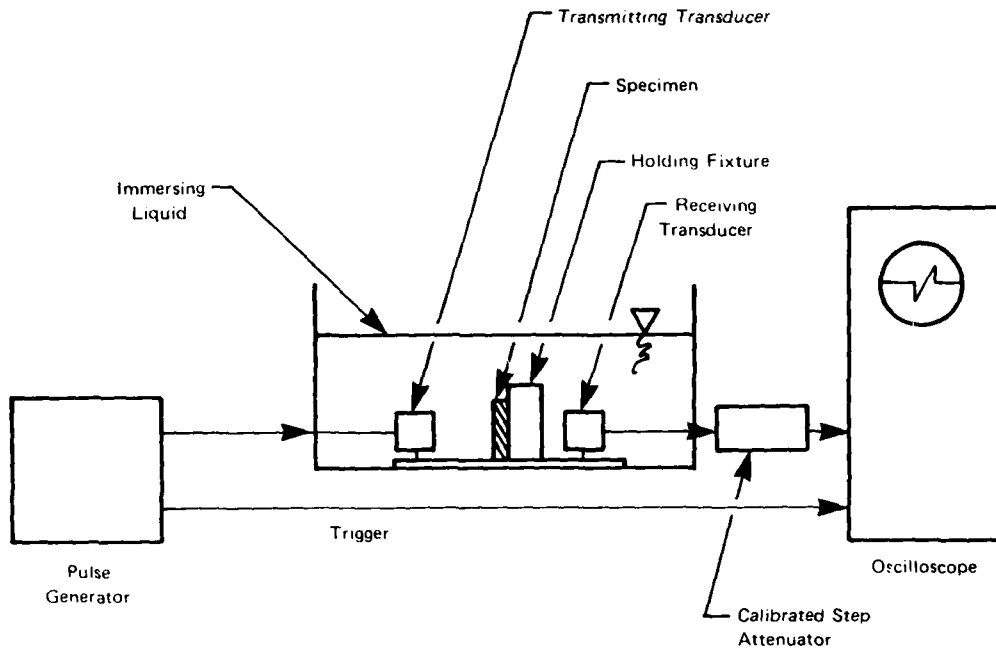


FIGURE 17. ULTRASONIC TRANSMISSION SETUP USING THE PULSED THROUGH-TRANSMISSION TECHNIQUE (From Ref. 19)

The A-scan presentation, shown schematically in Figure 18, simply provides for an oscilloscope display of;

1. the envelope of the initial voltage pulse applied to the transmitting transducer;
2. the envelope of the voltage pulses generated by the receiving transducer as reflections are received;
3. a timing trace (if available).

The ordinate of the oscilloscope trace is proportional to pulse amplitude, and the abscissa is proportional to elapsed time (which may be related to transmission time in the test medium). It is common practice to adjust the display so that the "main bang" is just off the oscilloscope presentation; the pulse from the front surface reflection appears at the start of the oscilloscope trace, and the pulse from the back surface reflection appears at the far right of the oscilloscope trace. Thus, the location of pulses resulting from echoes from a flaw with respect to the two surface-echo pulses enables the operator to gauge the depth of the flaw. The amplitude of the pulse representing an echo from a discontinuity cannot be simply related to the size or the severity of the

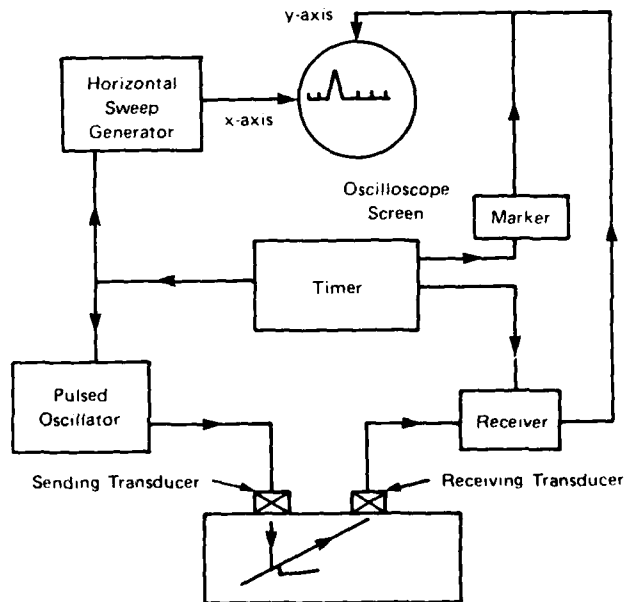


FIGURE 18. MAIN FEATURES OF A BASIC GENERAL-PURPOSE ULTRASONIC TEST UNIT IN THE A-SCAN MODE (From Ref. 6)

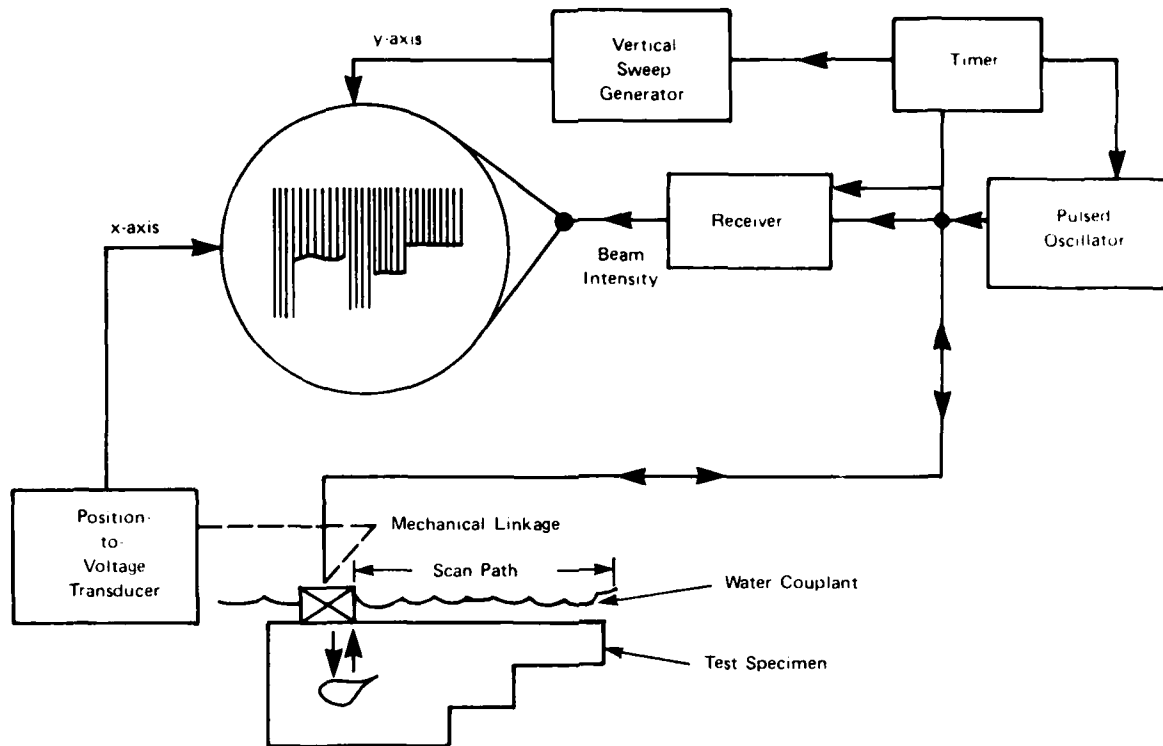


FIGURE 19. BASIC FEATURES OF B-SCAN SYSTEM WITH A PERSISTENT-PHOSPHOR CATHODE-RAY OSCILLOSCOPE DISPLAY (From Ref. 6)

flaw; only when there is sufficient auxiliary evidence as to the general nature of the flaw is this possible.

The B-scan presentation is illustrated in Figure 19. Here the internal vertical sweep (Y axis) of the oscilloscope spot is triggered by the timer. The beam is deflected horizontally (X axis) in synchronism with the usually linear scanning motion of a pulse echo transducer. The intensity of the oscilloscope spot is modulated in proportion to the amplitude of the received echo signal. If the resulting oscilloscope pattern is to be observed visually, the phosphor of the screen must be of the persistent type, and the scanning of the transducer must be repeated periodically to renew the image. The image itself represents a one-dimensional slice through the specimen with a profile of a discontinuity appearing as corresponding discontinuities in the oscilloscope screen pattern.

In practice, the B-scan method has serious deficiencies. Limits of phosphor persistence times restrict the scan range; the more persistent phosphors tend to produce a smeared image reducing resolution. Various alternatives to the cathode ray oscilloscope as a

means of displaying B-scan presentations have been tried without notable success. Consequently, the B-scan presentation is seldom used.

The C-scan presentation provides a plane view of a slice of the specimen at a selected depth below the surface. The essentials of this system are illustrated in Figure 20. Although a persistent phosphor oscilloscope could, in principle, be used for the C-scan presentation, in practice other means of recording the presentation are superior. Usually, some form of electromechanical recorder producing a permanent paper record is used. In the system illustrated in Figure 20, a permanent record is made with a helix-drum recorder. The rotation of the drum is electromechanically coupled with the transducer-scan-pattern mechanism. For a C-scan operation, the ultrasonic test unit must be equipped with an electronic gate that samples the received echo for a selected period, starting at a selected elapsed time after the initial transmitted pulse. The elapsed time selected is proportional to the distance from the depth to the top of the inspected slice of the specimen, and the length of time the gate is open is proportional to the thickness of the inspected slice. When used in conjunc-

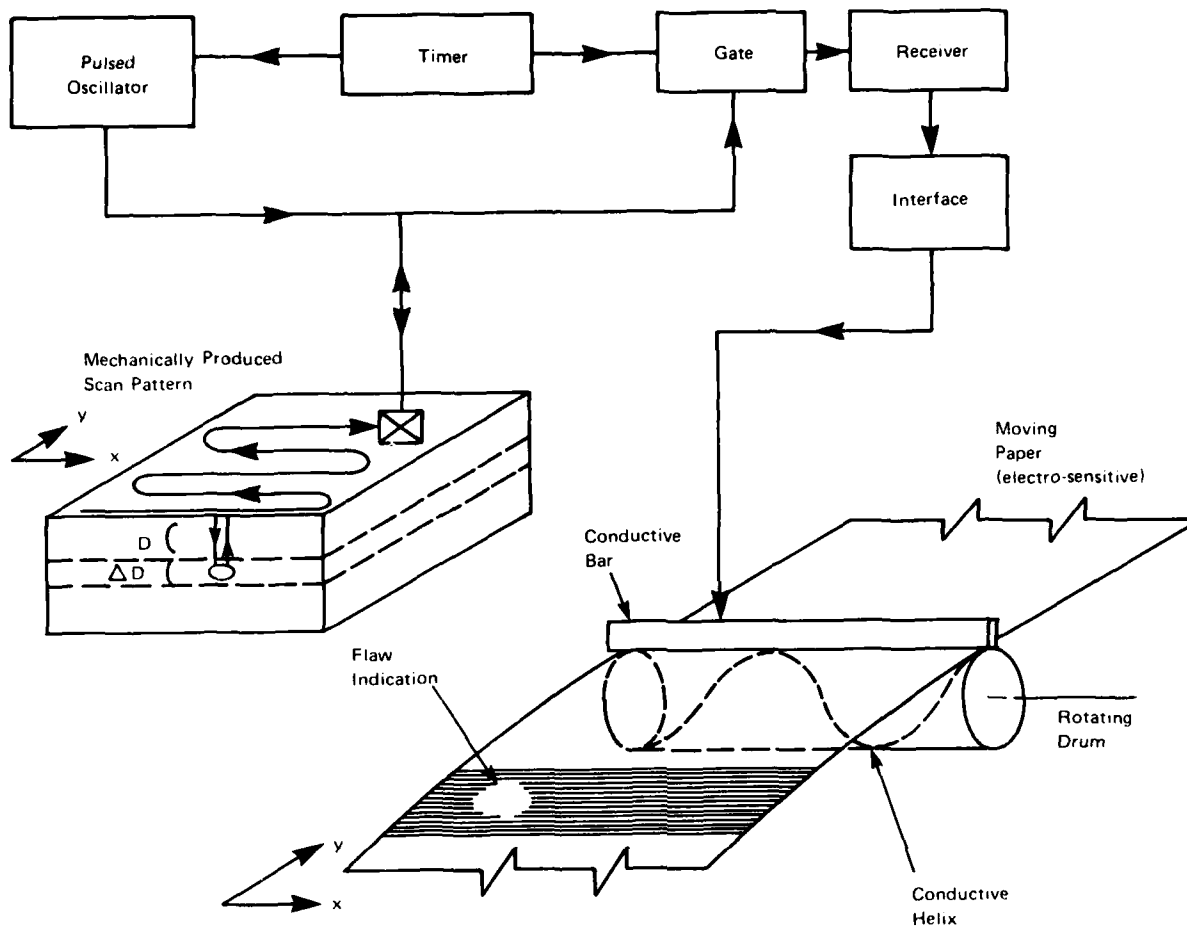


FIGURE 20. A PULSE-ECHO C-SCAN PRESENTATION SYSTEM (From Ref. 6)

tion with a large aperture focused transducer, the C-scan system is capable of generating a detailed record of well resolved discontinuities. The outstanding disadvantage of the C-scan presentation is that it produces a two-dimensional plane view of discontinuities within a given depth range, but does not provide information from other depths unless the material is scanned repeatedly at successively greater depths.

## 2. General Application to Composites

Ultrasonic inspection is the technique which has proved to be the most generally useful for carbon fiber reinforced plastic composites in the form of sheet material. The method is most suitable for detecting delaminations, inclusions, and surface scratches. The easiest way of assessing material quality is to scan the sheet and to measure the attenuation induced into an ultrasonic beam transmitted through it. Several approaches

are described by Stone (Ref. 20). Scanning can be accomplished by single transmission of the beam and the use of a pair of probes, as shown in Figure 21a. It is often convenient to use a single probe as both transmitter and receiver, and to let the ultrasonic beam return through the specimen, either by using a reflector plate (Figure 21b) or by examining the back surface echo (Figure 21c).

In interpreting ultrasonic inspection results, it is necessary to consider what causes the attenuation and what level of attenuation is acceptable. These factors have been discussed by Stone and Clarke in considerable detail (Ref. 21). The principal factors governing the level of attenuation are:

1. delaminations,
2. void content,
3. fiber volume fraction,
4. surface losses.

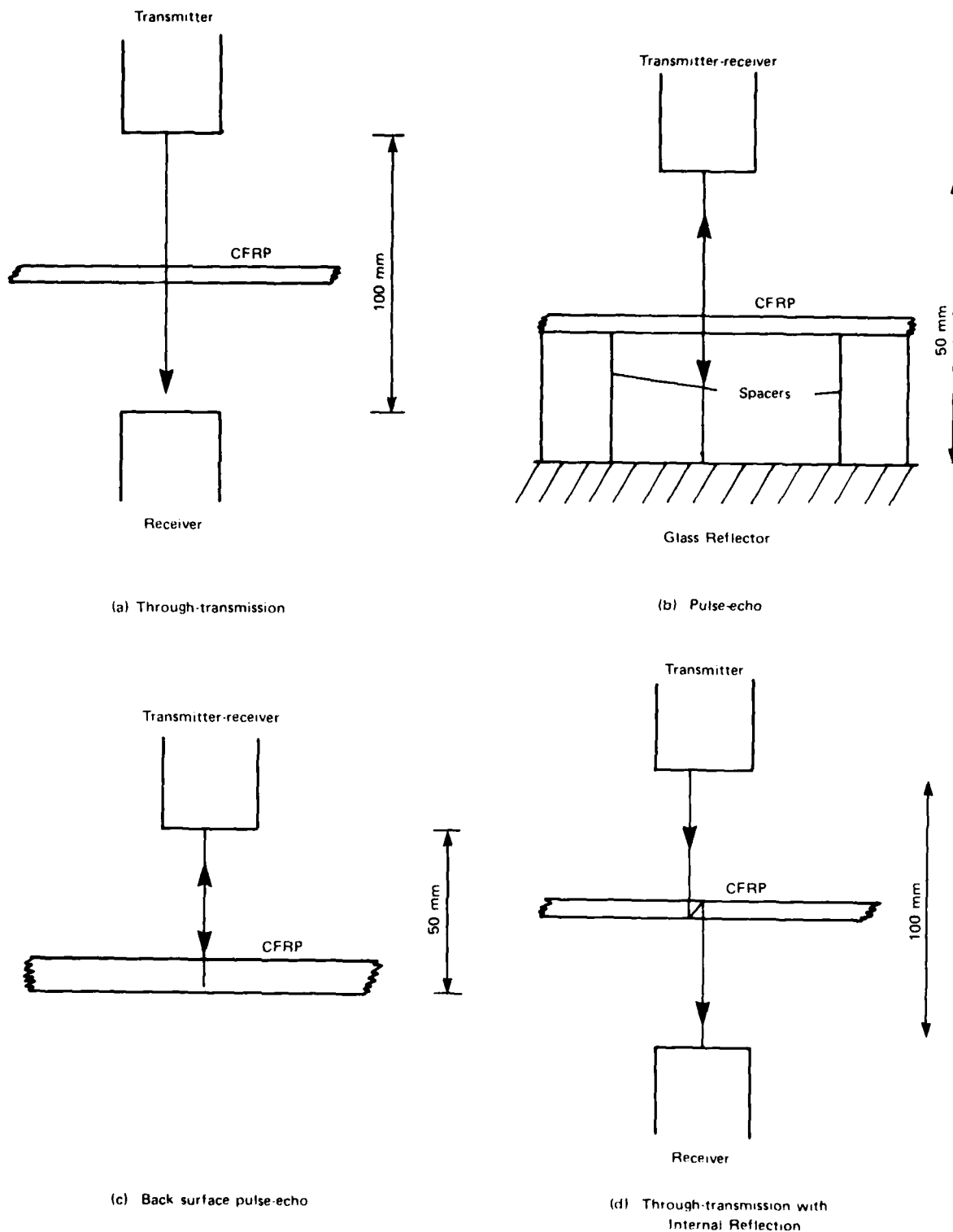


**FIGURE 21. ALTERNATIVE ULTRASONIC INSPECTION PROCEDURES (From Ref. 20, Reproduced by permission of The British Institute of Non-Destructive Testing, British Crown Copyright)**

Delaminations occur between individual plies and are thus aligned parallel to the surface of the laminate, and give a detectable back echo which may be displayed on an oscilloscope. In Reference 20, Stone shows how the use of high frequencies (25 MHz) and a weakly focused probe enables the through thickness depth of a delamination to be determined accurately. The size of delamination detectable depends on the area over which the ultrasonic beam integrates. While a focused beam will give the necessary resolution, it can cause problems in practice because small variations in probe-to-specimen distance can introduce unacceptable gradations in attenuation. A method to avoid this difficulty has been described by Jones and Stone (Ref. 22). The approach involves using a simple stop in front of a parallel probe. A standard 10-mm diameter plane probe with the center frequency of 7.5 MHz was found to integrate effectively over an area 6-mm in diameter; the addition of a 6-mm diameter stop reduced this area to about 2-mm diameter. Such a probe could detect a delamination 0.15-mm in diameter.

Translaminar cracks (i.e., cracks in one ply parallel to the fibers and normal to the plane of the sheet) can also be revealed on a C-scan by the use of high resolution probes. There is, however, a possibility of confusing crack indications with other defects which can occur in narrow bands aligned with the fibers (such as resin rich areas at a side butt joint between sheets of prepreg), and in cases of doubt, it is best to investigate the area further with a pair of conventional shear wave contact probes.

If there are no significant delaminations, then the attenuation suffered by an ultrasonic beam may be attributable either to surface losses or to internal losses caused by reflection and scattering mechanisms, usually at voids or internal damage. Stone (Ref. 20) indicates that adequate uniformity in terms of surface texture and surface profile is usually obtained on currently produced laminate material so that ultrasonic surface losses do not vary much from point to point. Also, although there are local changes in the fiber volume fraction, the quality of prepreg currently being produced results in very little variation in fiber volume fraction from point to point when integrated over the area interrogated by the ultrasonic beam. Thus, the primary questions faced are: What is the type and severity of void content present, and what effect does this have on the mechanical strength? A discussion of the nondestructive determination of void content by ultrasonics will be deferred until later in Section B.4.

In the case of complex composite structures, the interpretation of ultrasonic pulse-echo and through-

transmission results may be difficult. A supplementary approach utilizing ultrasonic spectroscopy has been described by Chang, et al (Ref. 23). The spectroscopic technique depends on the phenomenon of resonance interference of acoustical waves in materials. When the material thickness is an integral multiple of the half wavelength of the sound waves, destructive interference of a return echo by multiple reflections in the material produces anti-resonant dips in the frequency spectrum for the reflected signal. The period of the anti-resonant dips is related to the material thickness normal to the beam path. Delaminations or voids in a plane perpendicular to the direction of propagation of the sound waves may be observed through their characteristic anti-resonant frequencies. Correlations between anti-resonance frequencies of good specimens and specimens containing flaws lead to a determination of flaw size and location.

A block diagram of the experimental approach utilized by Chang, et al, is shown in Figure 22. The RF output of the Automation Industries UM771 reflectoscope is directed to a delay trigger circuit in a Tektronics R556 oscilloscope. A select portion of the RF output is displayed on a HP175A oscilloscope with a scanner plug-in. The horizontal drive of the scanner is stepped by the voltage generated by the D/A converter in the minicomputer in 256 equal intervals. The analog value of the RF waveform at each step is converted to digital form through an A/D converter channel and stored in the minicomputer memory. A Fourier transform is performed by the minicomputer providing output in the frequency domain.

The specimen investigated by the spectral analysis technique was a T-300/5208 graphite/epoxy composite plate 5.26 mm thick with  $[0, \pm 45]$  ply orientation. Three flat bottom holes were drilled from the back of the specimen with diameters of 6, 3, and 1.5 mm. The output characteristic of the transducer positioned over a flaw-free region was used as a reference function to compute a normalized frequency spectra. The normalized reflected frequency spectra for the transducer positioned over the 6, 3, and 1.5 mm diameter holes, as well as a spectrum from the flaw-free area, are shown in Figure 23. The order of anti-resonance frequency dips is shown plotted below each corresponding spectrum. The velocity of sound determined from the good area was used to compute the flaw depth in areas containing flat bottom holes from the slopes of these plots. The results are shown in Table VII.

Application of the spectral technique for detecting crack-like voids and delaminations was also in-

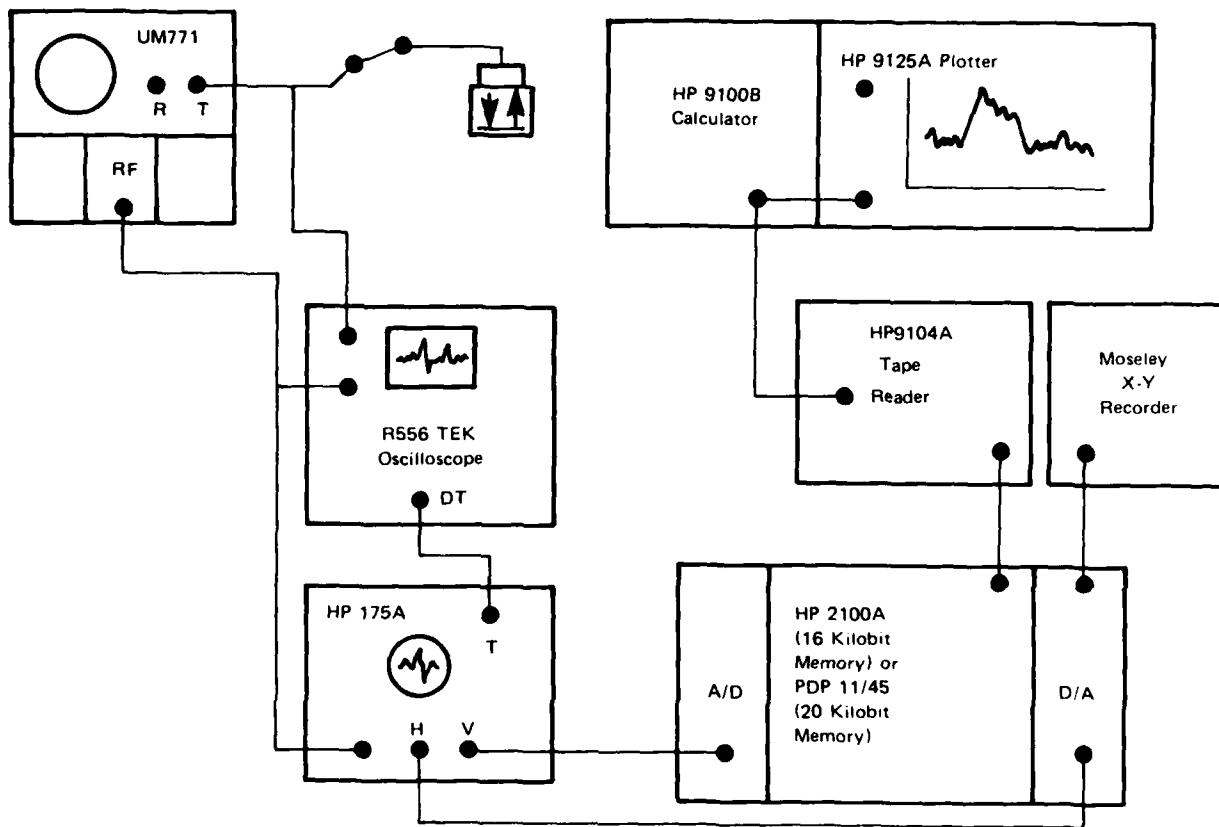


FIGURE 22. BLOCK DIAGRAM FOR SPECTRAL ANALYSIS OF ULTRASOUND FOR NDT (From Ref. 23, Reproduced by permission of IPC Science & Technology Press Ltd, England)

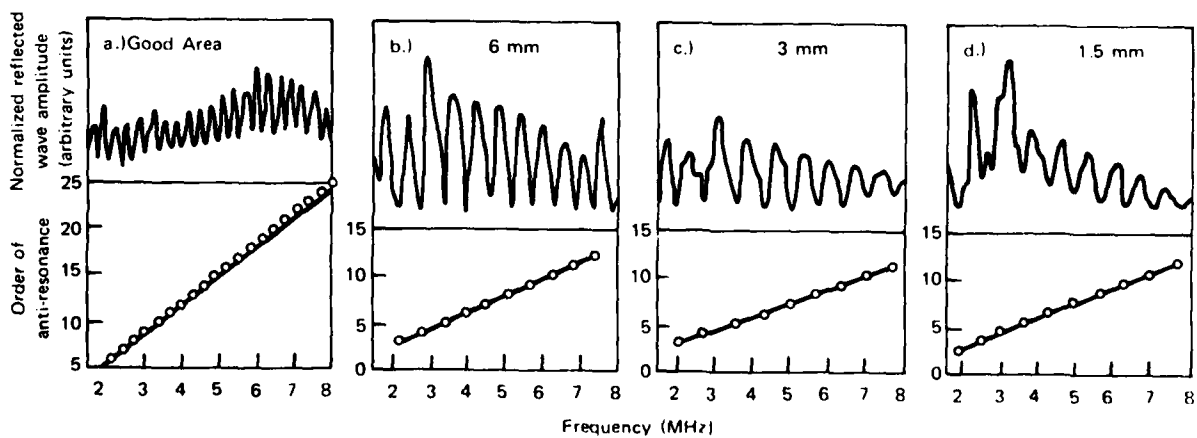


FIGURE 23. ULTRASONIC SPECTRA FROM FLAT-BOTTOM HOLES (b, c, d) AND A GOOD AREA (a) (From Ref. 23, Reproduced by permission of IPC Science & Technology Press Ltd, England)

TABLE VII  
RESULTS OF ULTRASONIC SPECTRAL ANALYSIS TECHNIQUE ON GRAPHITE-EPOXY  
COMPOSITE SPECIMEN WITH FLAT-BOTTOM HOLES (Ref. 23)

Hole Diameter (mm)	Thickness (mm)	Measured Frequency Period (MHz)	Standard Deviation (9%)	Calculated Specimen Thickness (mm)	Velocity of Sound (in km s <sup>-1</sup> )
0 (Sound area)	5.26	0.321	2	5.26	3.38
6	2.62	0.630	6	2.64	3.38
3	3.05	0.730	1	2.41	3.38
1.5	2.87	0.794	9	2.69	3.38

investigated. A graphite/epoxy specimen containing these types of defects was obtained. The existence of crack-like voids in delaminations was demonstrated by conventional ultrasonic through-transmission and enhanced x-ray radiography, as well as by dissecting the specimen and observing the cross-sectional surfaces of each section under a microscope. Spectral analysis results for certain areas of the specimen are shown in Figures 24 and 25. The curves show reflected wave ampli-

tude and the straight lines show order of resonance for the selected areas. Areas one and two were flaw-free. Areas three and five contained crack-like defects, while area four contained a large void about 5 mm × 20 mm. Comparison of the frequency spectra for the good areas and the areas containing flaws shows that the difference in characteristic spectra is sufficient to indicate the existence of flaws in this material.

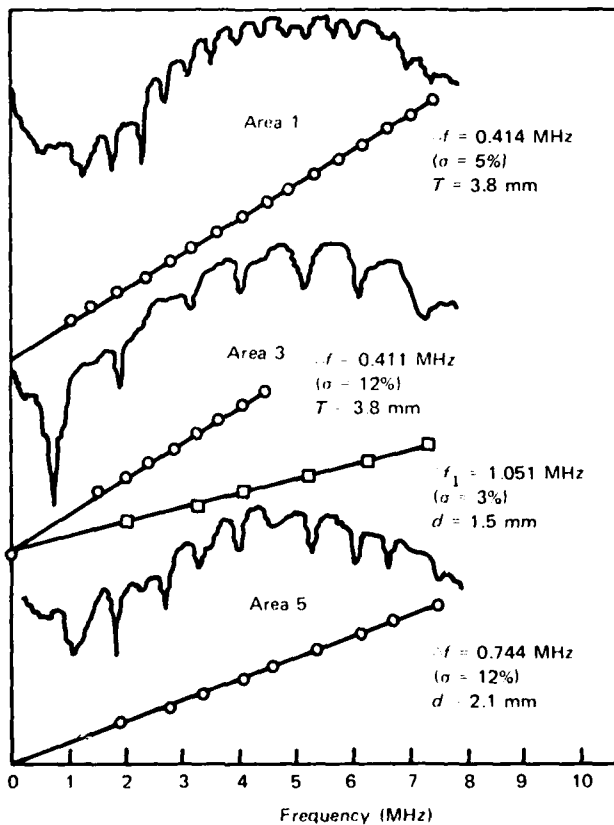


FIGURE 24. ULTRASONIC SPECTRA FOR CRACK-LIKE DEFECTS (From Ref. 23, Reproduced by permission of IPC Science & Technology Press Ltd, England)

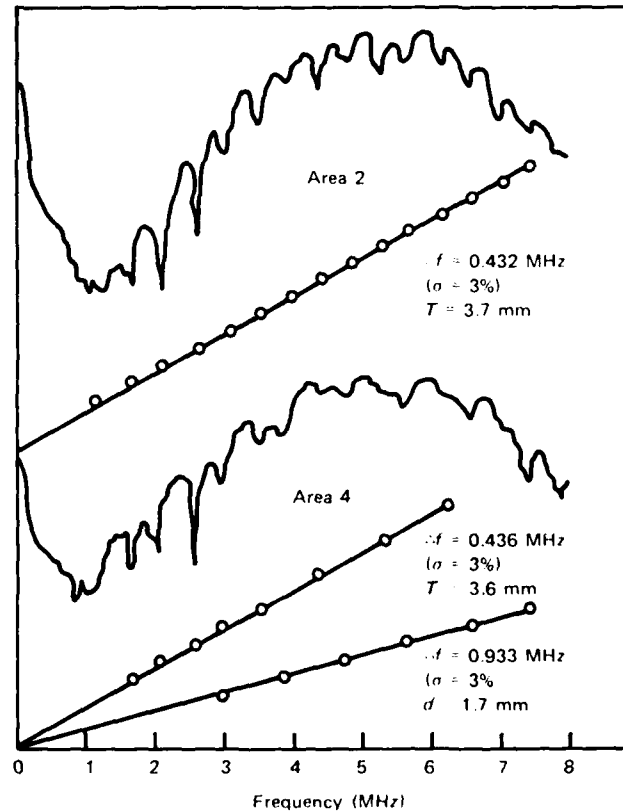


FIGURE 25. ULTRASONIC SPECTRUM FOR A VOID DEFECT (From Ref. 23, Reproduced by permission of IPC Science & Technology Press Ltd, England)

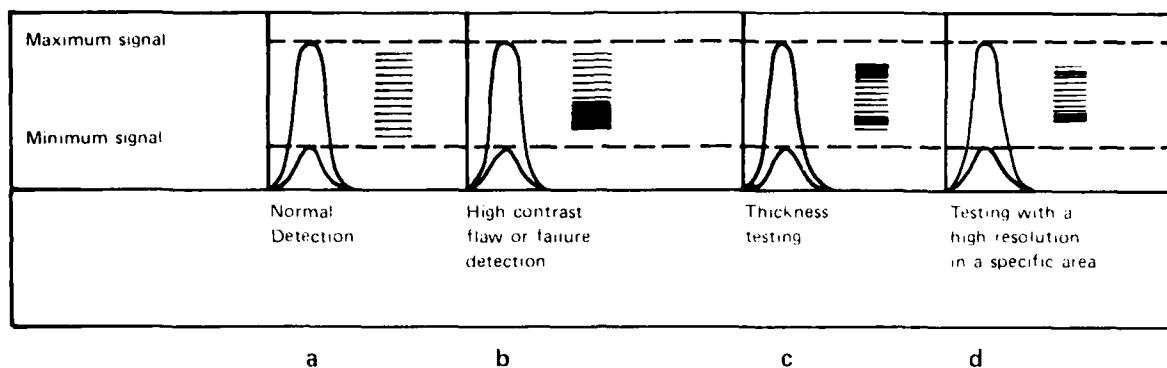


FIGURE 26. EXAMPLES OF DISCRIMINATOR LEVEL SETTINGS IN ULTRASONIC C-SCAN (From Ref. 24, Reproduced by permission of British Crown Copyright)

The sensitivity of ultrasonics to evaluate impact damage in graphite/epoxy composites was investigated by Bailey, et al (Ref. 13). A similar investigation by the same authors, using radiography, was previously discussed in Section III.A.3. As described in that section, impact damage was imparted by dropping a 0.906-kg (2-lb) weight from specified heights. Upon completion of nondestructive testing, destructive analysis was performed on the specimens to verify results and determine the characteristics of the damage. Internal fiber bundle fracture was determined by deplying the laminate accomplished by heating the specimen in a furnace long enough to char and partially remove the resin. The removed plies were examined with a variable magnification stereo-microscope to locate the fiber bundle fractures. The extent of ply delamination in the impacted zones was determined by microscopic examination of laminate cross-sections. This examination revealed both ply delamination and through-the-ply delaminations.

Results of ultrasonic testing showed that C-scan techniques provided clear indications of the location and size of the damage over the entire range of impact damage flaws examined. However, it provided no indication of the extent of fiber bundle fracture. Ultrasonic pulse echo examination, using a hand-held probe, exhibited the capability of locating the damage but the size determination was not as precise as the C-scan.

The application of ultrasonics C-scan techniques to composites and interpretation of results have been discussed by van Dreumel (Ref. 24). The author deals with the possibility of detecting and distinguishing defects in the following four categories of interest:

1. Voids and inclusions
2. Deviations in thickness and fiber content

3. Fiber misorientations
4. Delaminations and bond failures

The equipment used contained ten discriminator levels, each representing a gray tone on a display with which the amplified ultrasonic signal is compared. By varying the discriminator levels the gray tones can be adjusted to cover the total amplitude range of the received signal. By an appropriate choice of discriminator level distributions, a range of data displays for different applications can be obtained, as shown in Figure 26.

Results of the investigation showed that voids and inclusions are easy to detect, but in the gray tone pattern of the C-scan, they appear to be far larger than they really are. Thus, in contrast to x-ray radiography, ultrasonic C-scan is not a reliable method for quantitative void content determination. However, the method is useful for qualitative void detection.

Deviations in thickness of fibers may be measured under certain circumstances, but interpretation of C-scan gray tone patterns can be misleading. Quantitative measurement of energy loss of sound waves in a material is difficult. Surface flatness and parallelism, transducer impedance matching, angle of attack and coupling are all factors that have an influence on the results. It seems unlikely that when a C-scan method is applied to materials in construction, the above factors will be well controlled. Therefore, interpretation of C-scans in terms of thickness or void content should be made very carefully.

In laminates, fiber misorientation can be detected using ultrasonic C-scans. By concentrating the discriminator level settings halfway between the minimum and maximum signal amplitude, a large contrast

between the highest and the lowest amplitude in a relatively homogeneous panel is achieved. An example of using this technique to check fiber alignment is shown in Figure 27. The fibers are not fully parallel but follow curved lines.

Delaminations and bond failures are clearly indicated in the gray tone pattern of an ultrasonic C-scan. The scan in Figure 28 shows the damage of impact testing on a mixed laminate consisting of two layers of Kevlar 181 weave and 6 layers of unidirectional carbon fibers. The stacking order of this laminate was Kevlar ( $0^\circ$ ,  $45^\circ$ ), carbon fiber ( $0^\circ$ ,  $\pm 60^\circ$ ). The dark areas with sharp edges indicate delaminated areas where a steel ball struck the surface, while other dark areas indicate void concentrations formed during manufacture.

The ultrasonic C-scan method, as well as the A-scan and B-scan methods for display of ultrasonic data, are explored in detail by Blake (Ref. 25). Details are presented on the theory of operation of the various ultrasonic modes, as well as the application of these techniques to rapid scan systems. Examples of ultrasonic C-scans are given for both random and oriented fiber composites. Delamination characterization is explored in detail, and examples are given of natural, implanted, and propagated defects.

Although conventional ultrasonic C-scan techniques provide an acceptable means for detecting interlaminar defects, problems are often encountered in

the interpretation of test results, and validation and quantification of defects for material review decisions. To circumvent these difficulties, an acoustic imaging approach, having considerable versatility and not relying on interpretive procedures, has recently been described by Knollman, et al (Ref. 26).

Acoustic images of insonified objects are formed in a manner analogous to that in optical imaging. These acoustic images, in general, consist of amplitude and phase variations of an ultrasonic field and image plane—this field having interacted with a material undergoing nondestructive testing. Ultrasonic sensors are used to detect acoustic signal variations and sensor output is displayed photographically, may be shown videographically, and can be recorded.

Knollman, et al, point out that three methods are possible for acoustically imaging an anomaly in a composite material. One approach involves through-transmission of sound, wherein the structure under test is positioned between the insonification system and the acoustic receiver. This technique is designated "unfocused shadow imaging" since the shadow of the anomaly is cast directly on the receiver plane. "Focused shadow imaging" occurs if an acoustic lens is interposed between the transmitter and the test material, or between the test piece and the receiver, or both. The test piece is generally positioned at the focus of the single lens in the former case, or at the coincident focus of the two-lens arrangement. A third approach involves acous-



FIGURE 27. ULTRASONIC C-SCAN SHOWING POOR FIBER ALIGNMENT (From Ref. 24, Reproduced by permission of British Crown Copyright)



FIGURE 28. ULTRASONIC C-SCAN OF IMPACT DAMAGE (From Ref. 24, Reproduced by permission of British Crown Copyright)

tic energy scattered from the interior of the composite material. The receiver, together with an appropriate collector/focuser is positioned in the vicinity of the acoustic transmitter. A transmitter with focusing lens may also serve intermittently as an appropriate receiver. This method is known as "backscatter or echo imaging". In all circumstances, lenses may be replaced by concave, focused transducers.

Analysis of imaging considerations and sensitivity to small anomalies indicates that the focused shadow imaging mode is superior for the nondestructive evaluation of composite materials and structures. In the Lockheed Acoustic Imaging System, described in Reference 26, focusing at both the transmitter and receiver, is utilized. This double-focusing, shown schematically in Figure 29, concentrates acoustic energy on a point of the

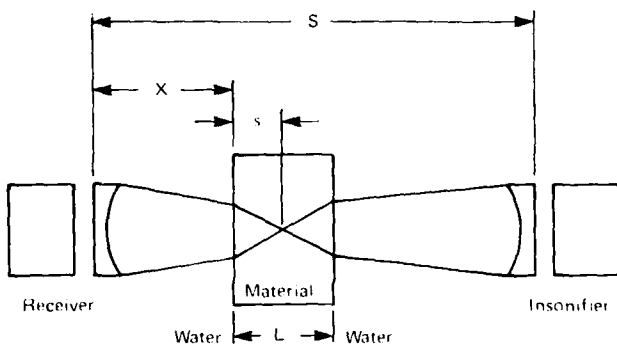


FIGURE 29. SCHEMATIC DIAGRAM OF A DOUBLE-FOCUSED IMAGING SYSTEM (From Ref. 26, Reproduced by permission of The American Society for Nondestructive Testing)

laminates being subjected to the nondestructive test, thereby permitting a point-by-point examination. In the Lockheed system, shown by block diagram in Figure 30, light emitted by a special glow-lamp is modulated in accordance with the transmitted or backscattered acoustic signals which have penetrated the composite. A photographic film is employed to record the emitted light intensity; thus, the inherent wide tonal range of optical photography is utilized in depicting the ultrasonic attenuation variations produced by the composite structure. Thus, for example, a total debond or delamination will be dark on the photograph, and a totally bonded region will be light, with more than 60 shades of gray possible in between. Large size transducers for high sensitivity and sharp focus are employed. Automatic systematic scanning of the transducer over the composite structure results in a two-dimensional acoustic image of the test piece in virtual real-time. Pulse operation and signal gating eliminate spurious signals.

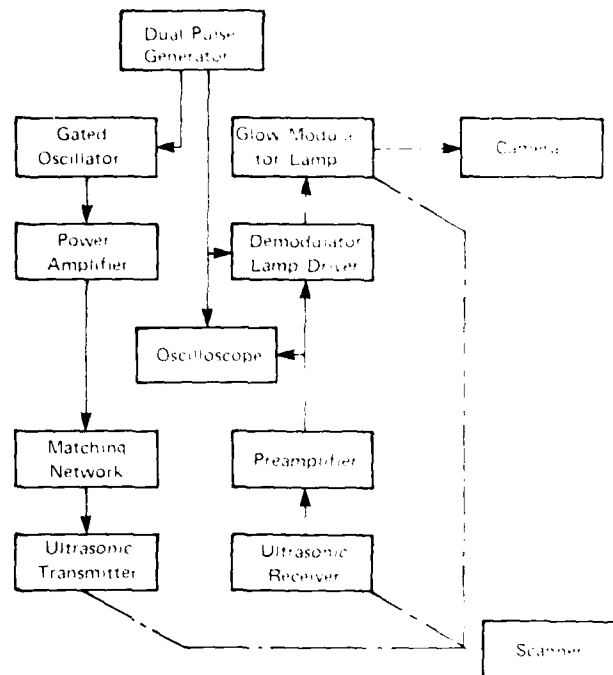


FIGURE 30. BLOCK DIAGRAM OF LOCKHEED ACOUSTIC IMAGING SYSTEM (From Ref. 26, Reproduced by permission of The American Society for Nondestructive Testing)

A typical acoustic through-transmission image, obtained at a frequency of 5 MHz, is shown in Figure 31 compared with a conventional ultrasonic C-scan. The specimen was a flat, 14-ply, 0° layup

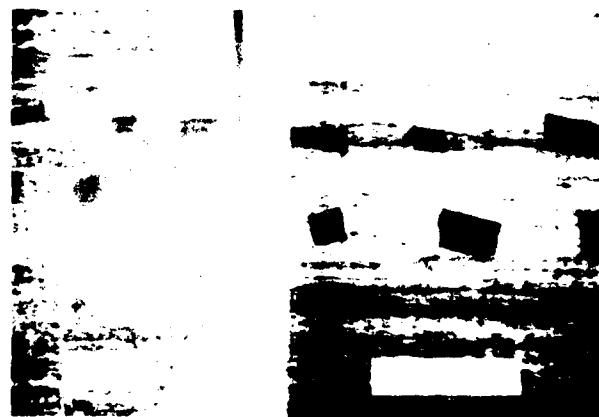


FIGURE 31. ULTRASONIC C-SCAN AND ACOUSTIC IMAGE OF A FLAT, 14-PLY GRAPHITE/EPOXY LAMINATE (From Ref. 26, Reproduced by permission of The American Society for Nondestructive Testing)

graphite/epoxy laminate. Induced debonds (Teflon film inserts between the plies) are portrayed (black areas), as well as acoustic attenuation patterns resulting from variations in thickness, presence of micro-porosity, and resin/fiber ratio variances (various gray shades). The inherently greater amount of significant information on structural content which is contained in the acoustic image over the C-scan presentation is obvious. In the acoustic image, even a strip of adhesive tape, which held one of the Teflon® films in place, is displayed clearly. Other acoustic images of composite specimens containing a variety of defects are given in Reference 26.

The authors indicate that advantages of acoustic imaging for inspection of composite materials include the presentation in real-time of a two-dimensional display representing with high sensitivity and resolution, interior structural variations and discontinuities, and requiring little or no interpretation. The wide tonal range of photographic film employed in detecting ultrasonic attenuation variation has considerable sensitivity to relatively small anomalies in material-property characteristics, and does not rely on sophisticated interpretation of the displays. As such, the Lockheed Acoustic Imaging System is readily adapted to on-line inspection of composite structures, and can even be used to monitor formation and growth of internal damage in composites during the application of programmed stress.

Development of an advanced ultrasonic technique for detecting, locating, and characterizing defects in co-cured graphite/epoxy composite skins and sandwich structures has been reported by Bar-Cohen, et al (Ref. 27). The method utilizes focused ultrasonic shock waves, that is, pulses of very short duration. Reflected pulses, in their RF configuration, are displayed on an oscilloscope screen. A reference pattern is established on the basis of defect-free areas of the specimen and any defect present in the area under test is manifested by a change in the ultrasonic reference pattern. This change can consist of one or more of the following parameters:

1. Additional reflection
2. Velocity change
3. Variations of attenuation
4. Reversal of reflection phase

Experiments were conducted on a specimen consisting of honeycomb core sandwiches between 10-ply graphite/epoxy laminates containing the following controlled defects:

1. Delaminations varying in size from 1-mm diameter to 10-mm diameter, lo-

cated at various depths in the laminate, including the bond line between the skin and the core;

2. Fiber gaps of 2-mm width at various depths;
3. Resin rich and resin starved areas.

Results of the experiments show that all of the defects could be located and identified using the shock wave pulse-echo approach. Skin delaminations and skin-to-core unbond defects were identified by evaluating the amount of energy reflected from the flaw. Gaps between fiber tows involve a local decrease in thickness and an increase in resin concentration at the defective area. These phenomena caused (a) splitting of the front echo, (b) decrease of transit time, (c) increased attenuation. Resin-rich and resin-starved areas could be characterized on the basis of (a) variation in transit time due to velocity change, and (b) variation in attenuation level.

### 3. Fatigue Damage

As pointed out by Stone (Ref. 20), the response of composite materials to a fatigue environment is complicated and depends on the layup employed and the nature of the applied stress field. For example, unidirectional graphite/epoxy composite shows a high level of resistance to fatigue damage when subjected to tensile loading along the fiber direction. But, in shear, fatigue effects are severe and significant creep is induced. With angle ply material, the presence of fatigue damage is not always accompanied by a loss of strength, and there is really no universal criterion by means of which the degree of fatigue damage can be specified. In some cases it is possible for damage to be beneficial. For example, it has been shown (Ref. 28) that the notch sensitivity of ( $0 \pm 45^\circ$ ) graphite/epoxy which is severe under monotonic loading, is much reduced in fatigue because of the occurrence of cracking which reduces the sensitivity to the stress riser. Thus, although internal damage can be detected by ultrasonic attenuation, care must be taken in the interpretation of such data.

Sturgeon (Ref. 8) indicates that no one inspection technique is sufficient by itself to give all the information desired regarding fatigue damage in composites, and some inspection techniques need to be used while fatigue testing is in progress; however, for inspection of damage after dynamic fatigue loading, the ultrasonic C-scan technique is probably one of the most useful methods, at least as a research tool. There are limita-

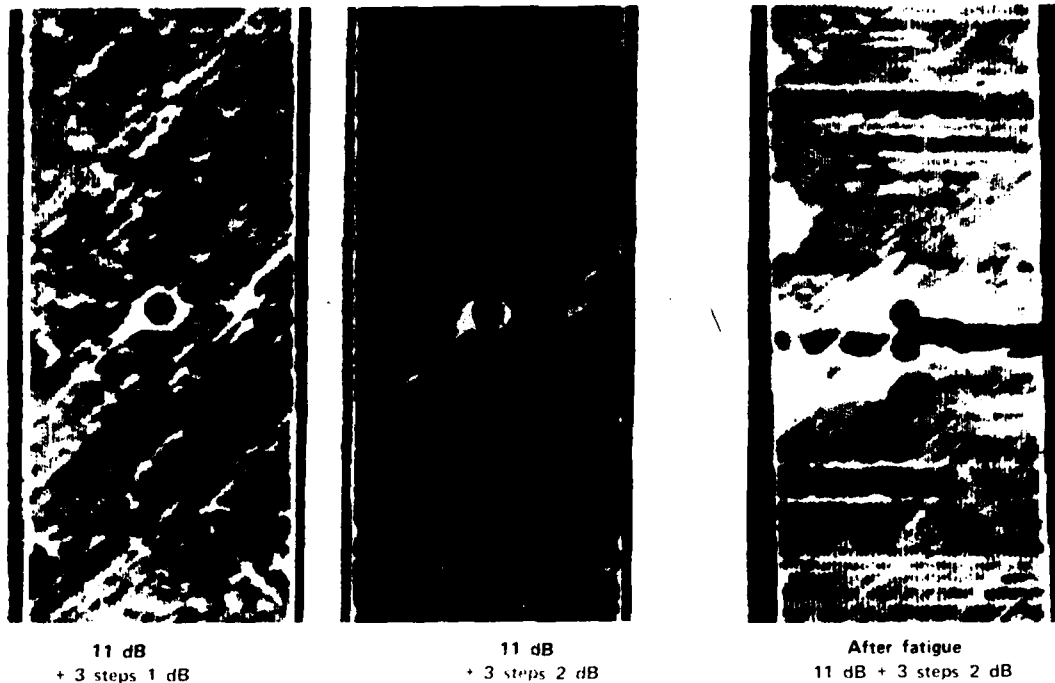


FIGURE 32. ULTRASONIC C-SCANS OF  $90 \pm 45^\circ$  CARBON FIBER COMPOSITE MADE BEFORE AND AFTER FATIGUING (From Ref. 8, Reproduced by permission of British Crown Copyright)

tions on the depth of material which may be scanned due to attenuation and scatter, but the technique is still useful. An example of the detection of fatigue damage is shown in Figure 32. The material is a  $90 \pm 45^\circ$  carbon fiber composite. The scan at 1 db steps before fatiguing shows details of surface imperfections in the outer  $45^\circ$  layers, and evidence of one or two thermal cracks in the  $90^\circ$  plies. To compare scans before and after fatigue, 2 db steps were used, and it is clear that considerable cracking occurred in the  $90^\circ$  plies. The final rupture lies across the hole accompanied by much delamination, which shows up as white areas on the scan. Some cracks are also found in  $45^\circ$  plies. There is also an overall lightening in shade of the C-scan after fatiguing, which may be due to progressive damage within the whole body of the composite—it may be crazing in the matrix or changes at the fiber-matrix interface. Outside the region of extensive delamination, each line on the scan in the  $90^\circ$  plies can be assigned to a crack as verified by sectioning and identifying cracks in polished specimens. Occasionally, cracks could be seen in the  $45^\circ$  plies. The carbon fibers are about 7 to 8  $\mu\text{m}$  in diameter, so the crack width is very small, but the dispersion of the ultrasound which it causes produces a much wider trace on the scan than the actual crack width. Some increase in the scan trace width is also due to cracks not running perfectly perpendicular through the laminate.

Sturgeon concludes that C-scan is a useful way of detecting delaminated and cracked areas, although it is not always possible to distinguish differences in the traces between surface imperfections and cracks without comparing the trace directly with the laminate surface.

An example of the application of ultrasonics to monitoring flaw growth and composite specimens subjected to fatigue loading is reported by Daniel and Liber (Ref. 29). Specimens were graphite epoxy of  $[(0 \pm 45 \ 90)_2]_2$  and  $[0_2 \pm 45]_2$  layups with four different types of initial flaws:

1. Circular hole
2. Imbedded film patch
3. Internal ply gap
4. Surface scratches

The specimens were subjected to fully reversed spectrum fatigue loading simulating the load environment experienced by the composite structure. One lifetime of exposure was simulated by 127,500 cycles of tension-compression loading at a frequency of 3 Hz, and at peak stress levels of 160.6 MPa (23.3 ksi) and 223.4 MPa (32.4 ksi). The specimens were tested to a maximum of four lifetimes. At intervals corresponding

to each half-lifetime of loading, the specimens were removed from the fatigue machine and inspected ultrasonically. The various C-scans obtained for each specimen were combined into maps illustrating the progressive flaw growth.

Contour maps obtained for specimens with the four types of initial flaws are shown in Figures 33 through 36. In general, it can be seen that flaw growth is greater in specimens of  $[(0/\pm 45/90)_2]_2$  layups than those of  $[0_2/\pm 45]_{2S}$  layup. In the case of specimens with circular holes (Figure 33) delaminations grow around the hole boundary in the early stages of load cycling, i.e., one to two lifetimes, but no further growth is seen up to four lifetimes. However, additional delamination growth sources develop in the interior, along the edges and along the edge of the tab. In the case of specimens

with imbedded patches (Figure 34), initial delaminations were present throughout. With increasing number of load cycles, these grew and additional ones developed throughout the specimens. In the specimens with internal ply gaps (Figure 35) some flaw growth followed along the gap but did occur at other locations as well. In the specimen of  $[0_2/\pm 45]_{2S}$  layup flaw growth was minimal (Figure 35b). Of the two types of specimens with surface scratches, the ones of  $[0_2/\pm 45]_{2S}$  layup failed during the first half lifetime of loading. The other specimen (Figure 36) showed delamination growth mostly around the horizontal scratch where surface  $0^\circ$  fibers had been broken.

Real-time ultrasonic attenuation measurements of fatigue damage in graphite/epoxy composites has been reported by Saluja, et al (Ref. 30). Two

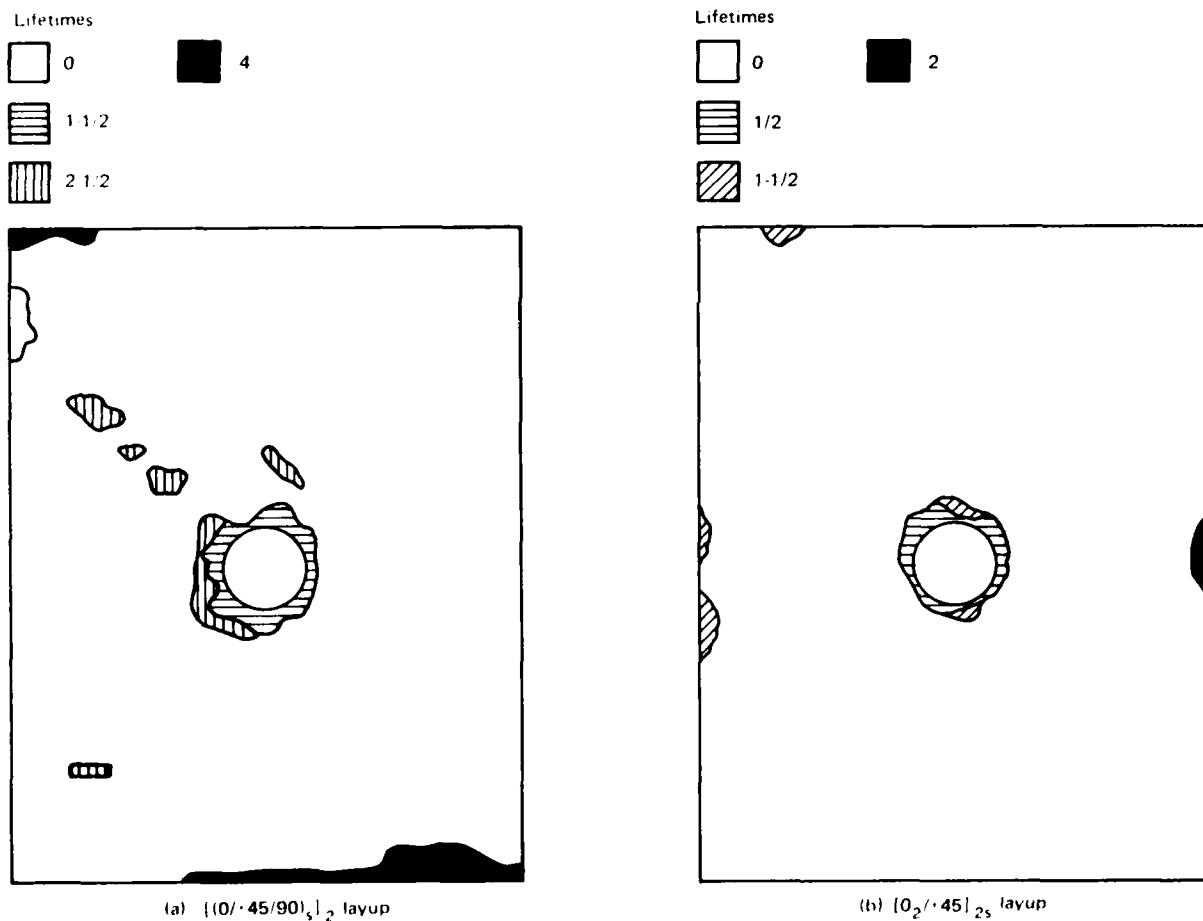


FIGURE 33. FLAW GROWTH UNDER SPECTRUM FATIGUE LOADING IN GRAPHITE/ EPOXY SPECIMENS WITH 6.4 mm (0.25 in.) DIAMETER HOLE (From Ref. 29, Reproduced from NTIAC publication, Proceedings of 12th NDE Symposium)

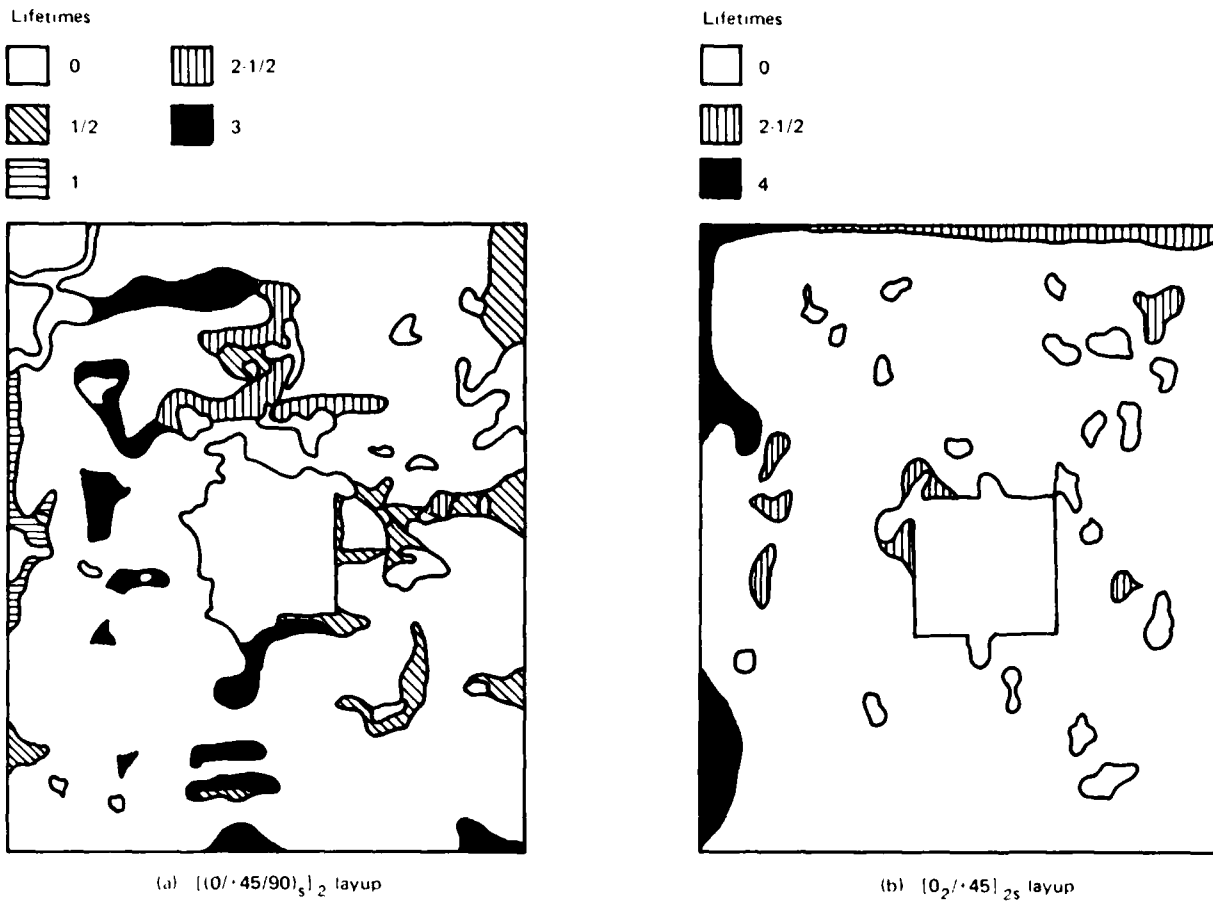


FIGURE 34. FLAW GROWTH UNDER SPECTRUM FATIGUE LOADING IN GRAPHITE EPOXY SPECIMENS WITH 9.4 mm (0.37 in.) SQUARE EMBEDDED KAPTON PATCH (From Ref. 29, Reproduced from NTLAC publication, Proceedings of 12th NDE Symposium)

different types of graphite/epoxy laminate were studied to determine damage development and growth along the edges and in the interior of the laminates. The laminates were constructed from A/S 3501 prepreg tape laid up in the configurations  $[0/\pm 45/90]_5$  (Type I) and  $[0/90/\pm 45]_5$  (Type II). The specimens were subjected to tensile-tensile fatigue loadings at a frequency of 15 Hz with a stress ratio of  $R = 0.1$ . The three maximum stress levels used were 172 MPa (25 ksi), 276 MPa (40 ksi), and 310 MPa (45 ksi).

Attenuation of ultrasonic stress waves was measured by Saluja, et al, in real-time during fatigue tests using a modified buffer rod technique (References 31 and 32). An automatic attenuation recorder was used which takes the ratio of the maxima of two signals appearing at preselected gates and provides an analog signal output proportional to the corresponding amplitude

ratio value in decibels. A real-time attenuation change is experimentally measured by the technique when the only changes taking place occur in the composite specimen due to load application. This attenuation change was experimentally verified to coincide with the development of the characteristic damage state of the laminate. The characteristic damage state consists of (a) transverse cracks in  $90^\circ$  plies that begin to occur at a load of approximately one-third of ultimate and reach a stable density at approximately two-thirds of ultimate; (b) delamination of the  $90^\circ$  plies at the free edge; (c) spreading of the transverse cracks into adjacent  $45^\circ$  plies; (d) delamination of the  $\pm 45^\circ$  interface; and (e) development of a uniform spacing of transverse cracks in the  $45^\circ$  plies. This damage state is dependent upon material properties and stacking sequence, but is independent of load history in the sense that the same damage state is observed under both quasi-static and fatigue

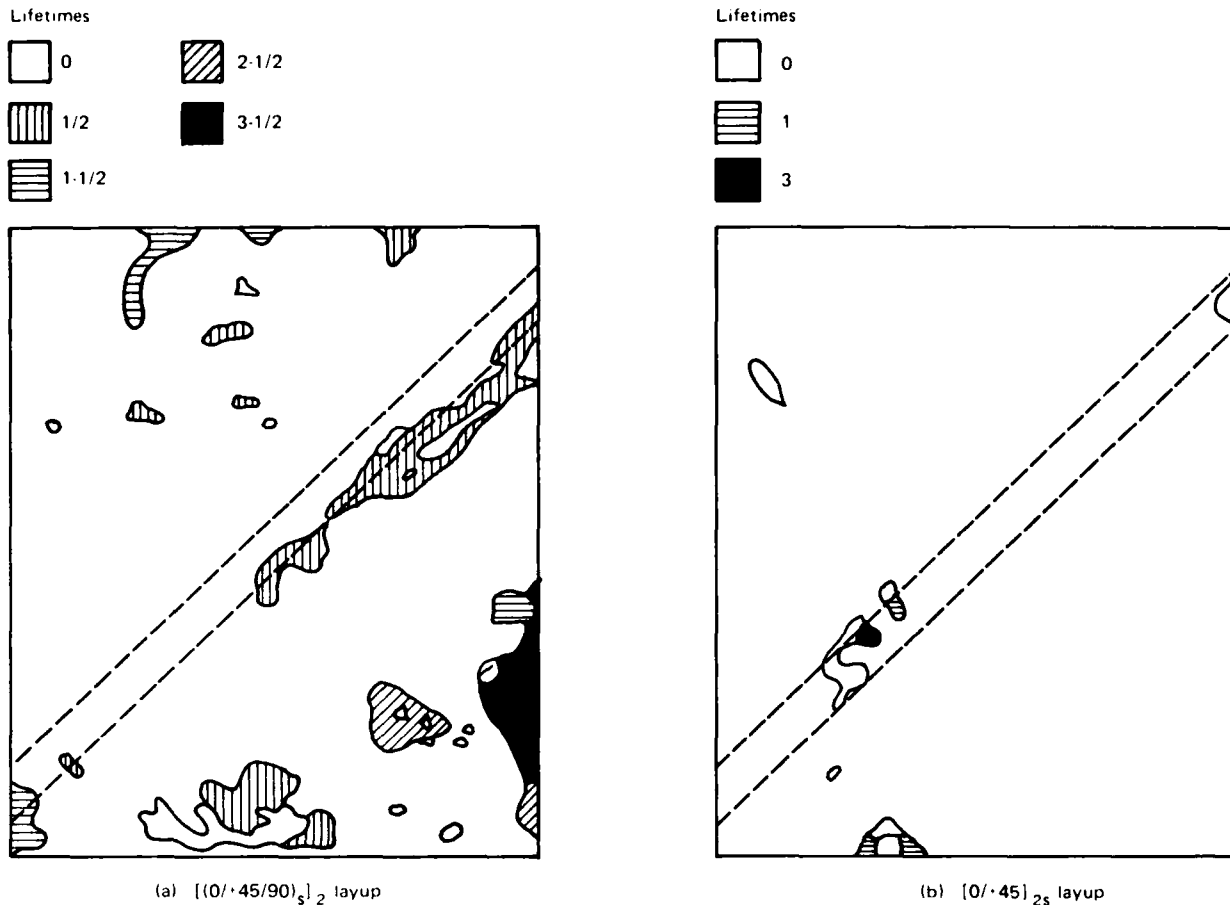


FIGURE 35. FLAW GROWTH UNDER SPECTRUM FATIGUE LOADING IN GRAPHITE/EPOXY SPECIMENS WITH 3.2 mm (0.125 in.) GAP IN OUTERMOST 45-DEG. PLY (From Ref. 29, Reproduced from NTIAC publication, Proceedings of 12th NDE Symposium)

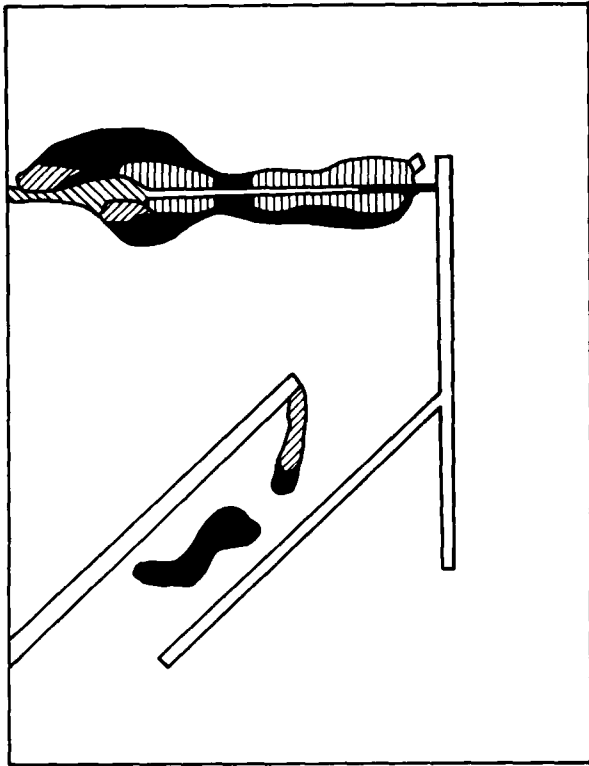
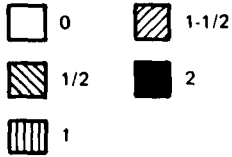
loadings. The damage state is developed at lower stress levels in fatigue than in quasi-static tension but the spacing of the transverse cracks is the same in either case.

Ultrasonic attenuation measurements made in real-time, while the specimen was being loaded, proved to be a very sensitive indicator of the development of the damage state. Examples are shown for both specimen types in Figures 37 and 38. A sharp increase in attenuation is noted during the initial period of cycling. The attenuation continues to increase with increasing number of cycles and levels off in the range of 500,000 to 600,000 cycles until the end of the test. Sectioning and replication studies performed on the specimens to determine the extent of damage in the interior showed that the real-time measurement of attenuation changes very closely paralleled the development of the characteristic damage state.

An attempt by Saluja, et al, to relate the attenuation change to the transverse cracks established in the specimens by use of an elementary diffraction model was only moderately successful. It predicted in a qualitative fashion the same trends in attenuation change observed experimentally. However, the quantitative agreement was not good. It was suggested by the authors that other work be performed either to modify the model or to develop a new one in order to obtain a better quantitative relationship between measured attenuation and the degree of damage in the composite.

An experimental study to investigate the ultrasonic attenuation and velocity as a function of the fatigue state of a graphite/epoxy composite subjected to trans-fiber compression-compression loading has recently been reported by Williams and Doll (Ref. 33). The specimens investigated were unidirectional Hercules

Lifetimes



$[(0/45/90)_2]_2$  layup

FIGURE 36. FLAW GROWTH UNDER SPECTRUM FATIGUE LOADING IN GRAPHITE/EPOXY SPECIMENS WITH 0.25 mm (0.01 in.) DEEP SURFACE SCRATCHES (From Ref. 29, Reproduced from NTIAC publication, Proceedings of 12th NDE Symposium)

AS/3501-6 graphite/epoxy composite having 72 laminae. The experiments consisted of alternately compression-compression fatiguing specimens at a frequency 30 Hz and measuring their narrow band longitudinal wave group velocity and attenuation properties. Velocity and attenuation measurements were typically made at intervals of  $3 \times 10^4$  fatigue cycles. The ultrasonic measurements were recorded at 4 narrow band center frequencies: 0.5 MHz, 1.0 MHz, 1.5 MHz, and 2.0 MHz.

Tests were conducted with a peak-to-peak stress amplitude of  $0.2\sigma_f$ ,  $0.4\sigma_f$ ,  $0.6\sigma_f$ , and  $0.8\sigma_f$ , where  $\sigma_f$  was the pre-fatigued static compressive fracture stress.

The correlation observed between pre-fatigued static fracture stress and initial ultrasonic attenuation is in agreement with results reported elsewhere (Ref. 34). No changes in attenuation or velocity

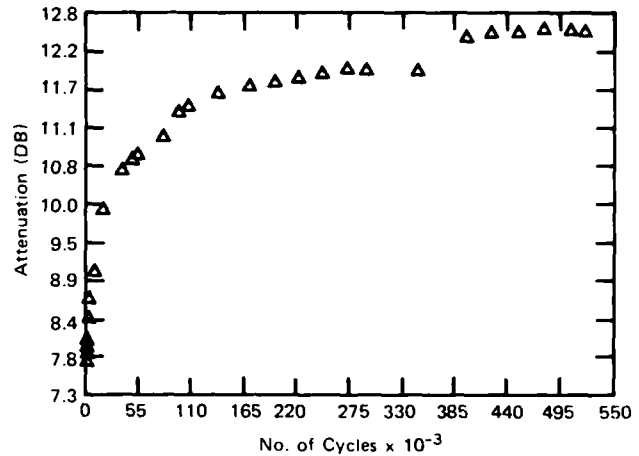


FIGURE 37. ATTENUATION CHANGE VERSUS NUMBER OF LOAD CYCLES FOR A TYPE I SPECIMEN (2309 #7) (From Ref. 30, Reproduced from NTIAC publication, Proceedings of 12th NDE Symposium)

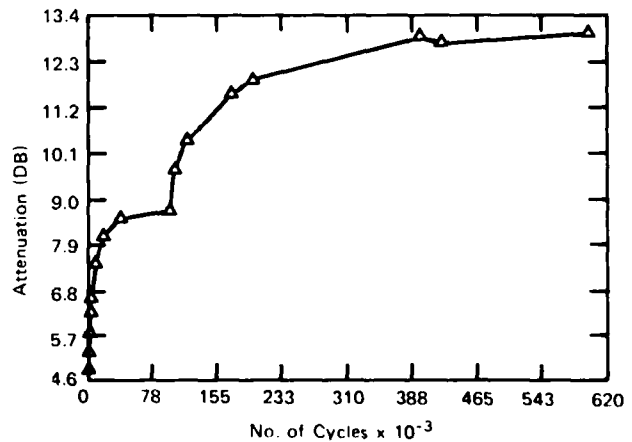


FIGURE 38. ATTENUATION CHANGE VERSUS NUMBER OF LOAD CYCLES FOR A TYPE II SPECIMEN (2649 #6) (From Ref. 30, Reproduced from NTIAC publication, Proceedings of 12th NDE Symposium)

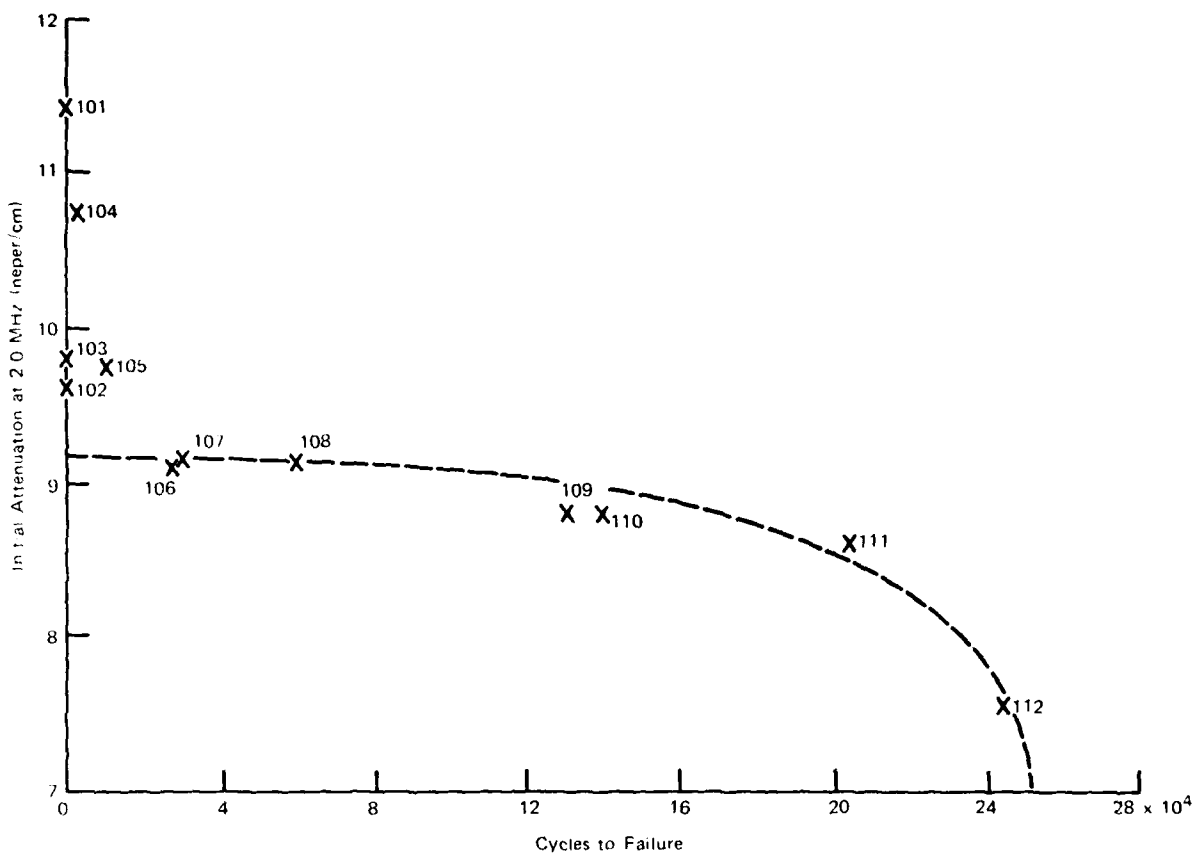


FIGURE 39. INITIAL ATTENUATION AT 2.0 MHz VERSUS CYCLES TO FAILURE FOR TRANSFIBER COMPRESSION-COMPRESSION FATIGUE OF LAMINATE NO. 1 SPECIMEN AT  $\sigma_{max} = 0.8\sigma_f$  (From Ref. 33, Reproduced by permission of The American Society for Nondestructive Testing)

and no fatigue fractures occurred for specimens fatigued to  $10^6$  cycles at maximum stress levels at or below  $0.6\sigma_f$ . When the peak stress level equaled  $0.8\sigma_f$ , there was generally a 5 to 10% increase in attenuation; however, this increase did not appear to be a fracture precursor. It was noted by the authors that the attenuation measurements were intermittent at about  $3 \times 10^4$  cycle intervals, and that the possibility of an attenuation precursor within a few cycles of failure cannot be discounted. The initial attenuation at 1.5 MHz and 2.0 MHz appeared to be an indicator of the relative survivability in the fatigue environment. There appeared to be ultrasonic frequency dependent "upper cutoff" attenuation values that define a minimal fatigue life and "lower cutoff" attenuation values that define a fatigue life limit. The "upper cutoff" value of approximately 9.4 nepers per centimeter is apparent in Figure 39, whereas the results shown plotted in Figure 40 suggest the existence of a "lower cutoff" value of attenuation below which specimens may be screened for survival to the fatigue limit.

#### 4. Measurement of Strength

A novel ultrasonic technique for measuring strength in fiber reinforced composites has been reported by Vary and coworkers (References 35 and 36). Development of the method was based on a perceived need for NDE techniques that go further than simply finding overt flaws in composite structures. Currently available NDE methods for composite structures usually fail to adequately predict mechanical property variations; typically they yield only qualitative data relative to strength. Therefore, Vary and coworkers concentrated on investigating NDE techniques that could measure variations in strength related properties. In particular, a new acoustic ultrasonic method was investigated that could measure the relative efficiency with which stress waves propagate in a given composite structure. The working hypothesis was that the presence of microvoids, for example, reduced both the composite strength and also the stress wave propagation efficiency. In the

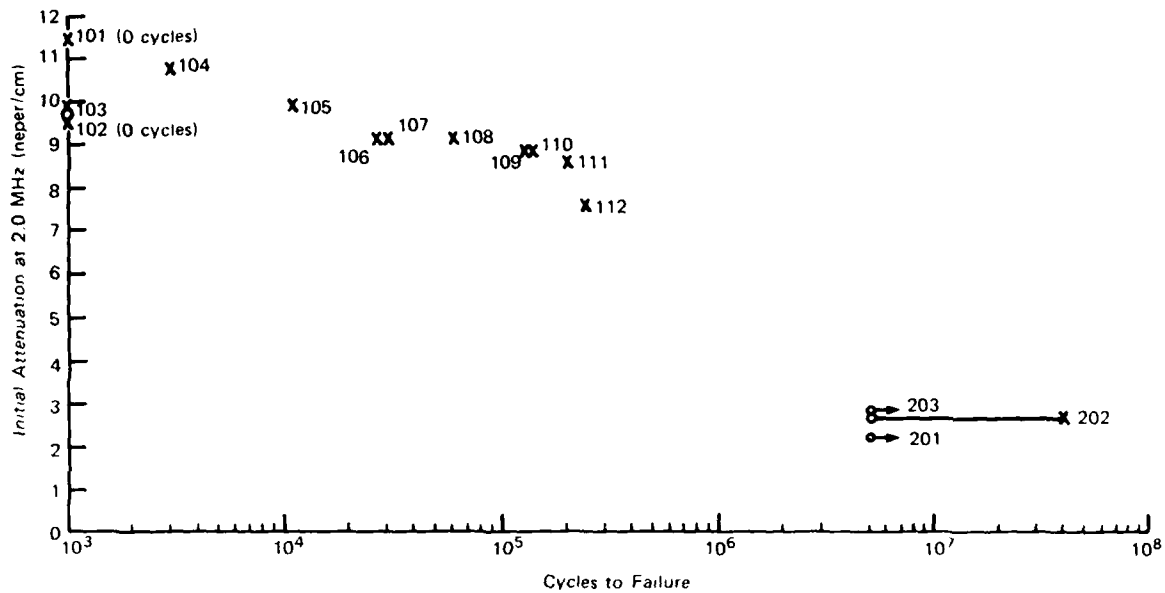


FIGURE 40. ATTENUATION AT 2.0 MHz VERSUS CYCLES TO FAILURE FOR TRANSFIBER COMPRESSION-COMPRESSION FATIGUE OF LAMINATES NO. 1 AND 2 SPECIMENS AT  $\sigma_{max} = 0.8\sigma_f$  (From Ref. 33, Reproduced by permission of The American Society for Nondestructive Testing)

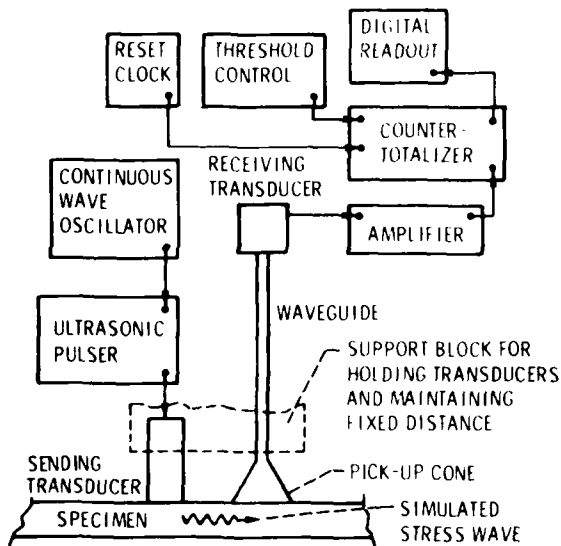
initial studies (Ref. 35), a significant correlation was found between an ultrasonically measured quantity termed the "stress wave factor" and the interlaminar shear strength. The stress wave factor is a measure of the relative efficiency with which stress wave energy will propagate in a given specimen, and is apparently determined by microstructural features such as void distribution and shape, and fiber-to-resin ratio variations.

The stress wave simulation method is illustrated in Figure 41. A sending transducer injects a repeating series of ultrasonic pulses into the material. Each of these pulses produces simulated stress waves that resemble acoustic emission waves in the material. The receiving transducer intercepts some of the simulated stress wave energy that radiates from the point of injection. The signals arriving at the receiver resemble "burst"-type acoustic emission events. After traveling through the composite, the simulated stress waves bear the imprints of dispersion and other effects that might alter an actual stress wave emanating from the injection zone.

The simulated stress waves are repeated at a fixed rate,  $r$ . The received signal roughly resembles a decaying sinusoid. Each successive burst is identical to its predecessors. After amplification, the received signals are sent to a counter that registers the number of oscilla-

tions,  $n$ , in each burst, exceeding a fixed threshold voltage. The counter is reset automatically after a predetermined time interval,  $g$ , and the previous count is held in memory and digitally displayed. The displayed count assumes a constant value soon after the specimen is coupled to the probe. The number that is displayed is  $\sigma_w = gn$ , the stress wave factor. The actual stress wave factor number is arbitrary and depends on factors such as signal gain, reset time, threshold voltage, repetition rate, probe pressure, coupling, etc. All these factors, however, are kept constant for any series of measurements so that  $\sigma_w$  reflects only the material variations of the specimens tested.

Results reported by Vary and Bowles (Ref. 35) on specimens of a unidirectional graphite-polyimide (AS/PMR-15) fiber reinforced composite showed good correlation between interlaminar shear strength and stress wave factor, as shown in Figure 42. The stress wave factor was measured for waves in the range from 0.1 to 1.0 MHz propagating parallel to the laminate surface and perpendicular to the unidirectional fibers. The data can be divided into two populations indicated by the curves marked U and L in the figure. Regression analysis for each curve gives a high coefficient of correlation, i.e., for each it is 0.98. Considering curves U and L as upper and lower bounds respectively, the stress wave factor alone can be used to give a conservative esti-



(a) APPARATUS FOR STRESS WAVE SIMULATION & MEASUREMENT

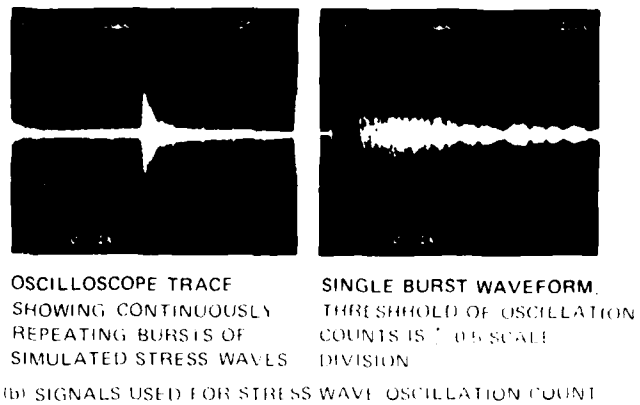


FIGURE 41. APPARATUS AND SIGNAL TREATMENT USED FOR MEASURING THE STRESS WAVE PROPAGATION FACTOR (From Ref. 35, Reproduced from NTIAC publication, Proceedings of 11th NDE Symposium)

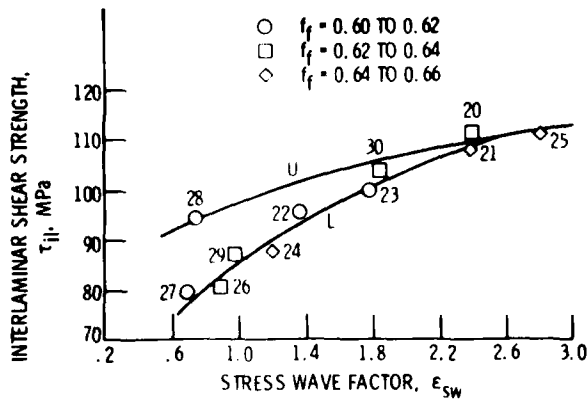


FIGURE 42. CORRELATION OF INTERLAMINAR SHEAR STRENGTH WITH STRESS WAVE FACTOR FOR GRAPHITE-POLYIMIDE COMPOSITE (From Ref. 35, Reproduced from NTIAC publication, Proceedings of 11th NDE Symposium)

mate of the shear strength by using the lower bound curve. Vary and Bowles show that if in addition the velocity of sound is measured parallel to the surface, then the interlaminar shear strength can be uniquely determined.

Results of the investigations reported by Vary and Bowles resulted in the following conclusions:

1. Ultrasonic measurements apparently provide a nondestructive means for predicting or estimating interlaminar shear strength of fiber composite laminate.
2. A quantity termed "the stress wave factor" was found to correlate strongly with interlaminar shear strength as well as with physical properties that determine strength, thus indicating the importance of stress wave transmission by fibers in determining composite strength.

In more recent work, Vary and Lark (Ref. 36) report on stress wave factor studies of graphite-epoxy composites in which fiber orientation was the primary variable, and fiber-resin bonding was a secondary variable. The objective was to find out if the stress wave factor was sufficiently sensitive to these two variables, and hence, accompanying strength variations.

The specimens were 8-ply panel laminates consisting of type AS-1 graphite fiber and PR-288 epoxy resin. The specimen designs included a number of fiber orientations that would lead to different ultimate strengths, moduli and fracture modes. The fiber-resin bonding was altered by coating the fibers in some specimens with PVA. None of the specimens contained intentional defects.

Prior to tensile testing the stress wave factor was measured at 15 locations along each specimen. After the specimens failed under tensile loading the separate pieces were reassembled and the fracture loci were noted. Figure 43 shows plots of the variation of stress wave factor versus linear distance along representative specimens. A scale drawing of the corresponding speci-

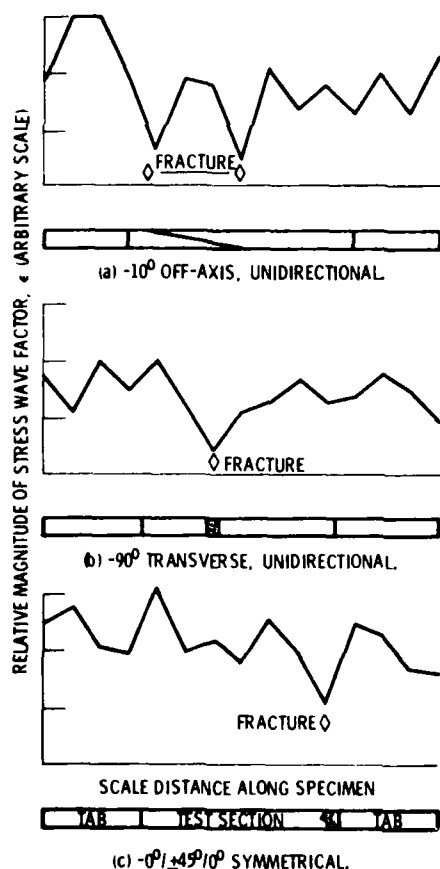


FIGURE 43. VARIATION OF STRESS WAVE FACTOR ALONG TENSILE SPECIMENS FOR THREE TYPICAL CASES (From Ref. 36, Reproduced by permission of American Society for Testing & Materials, 1916 Race Street, Philadelphia, PA 19103)

men accompanies each plot, and the failure locations are indicated. It is apparent that the failures tended to be near minimum stress wave factor values. These fracture loci gave no indications of overt defects such as delamination or excess void concentration in prior ultrasonic inspections. Thus, fracture apparently initiated at loci that were weakest because of microstructural variations rather than overt defects. Investigations of PVA-treated specimens compared with non-PVA specimens demonstrated that the stress wave factor could be used to correctly rank ultimate strengths despite porosity variations.

Vary and Lark suggest that their findings support the view that attenuated stress wave energy flow corresponds to decreased fracture resistance. The correlations that were obtained probably arose because stress wave propagation is a function of material elasticity which in turn controls ultimate strength in the composites tested. Apparently the stress wave factor provides a means of rating the efficiency of dynamic strain energy transfer in a given composite. The authors' view of the results is that a material that is more efficient in transfer of stress wave energy will exhibit greater strength. This is to be expected, they say, because attenuation is less along the direction of fiber orientation which is also the direction of maximum strength for fiber composites. Regions of low values of stress wave factor are regions of higher attenuation, which are also observed to be regions of weakness. Low values of the stress wave factor indicate places where dynamic strain energy is likely to concentrate and promote fracture.

## 5. Measurement of Void Content

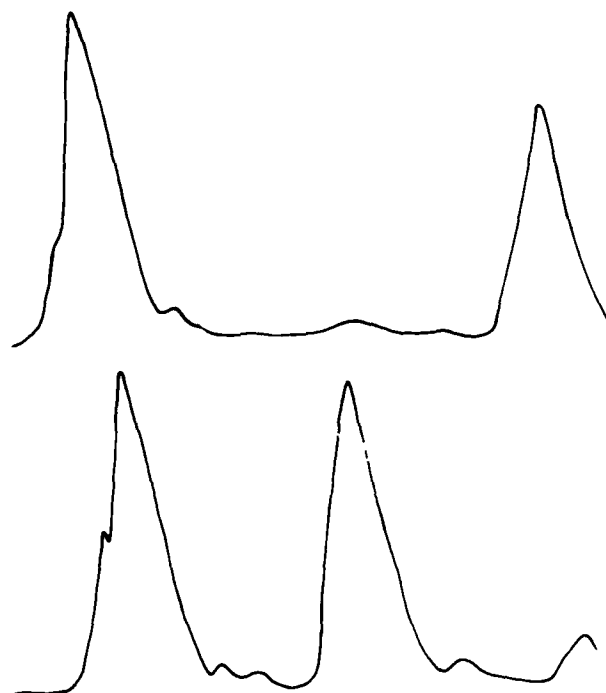
A useful appraisal of voids and their effects on the mechanical properties of composites has been recently presented by Judd and Wright (Ref. 37). In this report, brief accounts are given of (a) void types and their origins in fiber/resin composites, (b) methods of measurement of void content, and (c) the influence of voids on the mechanical properties of composites. The authors point out that voids in composites are caused by volatiles arising from the resin or its components during cure, from residual solvent, or from trapped air. Both theory and experiment indicate that there are decreases in mechanical properties in the presence of voids. The properties affected include interlaminar shear strength, longitudinal and transverse strength in modulus, fatigue resistance, and high temperature oxidation resistance. The available data indicate that regardless of resin, fiber type, or fiber surface treatment, the interlaminar shear strength of a composite decreases by about 7% for each 1% voids up to a total void content of at least 4%, be-

yond which the rate of decrease diminishes. Other mechanical properties are also affected, although not to the same degree or extent. An extensive tabulation compiled from 47 references is presented by Judd and Wright, listing the measured effect of voids on various composite systems.

The use of ultrasonic attenuation to measure void content in carbon fiber reinforced composites has been treated by Stone and Clarke (Ref. 38). Although there are a number of ways in which ultrasonics can be applied to inspection of composites, the most suitable method for production inspection of sheet material is to use a conventional pulse-echo or pulsed through transmission system with a C-scan presentation. In the work reported by Stone and Clarke, a 10 MHz probe was focused on the top surface and gated on the echo from a glass reflector plate, so that the pulse passed through the specimen twice. A quantized display was used so the various attenuation levels are presented as finite changes in tone density on a planned view of the specimen. The darkest regions are of lowest attenuation.

In addition to voids, other factors influencing ultrasonic attenuation are delaminations, state of cure of the resin, fiber volume fraction, condition of the fiber-matrix interface, and surface losses which are dependent on the surface texture. Delaminations will produce a high degree of attenuation. However, it should be possible to distinguish between voids and significant delamination by using a pulse-echo system because a delamination will produce a separate back-echo in between those from the front and back surfaces, as shown in Figure 44. It is difficult to separate the effect of the state of cure of the resin from that of voids because incorrect cure will often result in the production of voids. However, the converse is not true. Incorrect fabrication procedures can result in badly voided material, even though the resin is fully cured. Fiber volume fraction does not appear to have a very strong effect on attenuation, and it can be shown that this effect is small compared with that of voids and need only be taken into account when obtaining precise measurement of void content. With regard to the fiber/matrix interface, there is no evidence of the effect of fiber surface treatment on ultrasonic attenuation, although it seems likely that a failed or weak bond would increase the degree of internal scattering and hence the attenuation.

Stone and Clarke investigated the effect of void content on ultrasonic attenuation of a series of carbon fiber reinforced panels of unidirectional layup, having different void contents produced by varying the autoclave procedure. The surfaces of the panels were ground so that all the panels were of constant thickness



The upper oscillogram shows the normal back wall echo while the lower shows the reflection from the delamination.

**FIGURE 44. USE OF ULTRASONIC PULSE-ECHO TECHNIQUE FOR DELAMINATED DETECTION**  
(From Ref. 38, Reproduced by permission of British Crown Copyright)

and constant surface finish. Through transmission attenuation measurements were made using parallel probes on selected areas of various panels. Upon completion of the ultrasonic measurements, destructive tests were performed to determine interlaminar shear strength, fiber volume fraction, and void content.

The attenuation coefficient,  $\alpha$  is shown plotted against void content,  $V_v$  at three different frequencies in Figure 45. For a given frequency, the attenuation is strongly dependent on void content with the attenuation losses caused by voids increasing with frequency. The dashed curves in Figure 45 illustrate an attempt to approximate the relationship between  $V_v$  and  $\alpha$  by a parabola. The agreement with the experimental results is fair, although there is some discrepancy below about one percent  $V_v$  for the 5 and 7 MHz curves, while the curves for 2.5 MHz begin to deviate above 3%  $V_v$ .

In interpreting their data, Stone and Clarke point out that the total volume of voids may roughly be divided into two types. Up to about 1.5%  $V_v$  the voids tend to be spherical with the void diameter varying from about 5  $\mu\text{m}$  to 20  $\mu\text{m}$ . These voids are due to various vol-

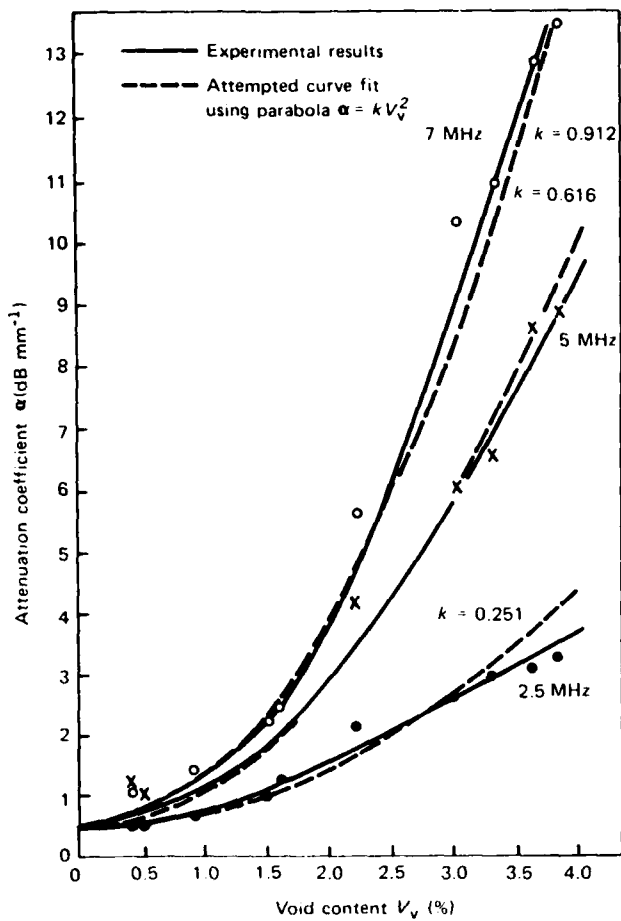


FIGURE 45. RELATIONSHIP BETWEEN THE COEFFICIENT OF ATTENUATION OF ULTRASOUND BY CFRP AND THE VOID CONTENT (From Ref. 38, Reproduced by permission of British Crown Copyright)

tile elements present, and there is some evidence that the size of individual voids increases with  $V_v$ . Beyond about 1.5%  $V_v$  interlaminar voids caused by air trapped between the laminates start to predominate; these are flattened and elongated and tend to be significantly larger than the volatile-induced voids. This two-stage process suggests that a bilinear relationship might be an alternative way of describing the variation of attenuation with void content. This approach to interpreting the experimental data is shown in Figure 46. Although there is some uncertainty at low values of  $V_v$ , the bilinear relationship appears to give a rather good fit to the experimental results.

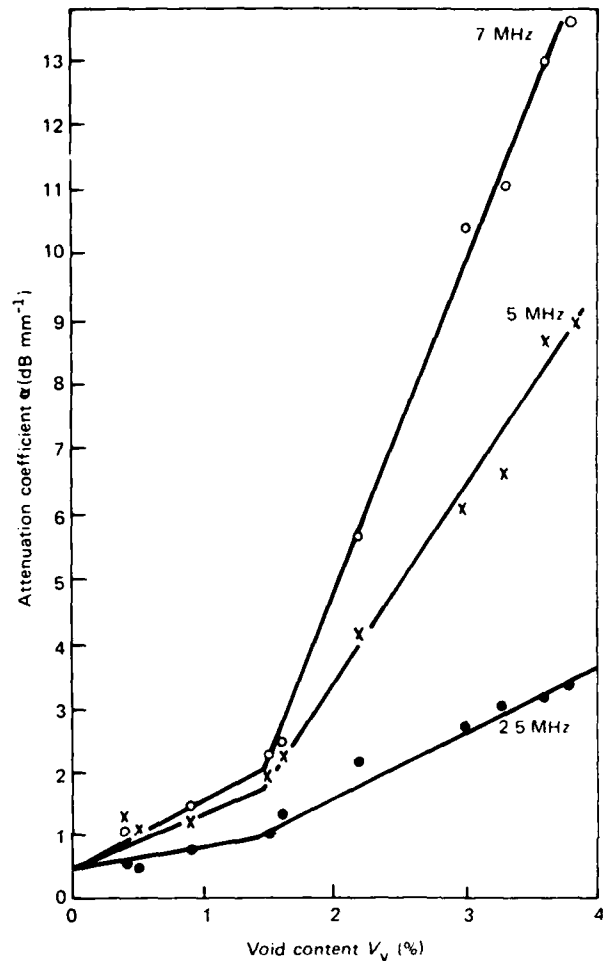


FIGURE 46. USE OF A BILINEAR FUNCTION TO DESCRIBE THE RELATIONSHIP BETWEEN VOID CONTENT AND ATTENUATION COEFFICIENT (From Ref. 38, Reproduced by permission of British Crown Copyright)

The ultrasonic attenuation method for measuring void content was further explored by Jones and Stone (Ref. 39). In this work the authors report on investigations using focused probes and on the relationship obtained between attenuation readings taken with focused probes, and those obtained with parallel probes. It was not found possible to correlate the readings taken with focused beam systems, notably because of the difficulty in establishing reliable data, but also because of the inherent scatter caused by the sensitivity of the system to small changes in the axial or angular position of the probe unit.

A simple stop was used in front of a parallel probe to produce a narrow parallel beam, giving improved resolution at the expense of some loss of power. The resolution of such a system is comparable with that of a focused probe, but since it does not exhibit a focal point, it is much less sensitive to positional errors. Difficulties, however, were still encountered in calibrating attenuation results obtained with a narrow beam against void content. This was because the narrow beam effectively integrated over too small a volume of material for the acid digestion method of void content determination to be used. Therefore, only tedious optical methods of calibration appear possible where a series of sections is taken in order to obtain a mean value of void content for the volume of material over which the beam integrates.

### 6. Detection of Moisture Degradation

One of the environmental conditions which is known to affect the mechanical properties of composites is moisture absorption (Ref. 40). As a result, there is continuing interest in the development of NDE techniques for the measurement of moisture and determination of strength degradation in composite materials. Several investigators have reported on the use of ultrasonics to determine moisture degradation in composite materials. In one study of environmental degradation, Kaelble performed an investigation to determine whether sound velocity or attenuation measurements were directly sensitive to the state of the interfacial bond as evaluated by moisture absorption, interlaminar shear strength, or fracture energy (Ref. 41). In experiments performed on graphite/epoxy specimens, Kaelble found that exposure to 95% relative humidity or water immersion at 100°C for times  $T \geq 200$  hours produces a 30 to 50% reduction in interlaminar shear strength, accompanied by a concurrent 2 to 5 fold increase in fracture toughness and acoustic absorption properties. These property changes were shown to be irreversible and directly related to cumulative moisture degradation of the fiber-matrix interfacial bond. The magnitude of the observed property changes were consistent with surface energy analysis and micro-mechanics predictions which show that fracture energy response optimizes at intermediate values of shear bond strength.

In follow-up work performed on a graphite/epoxy specimen subjected to length variable moisture exposure by partial submersion in a special container, Kaelble (Ref. 42) measured the longitudinal sound velocity  $C_L$  and acoustic absorption coefficient  $\alpha_1$ . Results of these measurements are shown in Figures 47 and 48. For ease of visual inspection, the curves in these figures

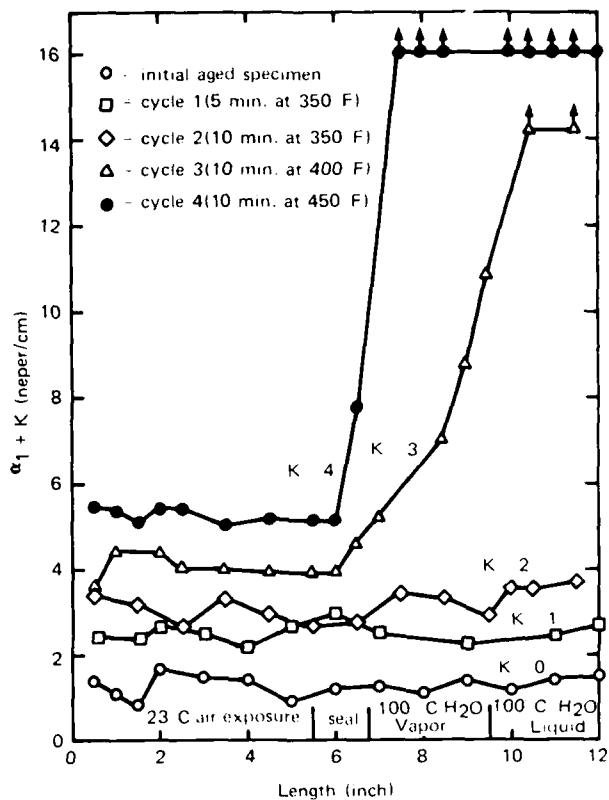
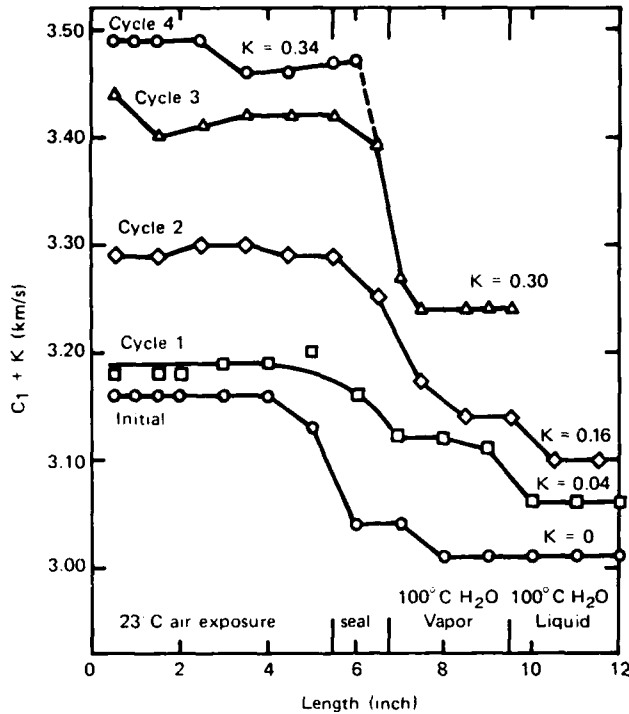


FIGURE 47. EFFECTS OF VARIED MOISTURE EXPOSURE AND SUBSEQUENT THERMAL CYCLES ON THE ACOUSTIC ATTENUATION  $\alpha_1$  OF COMPOSITE SC4 (From Ref. 42, Reproduced by permission of The American Society for Nondestructive Testing)

are separated by application of a vertical shift factor  $K$  to the actual measured values as indicated in the graphs. The lower curve of Figure 47 shows that acoustic absorption coefficient  $\alpha_1$  remains relatively constant with position, even though moisture exposure history varies with position. The 177°C (350°F) thermal shock cycles 1 and 2 indicated in Figure 47 also show nearly level  $\alpha_1$  values with position. In thermal shock cycles 3 and 4 with exposure at a temperature which exceeds the recommended service limit of 177°C (350°F), notable increases are observed in  $\alpha_1$  in the sections previously exposed to high moisture where  $L = 15.2$  to 30.5 cm (6 to 12 in.) In cycle 4, the high attenuation is due to internal cracking with visible evidence of internal delamination due to combined effects of high moisture and thermal cycling termed "hydrothermal damage". Conversely, in the lower moisture region, i.e.,  $L = 0$  to 15.2 cm (0 to 6 in.), the thermal shock cycles 1 through 4 leave  $\alpha_1$  essentially unchanged.



**FIGURE 48. EFFECTS OF VARIED MOISTURE EXPOSURE AND SUBSEQUENT THERMAL CYCLES ON THE ULTRASONIC VELOCITY  $C_1$  OF COMPOSITE SC4** (From Ref. 42, Reproduced by permission of The American Society for Nondestructive Testing)

Inspection of Figure 48 shows that the ultrasonic velocity at 23°C and 2.25 MHz is very sensitive to moisture content, as indicated by the variation of  $C_1$  with  $L$  shown by the lower curve. Thermal shock cycles 1 and 2 broaden the middle section region of variable  $C_1$ . Thermal shock cycles 3 and 4 produce more abrupt changes in  $C_1$  in the length region where a transition occurs from low to high moisture exposure, i.e.,  $L = 14$  to 16.5 in. (5.5 to 6.5 in.). Signal loss due to internal crack formation prevented  $C_1$  measurement for  $L$  greater than 16.5 cm (6.5 in.) subsequent to cycle 4.

Applications of ultrasonic inspection to moisture degradation in two graphite/epoxy systems were reported by Verette (Ref. 43). The specimens were immersed in 82°C (180°F) deionized water until saturation was reached. One specimen was prepared from "resin-starved" prepreg while the other specimen was of acceptable quality. Results of pulsed ultrasonic through transmission measurements taken in both the dry and saturated conditions are shown in Figure 49 and 50. Changes in acoustic velocity and attenuation in

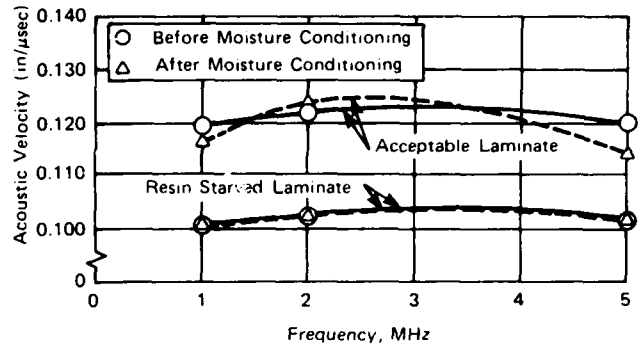


**FIGURE 49. MOISTURE EFFECT ON ACOUSTIC VELOCITY** (From Ref. 43, Reproduced by permission of American Institute of Aeronautics & Astronautics)

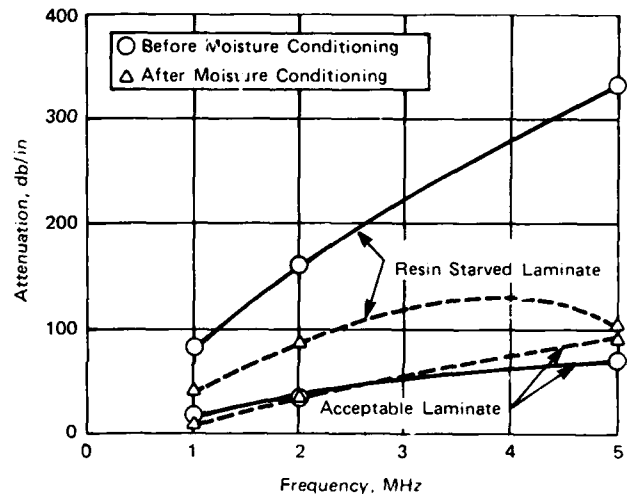


**FIGURE 50. MOISTURE EFFECT ON ACOUSTIC ATTENUATION** (From Ref. 43, Reproduced by permission of American Institute of Aeronautics & Astronautics)

going from the dry to wet condition were insignificant for the acceptable laminate, but the change was quite pronounced for the resin-starved laminate in the case of attenuation. The author suggests that the resin-starved laminate, which in the dry condition is quite attenuating possibly due to improperly coated fiber surfaces, takes on enough moisture to resemble the response of properly made laminate as far as ultrasonic attenuation is concerned.

A spectroscopic ultrasonic technique for measuring moisture in advanced composites was reported by Chang, et al (Ref. 44). The technique uses the

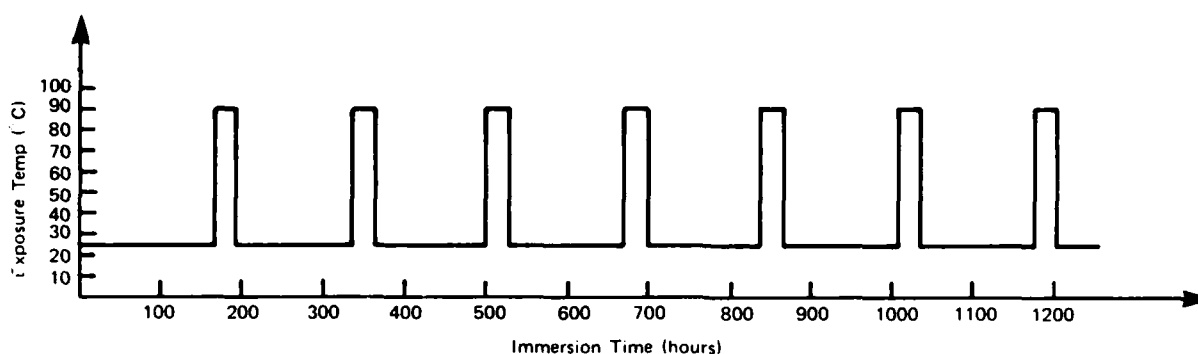


FIGURE 51. HYGROTHERMAL CYCLING HISTORY OF FRP SPECIMENS (From Ref. 45, Reproduced by permission of American Society for Testing & Materials, 1916 Race Street, Philadelphia, PA 19103).

principle of ultrasonic spectroscopy to obtain the interference of sound waves reflected from the front and back surfaces of the composite laminate. The frequency spectrum obtained by Fourier transform of the convoluted RF signals in the time domain provides information on the ultrasonic attenuation characteristics of the laminates. Experimental results obtained on 8-ply unidirectional laminates and cross-ply laminates treated under both hot and wet environmental conditions indicated an approximately 15% increase in attenuation in the frequency range of 12 to 20 MHz for laminates with approximately 1% moisture absorption. At an elevated temperature of 65.6°C (150°F) the ultrasonic attenuation differential increased to 20%.

A recent study of NDE of hygrothermal effects on fiber reinforced composites by ultrasonics has been reported by Bar-Cohen, et al (Ref. 45). In these tests, five-ply unidirectional carbon fiber reinforced laminates were immersed in room temperature (RT) water. Some of the specimens were transferred to hot (HT) water (90°C) immersion for one day each week. Water absorption was measured periodically by using an analytical balance. At certain stages in the hygrothermal history, specimens were simultaneously tested destructively and ultrasonically. A schematic diagram of the hygrothermal cycling history is presented in Figure 51.

Due to the complexity of internal processes that occur simultaneously under hygrothermal conditions (water diffusion in and out of the system, formation of voids and flaws, changes in matrix stiffness, fiber degradation, and disruption of interfacial or interlaminar bonding), it is difficult to justify a direct correlation between strength data and transient nondestructive test measurements. On the other hand, results of the measurements showed that when the effect of variations

in water absorption and desorption are deducted from the overall ultrasonic attenuation measurement, the net effect of material degradation may be detected and correlated with variations in strength derived from destructive tests. Such a correlation is shown in Figure 52 for carbon fiber reinforced plastic, as well as glass reinforced plastic and Kevlar reinforced plastic. The graph was obtained by plotting normalized flexural strength for the three composite systems with their respective ultrasonic attenuation data measured at RT conditions following a period of HT exposure. The trend in Figure 52 for normalized flexural strength versus ultrasonic attenuation is reasonably common for all three composite systems and agrees with the correlation between normalized tensile strength and attenuation found previously (Ref. 46). Based on these results, the authors conclude that ultrasonic attenuation data derived from nondestructive tests may provide an adequate means for the assessment of degradation in the structural performance of fiber reinforced composite materials under severe environmental exposure.

## 7. Commercial Aircraft Inspection

An example of the use of ultrasonics for nondestructive inspection of graphite/epoxy systems in the commercial aircraft industry has been reported by Hagemeyer (Ref. 47). The study described is part of a flight service evaluation of graphite/epoxy DC-10 rudders to determine the long-term behavior under actual service loads and environment. Various portions of the upper aft rudder are constructed of THORNEL 300/528 graphite/epoxy materials.

Because the geometry and size of the rudder makes immersion in a C-scan tank difficult, post-fabrication inspection is performed by contact pulse-echo ultrasonics or Fokker bond tester. In the pulse-echo ul-

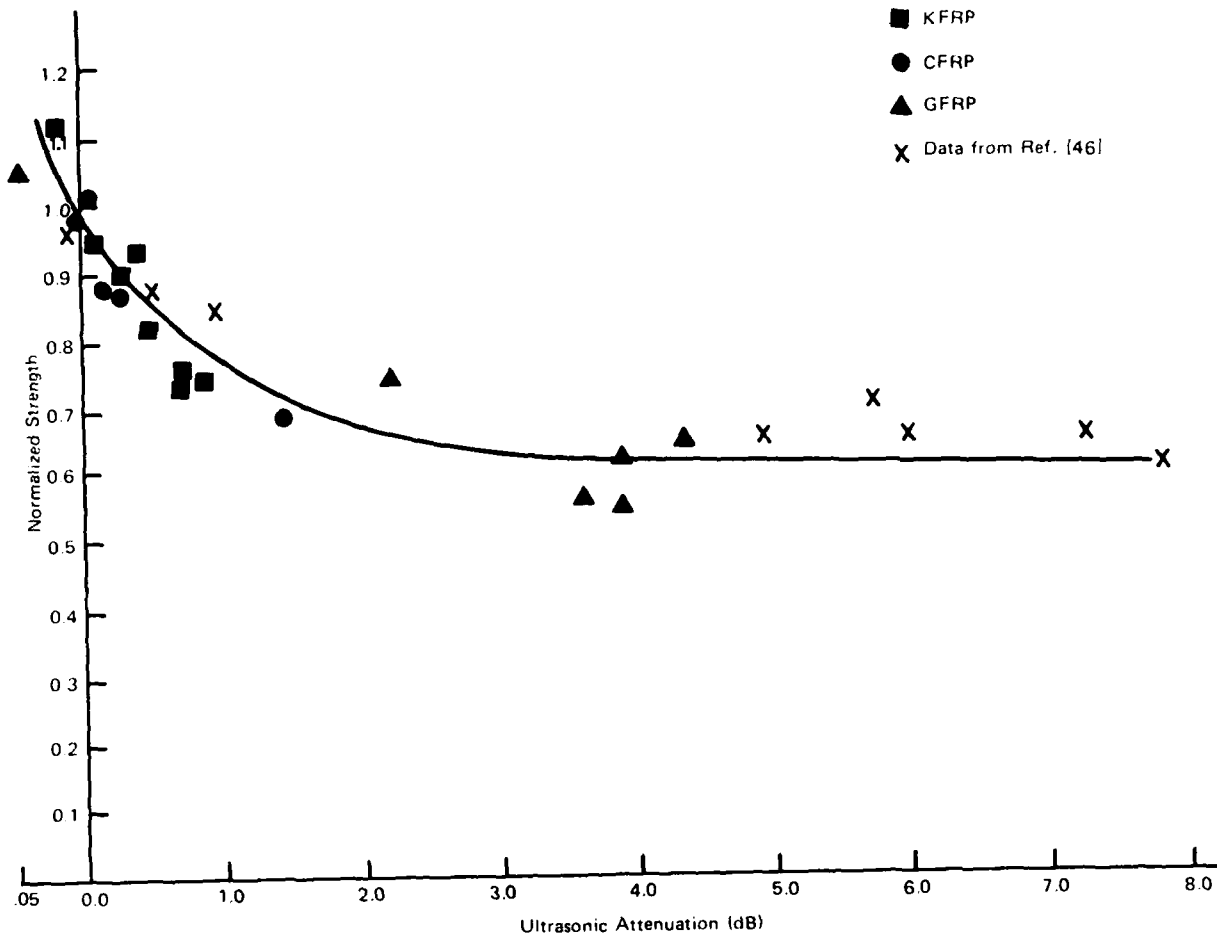


FIGURE 52. NORMALIZED FLEXURAL AND TENSILE STRENGTHS VERSUS ULTRASONIC ATTENUATION FOR DIFFERENT FIBER REINFORCED PLASTIC SYSTEMS (From Ref. 45, Reproduced by permission of American Society for Testing & Materials, 1916 Race Street, Philadelphia, PA 19103)

trasonic tests a longitudinal wave is transmitted through the laminate to inspect for delaminations and porosity. The Fokker bond tester is an ultrasonic resonance impedance type instrument employing a piezoelectric transducer as a sensor. It is used for the detection of porosity, voids, or delaminations.

During a five-year in-flight service exposure, ten graphite/epoxy rudders will be periodically inspected. In addition to visual inspection, ultrasonics will be used to inspect rib-to-skin and spar-to-skin bond areas adjacent to crank and hinge fittings every 3000 flight hours.

A description of nondestructive evaluation of other graphite/epoxy composite DC-10 structures

has been presented by Hagemeyer and Fassbender (Ref. 16). In addition to the radiography examinations previously described in Section III.A.5, ultrasonic inspections are also performed. Ultrasonic tests are usually performed at 10 MHz for thin laminates decreasing to 2.25 MHz for thicker laminates. Evaluation may be done by manual scanning or the evaluation may be automated using immersion techniques. Manual contact scanning has been used in conjunction with digital read-out ultrasonic thickness gauges to detect delaminations. If a composite laminate is sound, it will have a required thickness which can be measured with the ultrasonic thickness gauge. When the laminate is delaminated, the thickness reading indicates the existence of the delamination, and the thickness value indicates the depth of the delamination below the test surface. Complicated

shaped structures are usually inspected using the manual contact method.

Determination of interply porosity in composite laminates presents difficulties. Although methods have been described for measuring void content (Section III.B.5), it is doubtful if void content can be measured

with an accuracy much better than 0.5%, using any of the available techniques. Hagemaiier and Fassbender indicate an interest in establishing ultrasonic attenuation decibel-versus-thickness curves for 2.25, 5.0, and 10 MHz for pulse-echo, through transmission, and reflector plate techniques.

## IV. DISCUSSION

In this chapter, a general overview discussion will be presented of the state-of-the-art of nondestructive evaluation of graphite/epoxy composites, as determined from the literature review summarized in the preceding chapter. Included in this chapter is an application table which essentially serves as a guide to the literature on ultrasonic and radiographic inspection of graphite/epoxy composites. Also included is a summary narrative of side-by-side comparisons of several NDE techniques for inspection of composites.

To provide background for assessing the state-of-the-art using ultrasonic and penetrating radiation inspection techniques, additional information will be provided on the types and characteristics of defects found in composite materials (References 20 and 29). In general, defects arise in composites as a result of the fabrication process, or they are induced in service with age, loading, and environmental fluctuations. Although the definition of a "defect" is to some extent arbitrary, since features that are acceptable in one application may cause severe degradation in another, there are a number of fabrication-associated defects which have been identified as potentially detrimental to the mechanical strength of graphite/epoxy composites. These may be listed as:

1. Contaminates
2. Void contents (porosity)
3. Unpolymerized resin
4. Non-uniform matrix distribution
5. Condition of the fiber matrix interface
6. Foreign inclusions
7. Fiber volume fraction
8. Translaminar cracks
9. Delaminations
10. Incorrect fiber orientation
11. Cracking
12. Orientation and layup order of the plies
13. Ply end butt joints
14. Overlap or lack of side butt between plies

All of these factors acting singly, or in combination, can affect the structural performance of a component. The extent to which any combination of defects will prove detrimental is governed by the geometry of the structure, the exact location and orientation of the defects, the nature of the applied stress field, and the environment in which the component is required to operate.

In-service damage is caused principally by static overload, impact or fatigue, although other mechanisms such as creep and overheating are possible. This damage may take a number of forms varying from microscopic failures such as fracture or buckling of fibers due to interface failure and matrix cracking, to macroscopic events such as delaminations and visible cracks. In addition, there are changes in material properties caused by the environment. For example, in the case of aircraft, damage from lightning or bird strikes, rain or hail erosion, and the impact of debris on rough runways can occur with varying degrees of severity. Less obvious but equally important is the ingress of moisture caused by exposure to hot, moist atmospheres for long periods. Not only does moisture migrate along the fiber-matrix interface and weaken the interface bond, but it also diffuses through the resin itself and the rate of the diffusion is much increased if voids are present.

In assessing the current state-of-the-art in NDE, it appears that the techniques of x-ray radiography and ultrasonic pulse-echo or transmission attenuation are reasonably adequate for assessing the acceptability of laminates and inspecting fairly simple structures after fabrication. In their conventional form, these techniques yield only qualitative information concerning the inherent properties and service readiness of composite structures. The problems which seem to require most urgent attention are the quantitative evaluation of the significance of given defects, inspection of complex structures, and the study of the effects produced by service conditions of mechanical impact, fatigue, and hygrothermal degradation. Some advances are being made; for example, by combining NDE transducers and instrumentation with digital computers for improved signal acquisition and analysis, image generation and enhancement, and data storage and retrieval.

In the area of penetrating radiation, x-ray radiography is by far the most extensively used technique. It is an established production inspection tool, although safety considerations can impose restrictions. It is capable of detecting broken and misaligned filament, foreign objects or inclusions, and in certain cases, water intrusion and entrapment. With presently available x-ray equipment, it is possible to detect large flaws, air inclusions, and orientation and uniformity fluctuations in plastic composite materials as a function of material thickness, number of layers, and type of reinforcement. Radio-opaque penetrants, such as TBE, used in conjunction with radiography can help reveal the extent of

surface connected delaminations and voids. However, a less toxic alternative to TBE would be desirable.

The x-radiography method will no doubt become increasingly important with further development directed toward improving the detail that can be resolved by suitable choice of film-to-focus distance, acceleration voltage (i.e., energy level), x-ray film, and exposure time. Also, further development is expected of more sophisticated techniques such as stereo transmission methods, video radioscopy, computer-assisted radiography, and tomography.

In the area of ultrasonics, through transmission ultrasonic attenuation C-scan is probably the most sensitive and reliable technique for detecting defects such as delaminations, inclusions, and voids and for density evaluation. The application of ultrasonics, however, suffers due to the multiple scattering and attenuation accompanying wave propagation through a heterogeneous medium. In addition, the visco-elastic nature of the epoxy matrix produces a damping ratio which is an order of magnitude higher than in metals. Thus, crack detection that relies on scattering from flaws may be obscured by the dispersive nature of the matrix material. The combination of heterogeneity of composites, plus the dissipative nature of the organic matrix, makes crack detection by means of wave propagation considerably more complicated than in ordinary metals.

Despite these difficulties, ultrasonics is the most used and accepted NDE technique for inspection of composites; especially for discreet flaws, e.g., delaminations, cracks, inclusions, and voids. The ultrasonic method is also useful for determining property and geometric variations such as porosity, concentration differences, thickness, and elastic modulus. Measurement of these properties depends on a change in ultrasonic velocity or attenuation. As was pointed out in Chapter III, Section B.4, recent studies indicate that an acousto-ultrasonic NDE method may have potential for nondestructively determining the strength of composites. Although feasibility has been demonstrated, further experimental and theoretical development is needed. Application of the technique to diverse composite components awaits the refinement and adaptation of methods and instrumentation.

An interesting side-by-side comparison has been reported by Sendekyj, et al (Ref. 48) of damage indications obtained by using TBE enhanced x-ray radiography, through transmission ultrasonic C-scan, and holographic NDE methods on various composite specimens. Results were obtained for (a) graphite/epoxy specimens

containing fatigue induced damage regions growing from surface notches and through-the-thickness circular holes, and (b) hybrid composite specimens containing static loading induced damage regions near central through-the-thickness slits. In general, it was found that the TBE enhanced x-ray nondestructive inspection method gave the most detailed description of the damage, while the ultrasonic C-scan gave the least information.

In relation to the subject of this survey, the conclusions and recommendations reached by Sendekyj et al, relevant to the radiographic and ultrasonic detection techniques are presented below. (The reader is referred to the original document (Ref. 48) for additional details.)

#### Conclusions:

1. TBE enhanced x-ray photography gives the most detailed information on the nature and planar distribution of damage in composites. It is capable of finding fiber fractures, matrix cracks, and delaminations.
2. Through transmission ultrasonic C-scans show the planar extent of delaminations without giving any information on either matrix crack or fractured fibers.
3. Neither of these two NDE methods give a complete picture of the damage in composites.

#### Recommendations:

1. An x-ray opaque fluid that is not as toxic as TBE should be found and used in future applications of the enhanced x-ray NDE method.
2. A procedure for using enhanced x-ray photography for obtaining information on through-the-thickness distribution of damage in composites should be developed. Some of this desirable information may be obtained by x-raying the specimen edge-wise or making stereo pair x-ray photographs of the specimen. It may also be possible to construct a three-dimensional image of the damage by using tomography.
3. Since the through transmission ultrasonic C-scan method provides very limited informa-

tion in composites, it should not be used for damage documentation purposes. Instead, more sophisticated acoustic imaging techniques (e.g., the pulse-echo method) should be used.

4. Until a fully satisfactory NDE method for obtaining an accurate picture of damage in composites is developed, a combination of NDE methods should be used.

In Table VIII is presented an Application Table, based on the literature covered in this state-of-the-art survey to provide the reader with a guide to relevant documents. This table lists all pertinent documents cov-

ered in this survey and indicates which NDE techniques have been investigated, and/or applied, for specific defect and property determinations in graphite/epoxy composites. In the table, defects or properties are listed and categorized in the left-hand column, while NDE methods are listed along the top. The body of the table contains numbers keyed to the Bibliography (Appendix B) specifying which NDE methods have been reported for the various defects or properties. This table, together with the comprehensive Bibliography included in Appendix B, and the narrative presented in Chapter III, should provide the reader with a reasonably comprehensive survey of the state-of-the-art in the nondestructive evaluation of graphite/epoxy composites, using ultrasonics and radiography.

**TABLE VIII**  
**APPLICATION OF RADIOGRAPHY AND ULTRASONICS TO**  
**NONDESTRUCTIVE EVALUATION OF GRAPHITE FIBER**  
**REINFORCED PLASTIC COMPOSITES**

<u>Defects/Property Variations</u>	<u>Radiography</u>	<u>Ultrasonics</u>
Inclusions	1, 2, 3, 4, 56	3, 4, 56
Debonds/Delaminations	1, 5, 45, 6, 56	7, 8, 2, 9, 10, 11, 12, 13, 3, 14, 15, 16, 53, 54, 56
Voids	2, 17	7, 18, 19, 20, 4, 43, 17, 9, 42, 13, 21
Cracking	1, 45, 57	7, 12, 57
Defects (General)	22, 44, 23, 46, 21, 24, 52	22, 25, 24, 44, 26, 23, 46, 21, 52, 58, 59, 62, 63
Fatigue	27, 5, 6, 61	28, 27, 26, 48, 5, 29, 50, 61
Impact Damage	30, 4	30, 4
Resin Variations	3, 14	8, 3
Cure Variations	3	3
Fiber Alignment	2, 47, 31, 14	11
Broken Fibers	47, 31, 14	8
Volume Fractions	32	33
Porosity	4, 3	4, 10, 3, 7, 33
Density	3	3
Strength		34, 35, 49, 33
Moisture Degradation/Content		36, 37, 38, 39, 40, 25, 41, 55, 60
Reference Standards	3, 15	3, 15
Resin Content	32	
Thickness		51

## V. REFERENCES

1. Teller, C.M., Burkhardt, G.L., and Matzkanin, G.A., "Nondestructive Evaluation of Carbon-Carbon Composites: A State-of-the-Art Survey," TB-79-24, ADA071973, Final Report, Contract N00014-77-C-0510, ONR and AFSOR, November 1978.
2. Matzkanin, G.A., Burkhardt, G.L., and Teller, C.M., "Nondestructive Evaluation of Fiber Reinforced Epoxy Composites, a State-of-the-Art Survey," Final Report, Contract DLA-900-77-C-3733, U.S. Army AVRADCOM, 184 pp, April 1979.
3. Weeton, J.W. and Scala, E., eds., *Composites: State-of-the-Art*, pp 25-66, 1974.
4. Wehrenberg, Robert H. II, "The Reinforcing Fibers—Performance at a Price," MATERIALS ENGINEERING, pp 26-28, January 1980.
5. Vary, A., "Nondestructive Evaluation Technique Guide," NASA SP-3079, 105 pp, 1973.
6. "Nondestructive Testing, A Survey," NASA SP-5113, 282 pp, 1973.
7. Domanus, J.C. and Lilholt, H., "Non-Destructive Control of Carbon Fibre Reinforced Composites by Soft X-Ray Radiography," Proc. International Conference on Composite Materials, pp 1072-1092, 1978.
8. Sturgeon, J.B., "Fatigue Mechanisms, Characterisation of Defects and their Detection in Reinforced Plastics Materials," BRITISH J. NDT, 20, pp 303-310, November 1978.
9. Chang, F.H., Gordon, D.E., Rodini, B.T., and McDaniel, R.H., "Real-Time Characterization of Damage Growth in Graphite/Epoxy Laminates," J. COMPOSITE MATERIALS, 10, pp 182-192, July 1976.
10. Martin, B.G., "An Analysis of Radiographic Techniques for Measuring Resin Content in Graphite Fiber Reinforced Epoxy Resin Composites," MATERIALS EVALUATION, 35, pp 65-68, 75, September 1977.
11. Reynolds, G.M., "Neutron Gauging Systems," ASTM STP 586, pp 58-73, 1976.
12. Chang, F.H., Couchman, J.C., Eisenmann, J.R., and Yee, B.G.W., "Application of a Special X-Ray Nondestructive Testing Technique for Monitoring Damage Zone Growth in Composite Laminates," ASTM STP 580, presented at Symposium on Composite Reliability, Las Vegas, pp 176-190, April 1974.
13. Bailey, C.D., Freeman, S.M., and Hamilton, J.M., "Detection and Evaluation of Impact Damage in Graphite/Epoxy Composites," Mater. and Processes in Service Performance, 9th SAMPE Tech. Conf., pp 491-503, October 1977.
14. Crane, R.L., Chang, F.H., and Allinikov, S., "The Use of Radiographically Opaque Fibers to Aid the Inspection of Composites," MATERIALS EVALUATION, 36, pp 69-71, September 1978.
15. Roberts, E. and Vary, A., "Inspection of Composites Using a Computer-Based Real-Time Radiographic Facility," Proc. of Automated Inspection & Product Control Conf., pp 139-150, October 1976.
16. Hagemaiier, D.J. and Fassbender, R.H., "Non-destructive Testing of Advanced Composites," Douglas Aircraft Paper 6774, presented at 1978 SAE Aerospace Mtg., pp 1-9, November 1978.
17. Phelps, M.L., "Assessment of State-of-the-Art of In-Service Inspection Methods for Graphite Epoxy Composite Structures on Commercial Transport Aircraft," Interim Report, NASA Contract NAS 1-15304, pp 1-22, January 1979.
18. Chuang, S.N. and Starrett, H.S., "Thermal and Mechanical Properties of an FMI 2.2.1 Carbon-Carbon Composite Materials," AD-B021 9041, Final Report Contract F33615-74-C-5029, AFMI TR-76-134, April 1977.
19. Koenig, J.R. and Pears, C.D., "Thermal and Mechanical Properties of Carbon-Carbon Composites of Various Weave Spacings," AD-B016 1491, Final Report Contract N60921-74-C-0187, December 1976.

20. Stone, D.E.W., "Non-Destructive Inspection of Composite Materials for Aircraft Structural Applications," *BRITISH J. NDT*, pp 65-75, March 1978.
21. Stone, D.E.W. and Clarke, B., "Ultrasonic Attenuation as a Measure of Void Content in Carbon-Fibre Reinforced Plastics," *NON-DESTRUCTIVE TESTING*, 8, No. 3, pp 137-145, 1975.
22. Jones, B.R. and Stone, D.E.W., "Towards an Ultrasonic-Attenuation Technique to Measure Void Content in Carbon-Fibre Composites," *NON-DESTRUCTIVE TESTING*, 9, No. 2, pp 71-79, 1976.
23. Chang, F.H., Yee, W.G.W., and Couchman, J.C., "Spectral Analysis Technique of Ultrasonic NDT of Advanced Composite Materials," *NON-DESTRUCTIVE TESTING*, 7, No. 4, pp 194-198, August 1974.
24. van Dreumel, W.H.M., "Ultrasonic Scanning for Quality Control of Advanced Fibre Composites," *NDT INTERNATIONAL*, 11, pp 233-235, October 1978.
25. Blake, R.A., Jr., "Ultrasonic NDE of Composite Materials," The University of Delaware, 114 pp, 1979.
26. Knollman, G.C., Carver, D., and Hartog, J.J., "Acoustic Imaging of Composites—The Ultrasonic Test That Requires No Interpretation," *MATERIALS EVALUATION*, 36, pp 41-47, November 1978.
27. Bar-Cohen, Y., Arnon, U., and Meron, M., "Defect Detection and Characterization in Composite Sandwich Structure by Ultrasonics," *SAMPE J.*, 14, No. 1, pp 4-8, January-February 1978.
28. Sturgeon, J.B. and McLaughlin, K.S., R.A.E. Techn. Rep. 76153, 1976.
29. Daniel, I.M. and Liber, T., "Nondestructive Evaluation Techniques for Composite Materials," *Proc. of 12th NDE Symposium*, pp 226-244, 1979.
30. Saluja, H.S. and Henneke, E.G., "Ultrasonic Attenuation Measurement of Fatigue Damage in Graphite-Epoxy Composite Laminates," *Proc. of 12th NDE Symposium*, pp 260-268, 1979.
31. Papadakis, E.P., "Ultrasonic Attenuation in Thin Specimens Driven Through Buffer Rods," *J. OF ACOUS. SOC. AMER.*, 44, pp 724-734, 1963.
32. Hayford, D.T., Henneke, E.G., and Stinchcomb, W.W., "A Technique for Determining an Absolute Value of Ultrasonic Attenuation in Thin Composite Materials," *J. COMPOSITE MATERIALS*, 11, pp 429-444, 1977.
33. Williams, J.H., Jr. and Doll, B., "Ultrasonic Attenuation as an Indicator of Fatigue Life of Graphite Fiber Epoxy Composite," *MATERIALS EVALUATION*, 38, pp 33-37, May 1980.
34. Hayford, D.T., Henneke, E.G., and Stinchcomb, W.W., "The Correlation of Ultrasonic Attenuation and Shear Strength in Graphite Polyimide Composites," *J. COMPOSITE MATERIALS*, 11, pp 429-444, October 1977.
35. Vary, A. and Bowles, K.J., "Ultrasonic Evaluation of the Strength of Unidirectional Graphite-Polyimide Composites," *Proc. of 11th NDE Symposium*, pp 242-258, 1977.
36. Vary, A. and Lark, R.F., "Correlation of Fiber Composite Tensile Strength with the Ultrasonic Stress Wave Factor," *J. TESTING AND EVALUATION*, 7, pp 185-191, July 1979.
37. Judd, N.C.W. and Wright, W.W., "Voids and Their Effects on the Mechanical Properties of Composites—An Appraisal," *SAMPE J.*, 14, No. 1, pp 10-14, January-February 1978.
38. Stone, D.E.W. and Clarke, B., "Ultrasonic Attenuation as a Measure of Void Content in Carbon-Fibre Reinforced Plastics," *NON-DESTRUCTIVE TESTING*, 8, No. 3, pp 137-145, June 1975.
39. Jones, B.R. and Stone, D.E.W., "Towards an Ultrasonic-Attenuation Technique to Measure Void Content in Carbon-Fibre Composites," *NON-DESTRUCTIVE TESTING*, 9, No. 2, pp 71-79, April 1976.
40. "Proceedings Air Force Workshop on Durability Characteristics of Resin Matrix Composites," Battelle/Columbus Laboratories, September 30-October 2, 1975.

41. Kaelble, D.H., "Detection of Hydrothermal Aging in Composite Materials," Proc. of AR-PA/AFML Rev. of Quantitative NDE, pp 549-564, December 1975.
42. Kaelble, D.H. and Dynes, P.J., "Methods for Detecting Moisture Degradation in Graphite/Epoxy Composites," MATERIALS EVALUATION, 35, pp 103-108, April 1977.
43. Verette, R.M., "Temperature/Humidity Effects on the Strength of Graphite/Epoxy Laminates," AIAA Paper No. 75-1011, pp 1-10, 1975.
44. Chang, F.H., Bell, J.R., Carter, H.G., and Yee, B.G.W., "Measurement of Moisture Content in Advanced Composites by an Ultrasonic Technique," Proc. 11th NDE Symposium, p 69, 1977.
45. Bar-Cohen, Y., Meron, M., and Ishai, O., "Non-destructive Evaluation of Hygrothermal Effects on Fiber-Reinforced Plastic Laminates," J. TESTING AND EVALUATION, 7, pp 291-296, September 1979.
46. Meron, M., Bar-Cohen, Y., and Ishai, O., "Non-destructive Evaluation of Strength Degradation in Glass-Reinforced Plastics as a Result of Environmental Effects," J. TESTING AND EVALUATION, 5, pp 394-396, November 1977.
47. Hagemaiier, D.J., "NDT of DC-10 Graphite-Epoxy Rudder," MATERIALS EVALUATION, 36, pp 57-61, May 1978.
48. Sendeckyj, G.P., Maddux, G.E., and Tracy, N.A., "Comparison of Holographic, Radiographic, and Ultrasonic Techniques for Damage Detection in Composite Materials," Proc. of International Conf. on Composite Materials, Toronto, Canada, pp 1037-1056, April 1978.

## APPENDIX A LITERATURE SEARCH STRATEGY

Several computerized literature searches were conducted in the broad context of NDE of composites. Included in the searches in addition to graphite reinforced composite were glass and Kevlar reinforced composite. The files searched included the Nondestructive Testing Information Analysis Center (NTIAC) files, the Defense Documentation Center (DDC) files, and commercial open literature files. In each case the objective was to select a bibliography which would include virtually all the literature on NDE of composites in general, but more specifically on glass, Kevlar and graphite fiber reinforced composites. In order to do so, the searches were designed to encompass the broadest range possible commensurate with the retrieval of bibliographies which were of manageable size for manual review.

The NTIAC search strategy is shown in Table AI. In the search, one term from each group of terms separated by an "and" must be associated with a document for it to appear as a find. Some terms appear in both groups to assure that any document associated with only that term will be found. No NDE terms appear in this search since all NTIAC documents concern NDE.

Two searches were run in the DDC file; these strategies are shown in Tables AII and AIII. A different

group of terms is used in the DDC searches since descriptors in this file differ from those in the NTIAC file in some cases. A broad group of NDE terms is also included. The "%" symbol truncates the term in the same manner as in the NTIAC file. The DDC search excluded all NTIAC documents to avoid duplication.

The open literature searches utilized the Lockheed/DIALOG system to search the following files: (1) COMPENDEX (COMPUTERIZED ENGINEERING INDEX), (2) National Technical Information Service (NTIS), (3) ISMEC - Mechanical Engineering, and (4) Chemical Abstracts. The strategies for the open literature searches are shown in Tables AIV and AV. The "?" after some terms performs truncation. The (w) between multi-word terms is necessary to retrieve those groups of words as a single term.

The literature search results are shown in Table AVI. Out of a total of 2787 finds, 145 documents were judged relevant to NDE of graphite fiber reinforced composites based on a review of abstracts. Sixty-three of these documents contain information on applications of ultrasonics or radiography and formed the basis for this survey.

TABLE AI  
NTIAC SEARCH

<p>composite materials polymer matrix composites fiber reinforced composites filament wound construction reinforced plastics fibers matrix</p>	and	<p>polymers fiberglass glass plastics carbon graphite epoxy composite materials polymer matrix composites fiber reinforced composites filament wound construction reinforced plastics</p>
--	-----	---

TABLE AII  
DDC SEARCH NO. 1

%composite material		%aramid		%nondestruct
composite structures		%carbon reinforced		ultrasonics
%fiber reinforced		%carbon fiber		%ultrasonic test
matrix materials		%graphite fiber		%eddy current
%carbon reinforced		%graphite reinforced		x-ray diffraction
%carbon fiber		graphite composites		%radiogr
%graphite fiber		%glass fiber		%radiometr
%graphite reinforced	and	%glass reinforced	and	visual inspection
graphite composites		fiberglass		%microscop
%glass fiber		%fiberglass reinforced		%electrical resist
%glass reinforced		%epoxy		neutron radiography
fiberglass		%plastic		interferometry
%fiberglass reinforced		%polymer		holography
%aramid		%fiber		acoustic emissions
		%matrix		acoustics
		%filament		%penetra
		%polyamide		%thermogra
		%polyimide		liquid crystals
				microwaves
				acoustooptics
				x rays
				infrared image
				infrared images
				dielectric

TABLE AIII  
DDC SEARCH NO. 2

bulk modulus		%carbon fiber		%glass fiber
degradation		%carbon reinforced		%glass reinforced
%detect		%composite material		graphite composites
determination		composite structures		%graphite fiber
elastic properties	and	%fiber reinforced	and	%graphite reinforced
fatigue(mechanics)		fiberglass		%Kevlar
instrumentation		%fiberglass reinforced		matrix materials
%measur				reinforced plastics
mechanical properties				
%nondestruct				
strength				
tensile properties				
test methods				
toughness				

TABLE AIV  
OPEN LITERATURE SEARCH NO. 1

GROUP A	GROUP B	GROUP C	GROUP D
Carbon (w) Reinforced	Composite ?	Epoxy ?	Nondestruct ?
Carbon (w) Reinforcement	Fiber (w) Reinforced	Plastics ?	Ultrasonic ?
Carbon (w) Fiber	Fiber (w) Reinforcement	Polymer ?	Eddy (w) Current
Carbon (w) Fibers			Eddy (w) Currents
Carbon (w) Phenolic			X (w) Ray
Graphite (w) Reinforced			Radiograph ?
Graphite (w) Reinforcement			Radiometr ?
Graphite (w) Fiber			Visual
Graphite (w) Fibers			Microscop ?
Graphite (w) Composite			Electrical (w) Resistance
Graphite (w) Composites			Electrical (w) Resistivity
Glass (w) Reinforced			Neutron (w) Radiography
Fiberglass ?			Neutron (w) Radiography
Kevlar ?			Interferometry
			Holography (w) interfermetry
			Holography
			Acoustic (w) Emissions
			Acoustic (w) Emission
			Acoustic
			Penetrant
			Thermogra ?
			Liquid (w) Crystal
			Liquid (w) Crystals
			Gamma (w) Ray
			Dielectric

SEARCH STRATEGY:  
(Group A and Group D) or (Group B and Group C and Group D)

TABLE AV  
OPEN LITERATURE SEARCH NO. 2

measur?		composite(w)material?
detect?		composite(w)structure?
determination		fiber(w)reinforced
instrumentation		matrix(w)material?
nondestruct?		carbon(w)reinforced
degradation		carbon(w)fiber
mechanical(w)properties		graphite(w)fiber
bulk(w)modulus	and	graphite(w)reinforced
elastic(w)properties		graphite(w)composite?
fatigue		glass(w)fiber?
strength		glass(w)reinforced
tensile(w)properties		glass(w)reinforced
toughness		fiberglass
		reinforced(w)plastic?
		Kevlar?

TABLE AVI  
LITERATURE SEARCH RESULTS

FILE	TOTAL FINDS	NDE OF GRAPHITE COMPOSITES
NTIAC	552	41
NTIS	550	21
COMPENDEX	909	27
ISMEC	76	10
Chemical Abstracts	231	26
DDC	469	20
TOTALS	2787	145

## APPENDIX B BIBLIOGRAPHY

1. Domanus, J.C. and Lilholt, H., "Nondestructive Control of Carbon Fibre Reinforced Composites by Soft X-Ray Radiography," Proc. International Conf. on Composite Materials; 16-20 April 1978; Toronto, Canada; pp. 1072-1092.
2. Tober, Gustav and Schnell, Hilmar, "Detectability of Flaws in Boron and Carbon Composite Parts," AGARD Conf. Proc. No. 234-NDI Relationships to Aircraft Design and Materials; 27-28 September 1977; Voss, Norway; pp. 17/1-17/14.
3. Pless, W.M. and Lewis, W.H., "The Fabrication, Testing and Delivery of Boron/Epoxy and Graphite/Epoxy Nondestructive Test Standards," Lockheed-Georgia Co., Marietta, Georgia; Final Report, Contract NAS8-27565; Report No. NASA-CR-61374, ER-11199; December 1971; 70 pp.
4. Hagemaiier, D.J. and Fassbender, R.H., "Nondestructive Testing of Advanced Composites," Douglas Aircraft Paper 6774, presented at SAE Aerospace Meeting; November 1978; pp. 1-9.
5. Daniel, I.M. and Liber, T., "Nondestructive Evaluation of Composite Materials," Proc. 4th International Conf. Automated Inspection and Product Control; 7-9 November 1978; Chicago, Illinois; pp. 263-292.
6. Chang, F.H., Gordon, D.E., Rodini, B.T., and McDaniel, R.H., "Real-Time Characterization of Damage Growth in Graphite/Epoxy Laminates," J. COMPOSITE MATER.; Vol. 10; July 1976; pp. 182-192.
7. Hagemaiier, D.J., "NDT of DC-10 Graphite-Epoxy Rudder," MATERIALS EVALUATION; Vol. 36, No. 6; May 1978; pp. 57-61.
8. Bar-Cohen, Y., Arnon, U., and Meron, M., "Defect Detection and Characterization in Composite Sandwich Structure by Ultrasonics," SAMPE J.; Vol. 14, No. 1; January-February 1978; pp. 4-8.
9. Hagemaiier, Don, "Ultrasonic Applications in the Aerospace Industry," SAE Trans.; Vol. 83; 1974; Paper No. 740811; pp. 2767-2796.
10. Knollman, G.C., Carver, D., and Hartog, J.J., "Acoustic Imaging of Composites--The Ultrasonic Test That Requires No Interpretation," MATERIALS EVALUATION; Vol. 36, No. 12; November 1978; pp. 41-47.
11. Van Dremel, W.H.M., "Ultrasonic Scanning for Quality Control of Advanced Fibre Composites," NDT INTERNATIONAL; Vol. 11, No. 5; October 1978; pp. 233-235.
12. Sturgeon, J.B., "Fatigue Mechanisms, Characterization of Defects and Their Detection in Reinforced Plastics Materials," BR. J. NONDESTR. TEST.; Vol. 20, No. 6; November 1978; pp. 303-310.
13. Chang, Francis H., Yee, W.G.W., and Couchman, James C., "Spectral Analysis Technique of Ultrasonic NDT of Advanced Composite Materials," NON-DESTR. TEST.; Vol. 7, No. 4; August 1974; pp. 194-198.
14. Hagemaiier, D.J., McFaul, H.J., and Parks, J.T., "Nondestructive Testing Techniques for Fiberglass, Graphite Fiber, and Boron Fiber Composite Aircraft Structures," Paper presented to ASTM Committee D-30; Detroit, Michigan; 29 October 1969; 19 pp.
15. Blosser, E.G., McGovern, S.A., and Dhonau, O.E., "S-3A Graphite/Epoxy Spoiler Development Program, Volume II," LTV Aerospace Corp., Dallas, Texas, Vought Systems Div.; Final Technical Report No. 2-53443/4R-3172-Vol. 2; Contract No. N62269-73-C-0610; July 1975; 61 pp.
16. Stoecklin, R.L., "Development, Manufacturing, and Test of Graphite-Epoxy Composite Spoilers for Flight Service on 737 Transport Aircraft," Boeing Commercial Airplane Co., Seattle, Washington; Final Report No. NASA-CR-132682; Contract No. NAS1-11668; October 1976; 96 pp.
17. Judd, N.C.W. and Wright, W.W., "Voids and Their Effects on the Mechanical Properties of Composites--An Appraisal," SAMPE J.; Vol. 14, No. 1; January/February 1978; pp. 10-14.
18. Olster, Elliot F., "Effect of Voids on Graphite Fiber Reinforced Composites," Final Report; Contract No. N00019-71-C-0305; July 1972; 162 pp.
19. Lenoe, Edward M., "Effects of Voids on Mechanical Properties of Graphite Fiber Composites," Final Report; Contract No. N00019-70-C-0242; November 1970; 55 pp.
20. Lenoe, Edward M., "The Effect of Voids on the Mechanical Properties of High Modulus Graphite Fiber/Epoxy-Reinforced Composites," Report No. AVSD-0170-70-RR; Contract No. N00019-69-C-0208; March 1970; 191 pp.
21. Stone, D.E.W., "Nondestructive Inspection of Composite Materials for Aircraft Structural Applications," AGARD Conf. Proc. No. 234--NDI Relationships to Aircraft Design and Materials; 27-28 September 1977; Voss, Norway; pp. 14/1-14/18.

22. Sheldon, W.H., "Comparative Evaluation of Potential NDE Techniques for Inspection of Advanced Composite Structures," *MATERIALS EVALUATION*; Vol. 36, No. 2; February 1978; pp. 41-46.
23. Phelps, M.L., "Assessment of State-of-the-Art of In-Service Inspection Methods for Graphite Epoxy Composite Structures on Commercial Transport Aircraft," Interim Report NASA CR-158969; Contract No. NAS1-15304; January 1979; 56 pp.
24. Hagemaiier, D.J., McFaul, H.J., and Moon, D., "Nondestructive Testing of Graphite Fiber Composite Structures," *MATERIALS EVALUATION*; Vol. 29, No. 6; June 1971; pp. 133-140.
25. Stoecklin, Robert L., "737 Graphite Composite Flight Spoiler Flight Service Evaluation," Boeing Commercial Airplane Co., Seattle, Washington; 3rd Annual Rept.; NASA-CR-145207; Contract No. NAS1-11668; August 1977; 29 pp.
26. Ramkumar, R.L., Kulkarni, S.V., and Pipes, R.B., "Definition and Modeling of Critical Flaws in Graphite Fiber Reinforced Epoxy Resin Matrix Composite Materials," Materials Sciences Corp., Blue Bell, Pennsylvania; Final Rept.; NADC 76228-30; Contract No. N62269-77-C-0092; January 1978; 138 pp.
27. Sendekyj, G.P., Maddux, G.E., and Tracy, N.A., "Comparison of Holographic, Radiographic, and Ultrasonic Techniques for Damage Detection in Composite Materials," Proc. International Conf. on Composite Materials; 16-20 April 1978; Toronto, Canada; pp. 1037-1056.
28. Stalnaker, David O. and Stinchcomb, Wayne W., "An Investigation of Edge Damage Development in Quasi-Isotropic Graphite Epoxy Laminates," Interim Report, Contract No. F33615-75-C-5119; Report No. VPI-E-77-24; September 1977; 91 pp.
29. Saluja, Harminder S. and Henneke, Edmund G., "Ultrasonic Attenuation Measurement of Fatigue Damage in Graphite-Epoxy Composite Laminates," Proc. 12th Symposium on NDE; 24-26 April 1979; San Antonio, Texas; pp. 260-268.
30. Bailey, C.D., Freeman, S.M., and Hamilton, J.M., "Detection and Evaluation of Impact Damage in Graphite/Epoxy Composites," Mater. and Processes In-Service Performance; Soc. for Advancement of Mater. and Processing Eng.; 9th Tech. Conf.; Atlanta, Georgia; October 1977; pp. 491-503.
31. Crane, R.L., Chang, F., and Allinikov, S., "The Use of Radiographically Opaque Fibers to Aid the Inspection of Composites," *MATERIALS EVALUATION*; Vol. 36, No. 10; September 1978; pp. 69-71.
32. Martin, B.G., "An Analysis of Radiographic Techniques for Measuring Resin Content in Graphite Fiber Reinforced Epoxy Resin Composites," *MATERIALS EVALUATION*; Vol. 35, No. 9; September 1977; pp. 65-68, 75.
33. Vary, Alex and Lark, R.F., "Correlation of Fiber Composite Tensile Strength with the Ultrasonic Stress Wave Factor," *JOURNAL OF TESTING AND EVALUATION*; Vol. 7, No. 4; July 1979; pp. 185-191.
34. Hayford, D.T., Henneke, E.G. II, and Stinchcomb, W.W., "Correlation of Ultrasonic Attenuation and Shear Strength in Graphite-Polyimide Composites," *J. COMPOS. MATER.*; Vol. 11; October 1977; pp. 429-444.
35. Vary, Alex and Bowles, Kenneth J., "Ultrasonic-Acoustic Technique for Nondestructive Evaluation of Fiber Composite Quality," *POLYM. ENG. SCI.*; Vol. 19, No. 5; April 1979; pp. 373-376.
36. Verette, R.M., "Temperature/Humidity Effects on the Strength of Graphite/Epoxy Laminates," AIAA Aircraft Systems and Tech. Meeting, Los Angeles, California; August 4-7, 1975; Paper 75-1011; 11 pp.
37. Bar-Cohen, Y., Meron, Michael, and Ishai, O., "Nondestructive Evaluation of Hygrothermal Effects on Fiber-Reinforced Plastic Laminates," *JOURNAL OF TESTING AND EVALUATION*; Vol. 7, No. 5; September 1979; pp. 291-296.
38. Kaelble, David H., "Kinetics of Moisture Degradation in Graphite-Epoxy Composites," Proc. Interdisciplinary Workshop for Quantitative Flaw Definition; AFML-TR-74-238; November 1974; pp. 384-405.
39. Chang, F.H., Bell, J.R., Carter, H.G., and Yee, B.G.W., "Measurement of Moisture Content in Advanced Composites by an Ultrasonic Technique," Proc. 11th Symposium on Nondestr. Eval.; April 20-22, 1977; San Antonio, Texas; p. 69.
40. Kaelble, D.H. and Dynes, P.J., "Methods for Detecting Moisture Degradation in Graphite-Epoxy Composites," *MATERIALS EVALUATION*; Vol. 35, No. 4; April 1977; pp. 103-108.
41. Kaelble, D.H. and Dynes, P.J., "Nondestructive Tests for Shear Strength Degradation of a Graphite-Epoxy Composite," ASTM Spec. Tech. Publ. No. 617; Compos. Mater. Test and Des. 4th Conf.; Valley Forge, Pennsylvania; May 3-4, 1976; pp. 190-200.
42. Stone, D.E.W. and Clarke, B., "Ultrasonic Attenuation as a Measure of Void Content in Carbon-Fibre Reinforced Plastics," *NON-DESTRUCTIVE TESTING*; pp. 137-145; June 1975.

43. Jones, B.R. and Stone, D.E.W., "Towards an Ultrasonic-Attenuation Technique to Measure Void Content in Carbon-Fibre Composites," NON-DESTRUCTIVE TESTING; pp. 71-79; April 1976.
44. Epstein, George, "Nondestructive Test Methods for Reinforced Plastic/Composite Materials," Aerospace Corporation; Aerospace Report No. TR-0200(4250-20)-4; February 1969.
45. Chang, F.H., Couchman, J.C., Eisenmann, J.R., and Yee, B.G.W., "Application of a Special X-Ray Nondestructive Testing Technique for Monitoring Damage Zone Growth in Composite Laminates," ASTM Special Tech. Pub. 580, presented at Symposium on Composite Reliability, Las Vegas; pp. 176-190; April 1974.
46. Buhmann, K.P., Stellings, H.A., and Winkler, T., "Methods for Nondestructive Testing of Composite Materials," KUNSTSTOFFE; Vol. 64, No. 12; 1974; 50 pp.
47. Roberts, E. and Vary, A., "Inspection of Composites Using a Computer-Based Real-Time Radiographic Facility," Proc. of Automated Inspection and Product Control Conf.; pp. 139-150; October 1976.
48. Williams, J.H., Jr. and Doll, B., "Ultrasonic Attenuation as an Indicator of Fatigue Life of Graphite Fiber Epoxy Composite," MATERIALS EVALUATION, pp. 33-37; May 1980.
49. Vary, A. and Bowles, K.J., "Ultrasonic Evaluation of the Strength of Unidirectional Graphite-Polyimide Composites," Proc. of 11th NDE Symposium; pp. 242-258; 1977.
50. Henneke, E.G. II, Reifsnider, K.L., and Stinchcomb, W.W., "Vibrothermography and Ultrasonic Pulse-Echo Methods Applied to the Detection of Damage in Composite Laminates," Rockwell International, Thousand Oaks, California; Annual Report; January 1979; 4 pp.; Contract No. F33615-74-C-5180; Proc. of ARPA/AFML Review of Progress in Quantitative NDE; La Jolla, California; 1979.
51. Hayes, J., Fowler, K., Elfbaum, G., Fox, K., and Mel, B., "Nondestructive Thickness Measurement of Fiber Reinforced Plastic (FRP) Using Ultrasonic Techniques," Proceedings Reinforced Plastics/Composites Inst. Annual Conf., 33rd; Washington, DC; 7-10 February 1978; pp. 24/C1-24/C3; February 1978; 3 pp.
52. Jauch, P., "Methods and Techniques for the Inspection of CFRP Materials and Structures," in Italian (abstract in English); May 1978; 48 pp.; American Institute of Aeronautics and Astronautics, Inc.
53. Saksena, T.K. and Babbar, N.K., "Ultrasonic Investigation of the Curing Time of Epoxies," ULTRASONICS; Vol. 17, No. 3; May 1979; pp. 122-124.
54. Ramkumar, R.L. and Scott, W.R., "The Analytical, Experimental, and Nondestructive Evaluation of the Criticality of an Interlaminar Defect in a Composite Laminate," ICCM/2; Proc. 1978 International Conf. on Composite Materials; 16-20 April 1978; Toronto, Canada; pp. 1057-1071.
55. Turner, T.W. and Ashbee, K.H.G., "The Physical Mechanisms Responsible for the Weathering of Epoxy Resins and GFR Epoxy Resins," Bristol University (England); Final Technical Report; October 1978; 35 pp.
56. Kaitazidis, Michael, "Inspection of Carbon Fibre Parts After Fabrication and During Service," AGARD Conf. Proc. No. 234--NDI Relationships to Aircraft Design and Materials; 27-28 September 1977; Voss, Norway; pp. 16/1-16/16.
57. Moyzis, J.A. and Raney, J.M., "Exploratory Development of Nondestructive Evaluation Techniques," Systems Research Labs, Dayton, Ohio; Final Report; March 1978; 75 pp.; Contract No. F33615-76-C-5313.
58. Ting, C.S. and Sachse, Wolfgang, "Measurement of Ultrasonic Dispersion by Phase Comparison of Continuous Harmonic Waves," J. ACOUST. SOC. AM.; Vol. 64, No. 3; September 1978; pp. 852-857.
59. Tidswell, N.W. and Silvergleit, M., "Development of Ultrasonic Procedures and Calibration Standards for Determining Quality of Graphite Epoxy Composites," David W. Taylor Naval Ship Research and Development Center, Annapolis, Maryland; Report No. DTNSRDC/SME-78/36; June 1979; 45 pp.
60. Kaelble, D.H. and Dynes, P.J., "Nondestructive Tests for Shear Strength Degradation of a Graphite-Epoxy Composite," Rockwell International, Thousand Oaks, California; ASTM Spec. Tech. Publ. No. 617: Compos. Mater.: Test and Des., 4th Conf.; Valley Forge, Pennsylvania; May 3-4, 1976; pp. 190-200.
61. Whitcomb, J.D., "Experimental and Analytical Study of Fatigue Damage in Notched Graphite/Epoxy Laminates," NASA Langley Research Center, Hampton, Virginia; Report No. NASA-TM-80121; June 1979; 31 pp.
62. Treca, M., "Current Status and Development of Inspection of Carbon Fiber-Reinforced Composite Aircraft Structures," Lab Cent. Aerospace, Suresnes, France; AGARD Conf. Proc. No. 234—Meeting of the AGARD Struct. and Mater. Panel, 45th; (in French); Voss, Norway; September 27-28, 1977; pp. 18.1-18.7.
63. Dickson, J., "Ultrasonic Tests on Friction Materials," METROLOGY AND INSPECTION; Vol. 10, No. 1; January 1978; pp. 23-27.